Statistical Mechanics of Finite Length Semiflexible Wormlike Polymers

by

Nigel Thor Stanley Morgan Andersen

A thesis

presented to the University of Waterloo

in fulfillment of the

thesis requirement for the degree of

Doctor of Philosophy

in

Physics

Waterloo, Ontario, Canada, 2025

© Nigel Thor Stanley Morgan Andersen 2025

Examining Committee Membership

The following served on the Examining Committee for this thesis. The decision of the Examining Committee is by majority vote.

External Examiner	Hendrick de Haan Associate Professor Physics University of Ontario Institute of Technology
Supervisor	Jeff Z. Y. Chen Professor Physics and Astronomy University of Waterloo
Internal Member	Russell Thompson Associate Professor Physics and Astronomy University of Waterloo
Internal-external Member	Pierre-Nicholas Roy Professor Chemistry University of Waterloo
Other Member	Robert Wickham Associate Professor Physics University of Guelph

Author's Declaration

This thesis consists of material all of which I authored or co-authored: see Statement of Contributions included in the thesis. This is a true copy of the thesis, including any required final revisions, as accepted by my examiners.

I understand that my thesis may be made electronically available to the public.

Statement of Contributions

This thesis contains content that has been published elsewhere:

The content of Chapter 2 and Appendix A was published in The Journal of Chemical Physics in 2024 [1]. It was co-authored with Jeff Z. Y. Chen. It is reproduced from Andersen, Nigel T., and Jeff Z. Y. Chen. "Forced extension of a wormlike chain in the Gibbs and Helmholtz ensembles." The Journal of Chemical Physics 160.8 (2024)., with the permission of AIP Publishing.

The contents of Chapter 3 and Appendix B, with the exception of Section B.4, was published in Physical Review E in 2025 [2]. It was co-authored with Jeff Z. Y. Chen. It is reproduced here with permission from Andersen, Nigel T., and Jeff Z. Y. Chen. "Stretching semiflexible polymers: Gibbs versus Helmholtz ensembles." Physical Review E 111.4 (2025): 045402, ©2025 American Physical Society.

The contents of Chapter 4 and Appendix C was published in Macromolecules in 2023 [3]. It was co-authored with Jeff Z. Y. Chen. It is reprinted with permission from Andersen, Nigel T., and Jeff Z. Y. Chen. "Helical Wrapping of Cylindrical Tubes by Wormlike-Chain Polymers." Macromolecules 56.8 (2023): 3246-3254. Copyright 2023 American Chemical Society.
`http://pubs.acs.org/articlesonrequest/AOR-W2VDQ5UYGDXESVKMNTAI`

In all cases, I am the majority author of the works.

Abstract

The wormlike chain is a fundamental model in polymer physics used for describing the statistics of semiflexible polymers. It is a general model applicable to many polymers, with double-stranded DNA being a notable example. Previous theoretical work has focused on long polymers, where subtle differences in the choice of statistical ensemble are not relevant. This worked well in explaining early data on polymer stretching, but as more modern techniques have allowed for the stretching of shorter, more rodlike polymers, finite length ensemble effects have become visible in experimental measurements and computer simulations. Here, these effects are computed, and a full picture of wormlike chain statistical mechanics is presented. The new results are compared against several decades of polymer stretching literature, and are found to describe previously unexplained behaviour. Finally, the broad use of the model is demonstrated by applying it to DNA wrapped carbon nanotubes, a system that requires considering polymer flexibility, and predicting the pitch of the helical structure formed by these complexes.

Acknowledgements

First, I would like to thank my supervisor Professor Jeff Z.Y. Chen, for his support and guidance throughout the development of this thesis. Without him this work would not have been possible, and I could not have asked for a better mentor. It was my good fortune to have many good friends by my side throughout my graduate studies. I am also indebted to the many professors and teachers throughout my academic journey, who each contributed to my growth as a scientist. Finally, I would like to thank Meijing Jiang, for her continued love and support.

The development of this thesis was supported by the Ontario Graduate Scholarship (OGS), Queen Elizabeth II Graduate Scholarship in Science and Technology (QEII-GSST), and Canada Graduate Scholarship-Doctoral (CGS D) scholarships.

Table of Contents

Author's Declaration **iii**

Statement of Contributions **iv**

Abstract **v**

Acknowledgements **vi**

List of Figures **x**

List of Tables **xiv**

List of Abbreviations **xv**

1 Introduction **1**
1.1 Background and Motivation 1
1.1.1 Polymer Science 1
1.1.2 Single Polymer Theory 1
1.1.3 Motivation 2
1.2 Stretching Polymers Experimentally 3
1.2.1 Experimental Methods 3
1.2.2 Force-Extension or Extension-Force 4
1.2.3 Choosing an Ensemble Experimentally 5
1.2.4 Consideration for Shorter Polymers 6
1.3 Polymer-Wrapped Carbon Nanotubes 8
1.4 Modelling Single Polymers 8
1.4.1 Freely Jointed Chain 9
1.4.2 Wormlike Chain 11
1.4.3 Relevant length scales 14
1.5 Numerical Methods 15
1.6 Structure 16

2 Forced Extension of a Wormlike Chain in the Gibbs and Helmholtz Ensembles **17**
2.1 Introduction . . . 17
2.2 Stretched Wormlike Chain . . . 21
2.2.1 The Model . . . 21
2.2.2 Gibbs Ensemble . . . 21
2.2.3 Helmholtz Ensemble . . . 22
2.3 Strongly Stretched WLC in Different Ensembles . . . 23
2.4 Other Regions of the Parameter Space . . . 26
2.5 Conclusion . . . 29

3 Stretching Semiflexible Polymers: Gibbs Versus Helmholtz Ensembles **30**
3.1 Introduction . . . 30
3.2 Results . . . 32
3.2.1 Review of Experimental Results and Computer Simulations 32
3.2.2 Ensemble Dependent Analysis . . . 34
3.3 Summary . . . 38

4 Helical Wrapping of Cylindrical Tubes by Wormlike-Chain Polymers **39**
4.1 Introduction . . . 39
4.2 Scaling and Comparison with Experiment . . . 41
4.3 Theory . . . 44
4.3.1 WLC Model . . . 44
4.3.2 Cylindrical Surface . . . 45
4.3.3 Ground-State-Dominance Solution . . . 46
4.3.4 Small-R Theory . . . 47
4.3.5 Large-R Theory . . . 47
4.3.6 Numerical Solution . . . 48
4.3.7 Helix Pitch . . . 48
4.4 Comparison to a Previous Theory . . . 51
4.5 Summary . . . 51

5 Conclusion **53**
5.1 Summary . . . 53
5.2 Outlook . . . 54

Bibliography **56**

Appendices **70**

Appendix A Forced Extension of a Wormlike Chain in the Gibbs and Helmholtz Ensembles Appendix **71**
A.1 Derivation of the Strongly Stretched Gibbs Result . . . 71
A.2 Scaling Argument . . . 72
A.3 Contour Integral . . . 73

A.4 Re-summation 75
A.5 Gaussian Limit 76

Appendix B Stretching Semiflexible Polymers: Gibbs Versus Helmholtz Ensembles Appendix **77**
B.1 Wormlike-chain Theory 77
B.2 Scaling Argument 79
B.3 Helmholtz Interpolation Formula 79
B.4 Derivation of Solutions for Different Boundary Conditions 80
B.4.1 General Theory and Mapping 80
B.4.2 Two Fixed Ends 82
B.4.3 One Fixed End 83
B.4.4 Scaling behaviour for 1 and 2 fixed ends 84
B.5 Other Studies 86

Appendix C Helical Wrapping of Cylindrical Tubes by Wormlike-Chain Polymers Appendix **88**
C.1 Experimental Data 88
C.2 Comparison Against Lundberg and Strano 89

List of Figures

1.1 Schematic of a FJC. Because each monomer is uncorrelated with any other, the polymer is a series of random steps of length b_0. When used to model a real polymer, each step is replaced with the size of a Kuhn monomer b. The end-to-end vector $\mathbf{R}$ is shown. Since the direction of each step is random, the average end-to-end vector $\langle \mathbf{R} \rangle$ will be zero. 9

1.2 Schematic of the WLC. The polymer is modelled as a curve in space, with persistence length λ, and described by its position $\mathbf{r}(t)$ and orientation $\mathbf{u}(t)$, which are parametrized by the variable t. 11

2.1 Schematic of a stretched WLC under (a): the Gibbs ensemble, and (b) the Helmholtz ensemble. The Gibbs experiment has a constant applied force f, and the average extension $\langle Z \rangle$ can be determined from the Gibbs free energy, yielding an extension-force relationship. The Helmholtz experiments has a fixed extension Z, and the average force $\langle f \rangle$ required to maintain it can be obtained from the Helmholtz free energy, giving a force-extension relationship. The question is when, if at all, the Gibbs force-extension relationship is equivalent to the Helmholtz extension-force version. 18

2.2 Exact solutions of the force-extension relationships for a strongly stretched WLC under the Gibbs and Helmholtz ensembles Eqs. (2.3) and (2.4) (solid and dashed lines, respectively). Plot (a) shows extension-force relationships for $L/2\lambda = 4, 1/2, 1/16$ (flexible, semiflexible, and rodlike), corresponding to the bottom (grey), middle (light blue), and top (dark blue) curves. A reduced force is used to allow plotting of the curves on the same plot [4]. Curves for different $L/2\lambda$ collapse into a single universal scaling curve in (b) with use of the scaling variables, α and x. The Gibbs (solid) and Helmholtz (dashed) curves approach each other only when x is asymptotically large, in the thermodynamic limit. 20

2.3 Force-extension behaviour for a rodlike polymer in the Gibbs (solid line) and the Helmholtz (dashed line) ensembles. The average force required to maintain a given extension in the Helmholtz ensemble is zero as the thermodynamic fluctuations needing to be suppressed are isotropic. This holds until the rod is fully stretched, at which an infinitely large force is required in the stretching direction in order to completely suppress any deviations. 26
2.4 Regions of the stretched WLC parameter space. Blue indicates equivalence of the force-extension relations based on the Gibbs and Helmholtz ensembles, while red indicates no such equivalence. The behaviour in the strongly stretched (dashed box) region is the main contribution of this chapter. There, the force-extension relationships converge as the flexible (thermodynamic) limit is approached. 28

3.1 Theoretical behaviour for the two different types of polymer stretching experiment. The upper curve is the expected behaviour when the force is fixed and the fluctuating extension is measured by averaging [4–6]. The lower curve is when the extension is fixed and the fluctuating force is measured by averaging [1]. When the polymer is strongly stretched, only two scaled variables are relevant, regardless of polymer stiffness: the extension variation α defined in (3.1), and the reduced force x in (3.2). As the polymer length increases, they merge to the same asymptotic power law represented by the grey dash-dot line for a strongly stretched, infinitely long WLC [7]. 31
3.2 Collection of force-extension data from different experiments and computer simulations of semiflexible polymers in the literature. Table 3.1 lists the details for each study, including the molecule used, experimental setup, and corresponding symbols in the plots. Each data point is coloured based on its relative length, given by the ratio $L/2\lambda$, as indicated by the sidebar. (a) contains data for lower $L/2\lambda$, where the force was fixed, and the average extension measured. This is common in simulations, and some special experimental setups. (b) contains data for high $L/2\lambda$, such as the long dsDNA data used to validate the WLC model in Ref. [7]. A wide mix of techniques is employed with this data. (c) contains data for lower $L/2\lambda$ as well, but for cases where the extension was fixed, and the force was measured. This is typical for optical tweezers and AFM, or special simulations. In the background of each is the power law in (3.5) (grey dash-dot line), and the Marko-Siggia interpolation formula commonly used to fit experimental data (black dashed line) [7]. 35

3.3 The same data as Fig. 3.2 (a)-(c), re-plotted using the reduced variables α and x. The same colour scheme is employed. The solid lines are from the theoretical predictions, (3.3) and (3.4). Low- to mid-$L/2\lambda$ polymers follow different scaling behaviour, depending on how the experiment was conducted. This ensemble dependence is displayed in (a) and (c). High-$L/2\lambda$ experiments in (b) reside only along the asymptotic limit described by (3.5). 37

4.1 Schematic of a WLC wrapped on the surface of a nanotube in (a) 3D view, and (b) 2D expanded view. A nanotube having a smaller radius in comparison with the persistence length has a higher degree of confinement, yielding in a larger pitch P. The general behaviour of P depends on the polymer length, stiffness, and the nanotube radius. In the expanded view, the WLC can be thought of moving on a flat surface spanned by the spatial variables $[R, \Phi, z]$, subject to an effective potential $U_{\text{eff}}(\theta)$, as a function of the bond direction θ. The effective orientational ordering potential $U_{\text{eff}}(\theta)$ is caused by the cylinder's curvature. . . 40

4.2 (a) Helix pitch ratio P/R, and (b) reduced change in Gibbs free energy, for a polymer wrapped as a helix on a cylindrical surface. The numerical solution to the full WLC model is given by the solid black line in both figures. Data adopted from 10 different experimental and computer simulation studies in the literature is displayed by symbols. The data points are sourced as follows: The upwards pointing triangle marker is from [8], the downwards pointing triangle is from [9], the circles are from [10], the left pointing triangle is from [11], the right pointing triangle is from [12], the square is from [13], the pentagon is from [14], and the diamond is from [15]. The grey cross and plus in the top left, are data from Zheng et al. [16] and Campbell et al. [17] respectively, while the white plus and cross to the right are the same data points, shifted to approximate the persistence length of the "charge strip" 2x ssDNA structure suggested by Zheng et al. [16, 17]. Details are discussed in the text. The persistence lengths for each of the polymers were estimated based on the experimental conditions and existing literature [18–25]. The inset shows the power-law behaviour (dashed line) of the solution (solid line) for large λ/R as presented in Section 4.3.7. (b) is the difference between the reduced Gibbs free energy of the cylinder surface-confined WLC, and a 2D free-space WLC. The blue and red dashed lines are the respective small λ/R and large λ/R scaling laws, as presented in Sections 4.3.3 and 4.3.5. 42

4.3 (a) Density distribution function for the relative helix pitch as a function of said pitch, $R\,\rho_P(P)$, for three different values of the relative confinement; $\lambda/R = 1, 5, 25$. For $\lambda/R = 1$, the polymer is in a weakly confined, random coil configuration on the surface of the nanotube, and the most probable pitch is $P/R = 0$. As the nanotube radius is decreased relative to the persistence length λ, the most probable value for the pitch increases. (b) Rescaled pitch distributions showing convergence to the large-λ/R result as λ/R is increased. The dashed grey curves are the full solution, corresponding to 10 even spaced curves for λ/R values in the range $[1, 10^2]$. The dashed red line corresponds to the peak of the large-λ/R distribution (solid black line), the location of which determines the coefficient of the large-λ/R scaling law given in Eq. (4.6) and illustrated in Fig. 4.2 (a). 50
4.4 Numerical comparison between the helix-pitch predictions from the current chapter (solid curve) and from Ref. [26] (dashed curve). The relative percent difference is plotted as the dot-dashed line. 52

A.1 Diagram of the contour C running counter-clockwise over the complex plane $z = x + iy$, used to evaluate the Fourier transform integral. First-order poles are at $z = 0$, and at $z = -in^2\pi^2\lambda/L$, represented by circles. The contributions from the semicircle in the bottom half plane vanish as the radius of C is increased to infinity. The component along the real line is offset by $i\tau$, where τ is a small real parameter used to ensure we remain within the region of validity of the partition function. 74

B.1 Comparison of the exact Helmholtz result Eq. (3.4) in the main text, and the interpolation formula Eq. (B.11), which limits to the exact behaviour for both small and large α, and provides a reasonably accurate result in the intermediate regime, in a simple formula. 80
B.2 Finite length scaling behaviour for a strongly stretched WLC under different boundary conditions. The outer dot-dashed curves are with one end fixed, and one end free to rotate, as is the common setup in optical tweezer experiments. The inner dotted curves are for both ends fixed, as might be achieved in AFM experiments. In both cases, the Gibbs result is the upper curve, while the Helmholtz result is the lower curve. 85
B.3 Set of extra data not presented in the main text, see Table B.1 for the full list and corresponding systems. The studies are of high quality, but the force-extension data within does not have the resolution necessary to resolve the fine theoretical difference presented here. 86

List of Tables

3.1 Summary of the data used from experiments and computer simulations. The first column lists the first authors only. The method of study is labelled as Flow (applied fluid flow), OT (optical tweezers), MT (magnetic tweezers), AFM (atomic force microscopy), MFC (microfabricated cantilevers), MC (Monte Carlo simulation), PBD (pseudo-Brownian dynamics), or MD (molecular dynamics). The data has been categorized by fixed-f or fixed-Z and by symbols used for plotting in Figs. 3.2 and 3.3. Data with circles indicate high-$L/2\lambda$ data, plotted as one set in Fig. 3.2 (b) and Fig. 3.3 (b). 36

B.1 Collection of force-extension data not presented in the main text. The method of study is labelled by Flow (applied fluid flow), OT (optical tweezer), MT (magnetic tweezer), AFM (atomic force microscopy), MC (Monte Carlo simulation), PBD (pseudo-Brownian dynamics), or MD (molecular dynamics). All data points are represented by unfilled circles in Fig. B.3 87

C.1 Experimental data points, estimated persistence length, and nanotube radii 90

List of Abbreviations

AFM Atomic Force Microscopy

DNA Deoxyribonucleic Acid

dsDNA Double-stranded Deoxyribonucleic Acid

EPS Extracellular Polymeric Substance

FJC Freely-Jointed Chain

Flow Applied Fluid Flow

GC Gaussian Chain

GSD Ground-State-Dominance

MC Monte Carlo

MD Molecular Dynamics

MFC Microfabricated Cantilivers

MT Magnetic Tweezers

OT Optical Tweezers

PBD Pseudo-Brownian Dynamics

PbP2V Polystyrene-b-poly-2-vinylpyridine

PEG Polyethelyne Glycol

PMAA Poly(methacrylic acid)

PNES Poly[2,6-1,5-bis(3-propoxysulfonicacidsodiumsalt)naphthylene]ethynylene

PNiPAM Poly(N-isopropylacrylamide)

PPES Poly[p-2,5-bis(3-propoxysulfonicacidsodiumsalt)phenylene]ethynylene

ssDNA Single-Stranded Deoxyribonucleic Acid

SWNT Single-Walled Carbon Nanotube

WLC Wormlike-chain

Chapter 1

Introduction

This thesis deals with polymer physics, specifically the theoretical treatment of single polymer systems, and their associated statistical mechanics. The topics covered within can be broadly categorized under the umbrella of soft matter, itself sometimes listed as a subset of broader condensed matter physics. While the polymers themselves are abstracted as curves in space, the framework used to treat them is robust and applicable to a wide range of problems, as the following chapters will detail.

1.1 Background and Motivation

1.1.1 Polymer Science

Polymers are long chains of molecular units called monomers. The chains formed by these monomers can be of varying lengths and of varying structure. The focus here will be on linear chains, but branched chains and cross-linked networks are also possible and actively studied [27]. The variety in choice of individual monomers, polymer structure, and size, results in a myriad of quite different polymers and polymer systems with drastically different properties. Perhaps the most visible use is in plastics, the polymer polyethylene commonly used in plastic bottles (among many other things) being a key example [28]. Less visible is the role that single polymers play. Deoxyribonucleic acid (DNA), the molecule that encodes our genetic information, is a long polymer itself composed of individual nucleotide units [29]. DNA is stiff owing to its double-helical structure, and this makes its elastic properties readily apparent when probed [7]. It is still actively researched, and features prominently in experimental work discussed in later chapters.

1.1.2 Single Polymer Theory

The study of the physical properties of individual polymers necessitates having a physical model to describe the observed behaviour. Several have been pro-

posed over the years. At the most basic is the freely-joined chain model (FJC), which considers the polymer chain as composed of monomers that are free to rotate relative to each other [30]. This is broadly unphysical, as the molecular bonds linking the monomeric units together do not allow for this kind of free rotation. The inherent stiffness introduced by the monomer-monomer bonding is important, but the FJC model can be made to work by considering only segments separated by enough distance so that the backbone structure has no influence, rather than using the real monomeric units [27]. A FJC composed of these Kuhn monomers, as these are called, can do an excellent job of modelling a real chain as long as the important length scales at play in the system are larger than the size of the effective monomers.

When the system is deformed on length scales smaller than the size of a Kuhn monomer, b, the effective FJC model breaks down, and a more advanced model is needed. The wormlike chain model (WLC), which considers the inherent polymer stiffness, is one such model. The necessity for this was demonstrated convincingly by Marko and Siggia, who showed that measurements of stretched double-stranded DNA (dsDNA) failed to adhere to predictions by the FJC model. Explaining the experimental data required the WLC [7].

1.1.3 Motivation

The original work by Marko and Siggia made a comparison with experimental data by Smith et al. to show the validity of the WLC model [7, 31]. Smith et al. had measured the behaviour of dsDNA stretched by use of magnetic tweezers, and found that the resulting force-extension curve did not match with the FJC model. Marko and Siggia took this data and instead fit it to the WLC model. The resulting fit was much better, and provided a strong case using the WLC for experiments on semiflexible polymers.

A downside is that the WLC formalism admits no general solution, and so a numerical solution was originally used to fit the data [7]. To make the theory more accessible, they built a formula interpolating between the low force and high force limits, which both admit their own closed form results. This provided a reasonably accurate version of the WLC solution, but in a much more convenient form. The interpolation formula and its modifications are still in broad use today.

In order to obtain the numerical solution, Marko and Siggia looked at the WLC in the limit of infinitely long polymers, and so obtained a single curve. This valid for many polymers, so long as the length of the polymer L is much longer than twice the Kuhn monomer size. In the context of the wormlike chain, the characteristic correlation length of bond vectors along the chain backbone λ is used, and is equal to half the Kuhn length $\lambda = b/2$ [32]. Here, λ is also called the persistence length, and gives a direct measure of the stiffness of the polymer. Infinitely long in this context then means a relative length of $L/2\lambda \gg 1$. The DNA they compared against had a relative length of roughly $L/2\lambda \sim 300$, meaning the approximation worked well [7, 31]

However, computer simulations and continued experimental advances have

made possible measurements of shorter polymer segments [31, 33–68] . Outside of the $L/2\lambda \gg 1$ limit, a single curve is no longer sufficient to describe semiflexible polymer behaviour, but instead a spectrum of different behaviour is observed depending on the specific value of $L/2\lambda$ for the exact polymer system of interest. Furthermore, thermodynamic fluctuations which had been suppressed in the $L/2\lambda \gg 1$ limit (which is also the thermodynamic limit, discussed later in Chapter 2), now directly effect the response to deformation. This not only requires full evaluation of the WLC without approximation, but also an analysis of which statistical ensemble the experiment or simulation in carried out in [4, 69]. At the same time, other polymer system where the inherent stiffness of the polymers plays a central role are being investigated. One of the most interesting of these are polymer carbon-nanotube complexes, where the polymers are known to wrap the nanotubes in a regular helical pattern. The physics of these complexes is interesting on its own, and with the added importance these systems have in nanotube processing it is desirable to deepen our understanding of polymer-wrapped carbon nanotubes. Interplay between the polymer trapped on the nanotube surface, and the nanotube itself depends heavily on both the size of the nanotube and on the inherent flexibility of the polymer. This requires using more complex models such as the WLC to understand and model them. With this in mind, the goal of this thesis is to describe the fundamental behaviour of the full WLC model under different statistical ensembles, compare the new predictions to existing experiments, and demonstrate its broad applicability by using it to gain a fundamental understanding of polymer-wrapped carbon nanotubes.

1.2 Stretching Polymers Experimentally

1.2.1 Experimental Methods

To understand why previous theories are inadequate, we need to understand general procedure of how these long molecules are stretched experimentally. Conceptually the simplest way to stretch a polymer is to apply a force to one of its ends. For an unstretched polymer sitting in solution, its contour with follow an essentially random path through space. This reflects that a random walk is the most favourable state entropically. Because it is a random walk, the separation of the two ends of the polymer is on average, zero [30].

Fix one end in place, and apply a force to the other, and the polymer will start to unravel along the direction of the applied force. Any stretching is entropically unfavourable compared to the random walk configuration, however, and so there will be a resistance to the extension. This will be linear at first, commonly referred to as the entropic stretching regime, but will eventually plateau as the separation of the ends approaches the total contour length of the polymer L [27]. A polymer cannot be stretched further than its contour length, and often during an experiment the connection holding the polymer in place (or the polymer itself) will break before this point. Depending on its

molecular structure, deformation can also take place when the extension is near the contour length. For example, double-stranded DNA, a double helix formed of two single strands of DNA, when stretched too far will start to unravel back into single strands of DNA, causing an observable change in contour length [7]. On the other hand, M13 Bacteriophage (a type of virus) can display a smooth linear extension of its contour length when strongly stretched [58].

There are three common methods used to stretch the polymer in this way: Fluid Flow, Magnetic Tweezers, and Optical Tweezers. In a fluid flow experiment, the polymer is held in a contained with one end tethered to a wall, while the other is left free. Fluid is flowed through one end of the channel and out the other, stretching the polymer with it. This relies on the drag between the polymer and the fluid, though a bead can also be applied to the stretching end to increase the drag [33]. Magnetic tweezers stretch by applying a magnetic force to a bead that is attached to one end of the polymer, and the strength of the force is modulated by changing the distance between the magnet and the end of the polymer [70]. The final method, Optical Tweezers, is the most common of the three. As with magnetic tweezers, a bead is attached to one end of the polymer while the other remains fixed in place. Then the bead is picked up using a pair of Optical Tweezers. Optical tweezers use the intensity gradient of a laser beam to constrain the beat to the centre of an optical trap. Commonly, the fixed end of the polymer is then displaced. As the bead is shifted away from the centre of the optical trap, it experiences a force trying to return it to the centre, extending the polymer. The position of the bead in the trap can be calibrated so that the applied force on the polymer can be calculated [48]. Sometimes multiple techniques can be combined into a single measurement, as was done in an early work using both magnetic tweezer and fluid flow [31].

In all three of the applied force experiments, the polymer end is not constrained to be coaxial to the stretching direction, meaning that even at high force it will wander slightly and deviate from the direction in which it is being stretched. For this reason, the important parameter is the projection of the distance between the endpoints Z, simply called the extension.

It is also possible to fix the ends to be coaxial with the direction of stretching. Atomic Force Microscopy (AFM) is one method that does this. In such an experiment, one end is fixed to the surface of the container, and the other to an AFM tip. AFM is commonly used to measure the topography of a surface by seeing how much the tip is deflected when passed along a surface. In a similar manner, the polymer attached to the tip can be stretched by moving the tip a certain distance, and the force being applied can be calculated using the measured deflection of the tip at that distance [71, 72].

1.2.2 Force-Extension or Extension-Force

Polymers through statistical mechanics

Polymer behaviour is discussed theoretically in terms of statistical mechanics. Rather than predicting the behaviour of a single polymer, the distribution of

polymer configurations and other statistical properties are discussed instead. This allows us to evaluate the expected behaviour of the macroscopic polymer systems without needing to model the microscopic dynamics. This is exactly what is done for other physical systems such as gases, and the polymer physics discussed in this thesis is an application of statistical mechanics. The discussion of force-extension in how they compare to extension-force curves is fundamentally a discussion of the differences between statistical ensembles.

Statistical ensembles

These ensembles are then a logical framing for a discussion of stretching. Two are relevant for what is done here: the canonical ensemble, where the macroscopic states of the system are specified through a temperature and generalized set of coordinates, and the Gibbs canonical ensemble, where the states are specified through a temperature and generalized set of forces [69]. Here, "generalized coordinates" refers to parameters similar to volume, and "generalized forces" to quantities such as pressure. In the context of the experimental systems discussed in Section 1.2.1, the generalized coordinate in the canonical ensemble is the extension Z, while the generalized force in the Gibbs canonical ensemble is the applied force to the polymer f.

Both ensembles are also referred to under several other names. The following convention is used throughout the rest of the text: the canonical ensemble is called the Helmholtz ensemble, while the Gibbs canonical ensemble is simply the Gibbs ensemble. This is consistent with the broader polymer literature on the topic. The main qualities of interest will be the free energies, whose derivatives will give rise to the average forces and average extensions under each ensemble. For the Helmholtz ensemble this is the Helmholtz free energy, and for the Gibbs ensemble it is the Gibbs free energy — another reason for the choice of labels.

1.2.3 Choosing an Ensemble Experimentally

It is not uncommon for the terms force-extension or extension-force to be used interchangeably. Implicitly, force-extension suggests the force is fixed, while extension-force refers to the force response at a fixed extension. Fundamentally, this is a choice of statistical ensemble for the experiment. Measuring the average extension as a function of force places one in the fixed force (constant f) Gibbs ensemble, while measuring the average force as a function of the extension places one in the fixed extension (constant Z) Helmholtz ensemble.

Conceptually, applying a force to stretch a polymer is the more intuitive way to think about the problem, but both are readily realized experimentally, and have been used to study a range of polymer systems. Fluid flow is the clearest example of an experiment in the Gibbs ensemble. The drag of the solution applies a roughly constant force to the polymer, but the polymer end, being unconstrained, will move around slightly near its equilibrium position for a given force. This is monitored, and the extension for a given force is reported as the average position at that force: an average $\langle Z \rangle$ for a fixed force f.

AFM is the prototypical fixed-extension experiment. The AFM is set to a certain height, holding the polymer end there. The polymer is still undergoing random thermodynamic motion, fluctuation slightly in solution. These fluctuations mean that the force measured at a given moment for the fixed extension vary slightly, but the polymer is still always held at that extension. The force for reported for a given extension is the average force $\langle f \rangle$ at this fixed Z.

Optical tweezers are interesting, as both fixed extension and fixed force experiments have been done. The optical tweezer experiment described below is a typical example. One end of the polymer is attached to a bead held in the optical trap, while the other is attached to a moving slide. The bead never leaves the trap, so when the slide is extended, the polymer is stretched a fixed distance. Thermodynamic fluctuations or oscillations of the bead shift it slightly within the trap, but as it moves it changes the region of the optical potential it is sitting in, resulting in a larger or smaller force that compensates for the change. This brings the bead back to equilibrium, fixing its position. Hence, it is a constant extension experiment. However, the laser itself could also be fitted with a feedback mechanics to modulate the power of the laser, altering the potential so that the force remains constants regardless of the position of the bead (Ref. [42] has a clever implementation of this). This implements a fixed force experiment.

For classical experiments, this distinction did not matter. For example, Ref. [48] used both fixed force and fixed extension without issue. These first experiments on polymer stretching almost always used long polymers, and so did not encounter different behaviour based on fixing the force or extension. However, when shorter rodlike polymers are stretched, the choice of ensemble matters immensely. Analyzing this and its ramifications for interpreting experimental data forms a key part of this thesis in Chapters 2 and 3.

1.2.4 Consideration for Shorter Polymers

Rodlike or flexible polymers

What is meant by "rodlike" or "flexible" in the context of polymers? Often, rodlike and flexible will be used in conjunction with the length. For example, a short DNA segment will be rodlike, while a long DNA segment will be flexible. This is because the mechanism being the stiffness is the molecular structure of the polymer itself, which does not change based on length. In the context of DNA, this is the double helix structure, which is hard to deform and provides local stiffness, and which is encapsulated in the quantity called the persistence length λ mentioned earlier. How this local stiffness manifests on a macroscopic scale depends on the relevant macroscopic length scale, in this case the total polymer length L.

When the contour length of the polymer is much larger than the persistence length ($L \gg \lambda$), the polymer appears flexible. If the contour length is much smaller than the persistence length ($L \ll \lambda$) however, then the polymer will appear as a rigid rod. For different segment lengths of the same polymer, e.g. a

short and long strand of dsDNA, this will result in the shorter segment appearing more rodlike than the longer segment. This concept of a length dependent effect on apparent polymer stiffness is encapsulated in the idea of a relative length $\tilde{L} = L/2\lambda$. A large $\tilde{L}$ polymer is flexible, while a short $\tilde{L}$ polymer is rodlike.

The relative length is almost always what is meant during theoretical discussions on polymer statistics in this thesis, unless specifically stated otherwise. It is also conveniently dimensionless.

Thermodynamic limit for polymers

When dealing with small systems in statistical mechanics, the choice of ensemble matters. Fixing the force to a value and computing the average extension will not give the same result as fixing the extension to that value, and computing the average force. Concisely $f \neq \langle f \rangle$, and $Z \neq \langle Z \rangle$. This occurs because the probability distributions corresponding to the variables are asymmetric: the average of the distributions do not correspond to their most probable values [73]. If you were to compute both force-extension and extension-force curves ($\langle Z \rangle(f)$ and $\langle f \rangle(Z)$), and plot them on the same graph, they would not overlap.

This holds for finite systems. However, when the number of independent degrees of freedom increases, relative fluctuations in the free variables are reduced. Taking the limit of the degrees of freedom to infinity, and the mean of the distribution will overlap with the most probable value, and the differences between the ensembles will vanish [69]. Taking a classical gas of non-interacting particles as an example: for a system with ten molecules, a fluctuation in the number of particles by 5 will noticeably change the system. However, for the same system now with a million particles, a fluctuation of 5 will no longer be noticeable.

The question then becomes, how does this apply? What is the thermodynamic limit for a single polymer system? They key is in the correlations along the polymer backbone. For a rodlike molecule (as defined above), every point along the backbone is strongly correlated; the orientation of the initial point will determine the position of the final point, as the rod is effectively a straight line. For a flexible chain, there are many uncorrelated segments. As a result the end point of a flexible chain is unrelated to its initial point, in both orientation and position.

As was the case with the discussion on what makes a polymer rodlike or flexible, this depends not on the true length, but on the relative length $\tilde{L}$. The relative length is actually the measure of the number of uncorrelated segments, meaning it gives the number of independent degrees of freedom. This is a key point, and more detail is given in Section 2.5 and in the whole of Chapter 2 more broadly.

1.3 Polymer-Wrapped Carbon Nanotubes

The second system of interest is polymer-wrapped carbon nanotubes. This refers to a single carbon nanotube wrapped by a single polymer strand. A common polymer choice is single-stranded DNA (ssDNA), though there are many others. Several reasons make this interesting to study experimentally.

First is solvation: carbon nanotubes are in general poorly soluble, and form aggregates in solution instead of individually dispersing [74]. Several methods were developed to try to combat this, including adding surfactants to solution to aid in dispersing the polymers, as well as chemically modifying the surface of the nanotubes to make them more soluble. The surfactant method allows for only a limited concentration of nanotubes, and the surfactants themselves could be problematic depending on the system of interest [75, 76]. Chemical modifications involve bonding molecules to the surface of the nanotubes, inherently modifying their electronic properties. [77]. Neither are the most desirable. Wrapping them with polymers provides a clean solution to this, where the nanotubes are individually solvated with minimal modification to their electronic properties [76, 78–82]. The solvation is enabled by having a polymer that can interact favourably both with the solution and the nanotube itself. Taking ssDNA as an example, the nucleotide bases in the ssDNA strand interact (without forming chemical bonds) with the carbon nanotube, while the sugar-phosphate backbone (which is hydrophilic) allows it to be dissolved in aqueous solution [78].

This introduces the second point. The polymer-nanotube structure is interesting because the polymer wraps the nanotube in a regular helix [83, 84]. While from a bending energy standpoint, aligning the polymer backbone along the long axis of the nanotube to minimize bending would be the most energetically favourable, the loss of entropy in this configuration is too great, and so the polymer bends. This competition between the bending energy penalty for forcing the polymer to follow the contour of the tube surface and the entropic desire for a more random configuration give rise to a helix with a well-defined pitch that depends both on the polymer and the size of the nanotube. If these parameters can be captured in a theory, then the pitch should be able to be predicted. Given the range of experiments that have been done, a comparison between the data and such a theory can readily be made.

1.4 Modelling Single Polymers

To understand the stretching behaviour of real polymers, the ensemble dependent effects that could emerge for shorter rodlike systems, and the behaviour in hybrid systems like DNA wrapped carbon nanotubes, a model is needed. Two of the most fundamental models in polymer physics are the Freely Jointed Chain (FJC), and the Wormlike Chain (WLC). We will see that for the purposes of the systems that we aim to describe here, the FJC is inadequate and the WLC must be used.

1.4.1 Freely Jointed Chain

The FJC model describes the polymer as chain of N monomers, with a bond length b_0 separating them [30]. The monomers are free to rotate around each other without hindrance, but the bond length is fixed and does not vary (see Fig. 1.1). One of the basic parameters that is of general importance, and that we would like to predict, is the approximate size of the undisturbed polymer system in free space. Some nuance is required in selecting a suitable quantity to characterize this. A straightforward choice might be the average end-to-end separation of its endpoints, $\langle \mathbf{R} \rangle$, but as the orientation of the bonds are uncorrelated in the FJC, summing over the individual bond vectors $\mathbf{r}$ gives

$$\langle \mathbf{R} \rangle = \sum_{n=1}^{N} \langle \mathbf{r_n} \rangle = 0 \tag{1.1}$$

as $\langle \mathbf{r_n} \rangle = 0$ regardless of the bond vector in question.

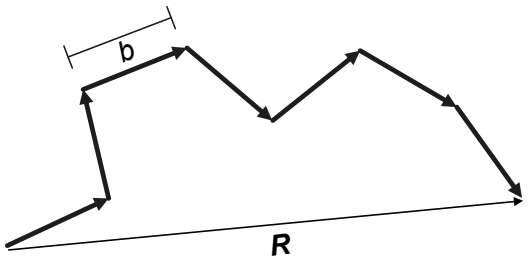


Figure 1.1: Schematic of a FJC. Because each monomer is uncorrelated with any other, the polymer is a series of random steps of length b_0. When used to model a real polymer, each step is replaced with the size of a Kuhn monomer b. The end-to-end vector $\mathbf{R}$ is shown. Since the direction of each step is random, the average end-to-end vector $\langle \mathbf{R} \rangle$ will be zero.

Therefore, the average of the square of the bond vectors is typically used instead [27].

$$\langle \mathbf{R}^2 \rangle = \sum_{n,m=1}^{N} \langle \mathbf{r}_n \cdot \mathbf{r}_m \rangle \tag{1.2}$$

This can be quickly verified to give a finite quantity: due to a lack of correlations, the $n \neq m$ terms are zero, and the sum simplifies to

$$\langle \mathbf{R}^2 \rangle = \sum_{n,m=1}^{N} \langle \mathbf{r}_n^2 \rangle \tag{1.3}$$

$$= N b_0^2 \tag{1.4}$$

which provides the basic measure of the size of the FJC.

As written, this does not apply to real polymers due to their inherent bond-bond correlations along the backbone. Instead, the bond length b_0 is replaced with the distance between two uncorrelated segments in the real polymer, b, called the Kuhn length. This gives a FJC of Kuhn monomers, which can serve as an effective representation of the real polymer so long as distances shorter than a Kuhn monomer do not have an effect on the behaviour of interest. Each Kuhn length is many times the size of the molecular bonds, with the exact correspondence depending on the inherent flexibility of the polymer in question: an inherently flexible polymer will have fewer molecular monomers per Kuhn monomer, while a more rodlike polymer will have more. In all cases, the total length L of the freely jointed chain and the real polymer are constrained to match, giving

$$L = Nb \tag{1.5}$$

Conceptually it is convenient to view the FJC in its discretized form as described above, but mathematically it can be easier to treat it in its continuum version. The continuum analogue of the FJC is the Gaussian Chain (GC), and it displays the same statistics as the FJC [27, 30, 32]. The difference is that the model treats the polymer as a smooth curve through space, where the distribution of the distance between of any two points along the chain $\mathbf{R}_n - \mathbf{R}_m$ is a Gaussian [30]. Here the Kuhn length no longer represents the effective monomer-monomer bond, but it is still an important local length scale describing the overall size of the polymer [32].

The Gaussian chain model is described by a Hamiltonian

$$\beta H = \int_0^1 \mathrm{d}t \left[\frac{3}{2Lb} \left| \frac{\mathrm{d}\mathbf{r}(t)}{\mathrm{d}t} \right|^2 + U[\mathbf{r}(t)] \right] \tag{1.6}$$

Here, $\beta = 1/k_B T$ is the inverse of the Boltzmann constant times the temperature. The variable t ranges from 0 to 1 and parametrizes the curve, with the vector $\mathbf{r}(t)$ specifying the position of the point at t along the curve. L and b are the total contour length and Kuhn length as before. An addition potential field U that depends on the position has been included, which can be used to reflect the system that is being modelled. The size of the polymer is unchanged from the FJC, and is given by

$$\langle \mathbf{R}^2 \rangle = Lb \tag{1.7}$$

equivalent to Eq. (1.4) through Eq. (1.5).

Similar to the path integral formalism in quantum mechanics, the Hamiltonian Eq. (1.6) can be used to derive a differential equation for the propagator of the GC system [30, 85]:

$$\frac{\partial}{\partial t} q_{GC}(\mathbf{r}, t) = \left[\frac{Lb}{6} \nabla_{\mathbf{r}}^2 - U(\mathbf{r}) \right] q_{GC}(\mathbf{r}, t) \tag{1.8}$$

where in the above the variable $\mathbf{r}(0)$ has been integrated out. The propagator, or Green's function, q represents the statistical weight of chain segment Lt that

ends at position $\mathbf{r}(t)$ [30, 32]. By integrating this function for $t = 1$ over all possible positions $\mathbf{r}$, the total partition function Q_{GC} is obtained,

$$Q_{GC} = \int \mathrm{d}t q_{GC}(\mathbf{r}, t = 1) \tag{1.9}$$

which is then used to determine the underlying statistics of the system.

As was mentioned earlier, this formalism works so long as the length scale being probed is significantly larger than that of the Kuhn length, such that the underlying structure of the physical polymer is not seen. When this assumption breaks down, a model that can account for the inherent correlations between monomers is required.

1.4.2 Wormlike Chain

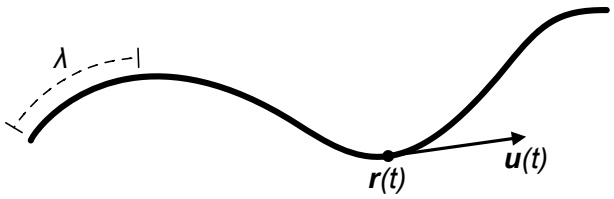


Figure 1.2: Schematic of the WLC. The polymer is modelled as a curve in space, with persistence length λ, and described by its position $\mathbf{r}(t)$ and orientation $\mathbf{u}(t)$, which are parametrized by the variable t.

The wormlike chain (WLC) is a continuum polymer model that aims to rectify the deficiencies in the FJC model by incorporating the inherent stiffness of the polymer as a parameter. It was first described in the context of discrete chains, where it is called the Krakty-Porod model [86], but is more useful for the purposes of this work in its continuous form, most notably formulated by Saitô et al. [87]. Its continuous version obeys the following Hamiltonian

$$\beta H = \int_0^1 \mathrm{d}t \left[\frac{\lambda}{2L} \left| \frac{\mathrm{d}\mathbf{u}(t)}{\mathrm{d}t} \right|^2 + U[\mathbf{r}(t), \mathbf{u}(t)] \right] \tag{1.10}$$

The persistence length now appears prominently in the numerator of the first term, which now has a dependence on the tangent vector $\mathbf{u}(t) = \mathrm{d}\mathbf{r}(t)/\mathrm{d}t$ at a point Lt along the backbone. The external potential $U[\mathbf{r}(t), \mathbf{u}(t)]$ can now also depend on the orientation, in addition to the position. This dependence on the orientation in addition to just the position is one of the fundamental characteristics of the WLC.

Persistence Length

A proper discussion of the persistence length is due in order to understand the WLC. It is related to the bending stiffness K of the polymer itself, but includes a dependence on the temperature T through the thermodynamic factor $\beta = 1/k_bT$, giving $\lambda = \beta K$. Therefore, it is not a static temperature, but depends on the parameters of the experimental system. It is also related to the correlations between tangent vectors $\mathbf{u}(t)$ at two points at t and t' along the polymer [87]

$$\langle \mathbf{u}(t) \cdot \mathbf{u}(t') \rangle = e^{-L|t'-t|/\lambda} \tag{1.11}$$

where it serves as the characteristic decay length of the correlations along the backbone.

Other factors can also influence the observed persistence length. For example, the persistence length of dsDNA, one of the most common polymers used in experiments, has a well documented dependence on the ionic strength (concentration of ions) in the solution [34]. Electrostatic repulsion between segments along the backbone of the DNA causes stiffening. When the ionic strength of the solution is increased, the ions screen these electrostatic interactions and reduce the observed persistence length. Overall, this causes the persistence length to decrease as the concentration of ions increases [88, 89].

The inherent stiffness now included in the model affects the overall size of the unconstrained semiflexible polymer as well. In general, the mean-squared end-to-end distance now depends on λ, with size of the chain given by the Kratky-Porod mean-squared end-to-end distance, which was first derived for the discrete version of the WLC (the Kratky-Porod model) [86]

$$\langle \mathbf{R}^2_{\mathrm{KP}} \rangle = 2\lambda^2 \left[L/\lambda + e^{-L/\lambda} - 1 \right]. \tag{1.12}$$

Taking the flexible limit $L/2\lambda \gg 1$, we find

$$\langle \mathbf{R}^2 \rangle = 2L\lambda \tag{1.13}$$

which when compared to the expression for the Gaussian chain Eq. (1.7) allows us to make the connection $b = 2\lambda$. On the other hand, when $L/2\lambda$ is taken to zero we have

$$\langle \mathbf{R}^2 \rangle = L^2 \tag{1.14}$$

as the polymer has become a rigid rod of length L.

Effects of Dimensionality

The above discussion assumes the context is a WLC in three spatial dimensions. However, the number of spatial dimensions will have an effect on the decay length of correlations along the backbone of the polymer. The proper expressions for the correlations and mean-squared end to end distance that take into account the number of spatial dimensions D, are [32]

$$\langle \mathbf{u}(t) \cdot \mathbf{u}(t') \rangle_D = e^{-L|t'-t|/\lambda_D} \tag{1.15}$$

and

$$\langle \mathbf{R}_D^2 \rangle = 2\lambda_D^2 \left[L/\lambda_D + e^{-L/\lambda_D} - 1 \right] \tag{1.16}$$

where the three-dimensional persistence length λ has been replaced with the D-dimensional persistence length λ_D, given through

$$\lambda_D = \frac{2\lambda}{(D-1)}. \tag{1.17}$$

For two-dimensional systems ($D = 2$), the reduced spatial freedom result in a longer correlation length and larger overall polymer size, reflected in the increase in the two-dimensional persistence length λ_2. This is relevant in quasi two-dimensional systems such as the polymer-wrapped nanotubes discussed in Chapter 4, where the polymer is confined to the surface of the nanotube. There are two ways to deal with this. The first is use the dimensionally dependent persistence length in the WLC Hamiltonian, which would introduce an explicit D dependence in Eq. (1.10), but have the expressions for $\langle \mathbf{R}_D^2 \rangle$ and $\langle \mathbf{u}(t) \cdot \mathbf{u}(t') \rangle_D$ remain identical to their three-dimensional counterparts $\langle \mathbf{R}_{\mathrm{KP}}^2 \rangle$ and $\langle \mathbf{u}(t) \cdot \mathbf{u}(t') \rangle$. The other method is to leave the persistence length in Eq. (1.10) as λ ($D = 3$), but use the dimensionally dependent λ_D for the correlations and mean-squared end-to-end distance. This latter approach is used here throughout, and λ always refers to the $D = 3$ persistence length.

Wormlike Chain Propagator and Diffusion Equation

As with the GC, the formalism is easier to treat when re-expressed in terms of the propagator $q(\mathbf{r}, \mathbf{u}, t)$ [32, 86, 87]

$$\frac{\partial}{\partial t} q(\mathbf{r}, \mathbf{u}, t) = \left[\frac{L}{2\lambda} \nabla_{\mathbf{u}}^2 - L\mathbf{u} \cdot \nabla_{\mathbf{r}|\mathbf{u}} + U(\mathbf{r}, \mathbf{u}) \right] q(\mathbf{r}, \mathbf{u}, t) \tag{1.18}$$

The WLC partition function Q is given by the integral of the propagator (Green's function) for the chain end

$$Q = \int \mathrm{d}t \, q(\mathbf{r}, \mathbf{u}, t = 1) \tag{1.19}$$

from which the desired conformational statistics can be obtained. When modelling polymer stretching in the Gibbs ensemble, this involves computing the Gibbs free energy

$$\beta G = -\ln Q(f) \tag{1.20}$$

from the Gibbs ensemble partition function $Q(f)$, which in turn allows computing the average extension $\langle Z \rangle$ through the thermodynamic relation

$$\langle Z \rangle = -\frac{\partial G(f)}{\partial f} \tag{1.21}$$

A similar process is done for the Helmholtz ensemble: the Helmholtz free energy

$$\beta F = -\ln Q(Z) \tag{1.22}$$

is computed from the Helmholtz ensemble partition function $Q(Z)$, then using the thermodynamic relation

$$\langle f \rangle = \frac{\partial F(Z)}{\partial Z} \tag{1.23}$$

the average force $\langle f \rangle$ is obtained.

When discussing the differences in polymer stretching behaviour caused by ensemble effects, the free energies and the associated average forces and extensions are the key parameters. However, in the context of polymer-wrapped carbon-nanotubes, the main parameter of interest is the pitch P of the helix the polymer forms on the surface of the nanotube. Calculating this requires analysis of probability density function ρ. It is given by

$$\rho(\mathbf{r}, \mathbf{u}) = Q^{-1} \int_0^1 \mathrm{d}t \; q(\mathbf{r}, \mathbf{u}, t) q(\mathbf{r}, -\mathbf{u}, 1-t) \tag{1.24}$$

which gives the polymer density at a point $\mathbf{r}$ with orientation $\mathbf{u}$. The integrand is the product of the propagator (statistical weight) bridging the start to the point of interest Lt along the backbone, with the propagator from the terminal end to the same point of interest. Only $q(\mathbf{r}, \mathbf{u}, t)$ is required to be computed, with $q(\mathbf{r}, -\mathbf{u}, 1-t)$ obtained by inverting the orientation and setting $t \to 1-t$. In practice, the distribution in the nanotube system will be a function of the angle θ (where $\theta = 0$ points parallel to the long axis of the nanotube), giving $\rho(\theta)$, which is then transformed into a probability distribution for the pitch.

Equation (1.18) is the fundamental equation that is used throughout this work. It admits in general no closed form solution, but its numerical solution, and exact solutions under different limits, are of central importance. Because of the focus on the WLC model, Q, q, H, or other parameters without subscripts will be referring implicitly to the WLC, rather than the GC or other models.

1.4.3 Relevant length scales

Good success has been had using only the GC (or FJC) model, regardless of the underlying persistence length of the polymer being studied. Given enough distance between, segments in the real polymer will also be uncorrelated. This allows a mapping of the real polymer to the GC, through use of the Kuhn length b, mentioned earlier. When does this work, and when does it break down?

Mapping the GC model to a real chain in this way applies as long as the contributions from the correlated segments in the underlying polymer are not revenant to what is being modelled. For a long polymer in random coil configuration in solution, the GC will give the correct distribution of the end-to-end vector, and will also correctly describe the behaviour of a weakly-stretched real polymer [27].

Issues in applying the GC model arise when the system is probed on a length scale in which the inherent stiffness of the backbone is visible, breaking the assumption of uncorrelated segments that the GC depends on. The GC remains valid when: the polymer is long in the sense $L/\lambda \gg 1$, variation in the

system occurs on length scales on the order of $\sqrt{Lb}$ or larger, and the external potential is weak with order $(b/L)^0 = 1$ or smaller. Under these conditions, the WLC reduces to the GC, and there is no issue in applying the GC model to the system [32]. When any of these conditions are broken, for example when considering rodlike molecules or a heavily deformed polymer under a strong stretching potential, then the WLC model must be used in order to properly capture the behaviour.

1.5 Numerical Methods

Chapter 2 and Chapter 3 contain a purely theoretical discussion, where the results are expressed through analytic equations. However, for the theory in Chapter 4, while closed form solutions are derived in certain limits, a general comparison to experiment requires a numerical solution over the full parameter space. This is discussed in Section 4.3.6, but here some additional background information is presented.

Typically, a diffusion type partial differential equation will contain term corresponding to a first derivative in time $\partial/\partial t$, as well as first and second derivatives in space $\partial/\partial x$, $\partial^2/\partial x^2$. In order to numerically integrate such equations, the derivatives are approximated as a finite difference across a grid [90]. There are multiple ways to choose the approximation. Given a function $f(x)$ over a grid with spacing Δx, one could take the forward difference at a point x_k:

$$\frac{\partial f(x)}{\partial x} = \frac{f(x_{k+1}) - f(x_k)}{\Delta x} \tag{1.25}$$

the backwards difference

$$\frac{\partial f(x)}{\partial x} = \frac{f(x_k) - f(x_{k-1})}{\Delta x} \tag{1.26}$$

or the central difference

$$\frac{\partial f(x)}{\partial x} = \frac{f(x_{k+1}) - f(x_{k-1})}{2\Delta x} \tag{1.27}$$

Higher order differences follow the same idea, and can be derived by recursively taking the finite difference. For example, the second order central difference is

$$\frac{\partial^2 f(x)}{\partial x^2} = \frac{f(x_{k+1}) - 2f(x_k) + f(x_{k-1})}{\Delta x^2} \tag{1.28}$$

A common choice is a forward difference or backwards difference for a time derivative, and a central difference for the space derivative.

Because of the specific problem being solved in Section 4.3.3, the solution is dominated by the ground-state eigenfunction, and so the eigenvectors and eigenvalues can be solved for instead of computing the full numerical integral of the equation. To do this, the equation is first written as an eigenfunction equation for some function ψ. Then the differential operator (derived from the

right-hand side of Eq. (1.18)) acting on ψ is discretized using a central difference, and the solution is given by the eigenvector, which is computed numerically. In the case of Section 4.3.3, the associated eigenvalue represents the reduced confinement free energy of the polymer on the nanotube surface.

1.6 Structure

The rest of this thesis tackles the problems outline in this introduction, using the WLC model. Chapter 2 investigates how the stretching response changes as a function of $\tilde{L}$, by deriving the strongly-stretched behaviour of a WLC in the Helmholtz ensemble, and comparing it to the Gibbs ensemble, highlighting the differences and how they converge in the thermodynamic limit. Chapter 3 continues this by reviewing two decades of experimental and simulation data on stretched polymers in both ensembles, and showing how the ensemble dependent theory derived in the previous chapter allows previously unexplained behaviour to be understood using the WLC. Finally, Chapter 4 uses the WLC to model polymer-wrapped carbon-nanotubes. It is shown that the WLC can predict the helix pitch formed by the polymer on the surface, as a function of nanotube radius and the persistence length. Comparisons are made to a previous approximate theory and experimental data.

Each of the main chapters, Chapter 2, Chapter 3, and Chapter 4 have been published elsewhere. See the Statement of Contributions at the beginning of this thesis for details and a statement of copyright. While the bodies of each chapter adhere closely to the contents of the published versions, several changes were made. The introductory paragraphs were based on modified versions of the abstracts, to have them fit better within the context of this thesis. Similarly, several of the figures were changed to better take advantage of the layout of this document. Information previously included as supplementary materials has been instead included here as appendices. Accordingly, references in the text of each to supplementary materials or supplementary information have been changed to references to appendices. Likewise, self references such as "this work" have been changed to "this chapter" or similar. References for each were also combined into a central bibliography, listed at the end of the thesis before the appendices.

In general, only the minimum amount of mathematics and theoretical details required to understand the contents of each chapter are presented in the main body of the text. Details and derivations are placed into the appendices, to avoid overwhelming the reader.

Chapter 2

Forced Extension of a Wormlike Chain in the Gibbs and Helmholtz Ensembles

A semiflexible polymer can be stretched by either applying a force to it or by fixing the positions of its endpoints. The two approaches generally yield different results and correspond to experiments performed in either the Gibbs or Helmholtz statistical ensembles. In this chapter, the Helmholtz force-extension relationship for WLC polymers in the strongly stretched regime is derived. By analyzing it in comparison with the Gibbs ensemble result, we show that equivalence between the two relationships is achieved only in the long-chain thermodynamic limit. The contents of this chapter was published in Ref. [1] in 2024.

2.1 Introduction

When stretching a polymer, there are two conjugate physical quantities one can measure: the extension in response to a given force, or the force required to maintain a fixed extension. The question that then arises is when, if at all, the two procedures generate the same results. In thermodynamics, the choice of fixing either the force or the extension corresponds to a choice of statistical ensemble. Fixing the extension corresponds to performing the experiment in the Helmholtz (canonical) ensemble, and the average force needed to maintain a specific extension is then obtained from the Helmholtz free energy. Fixing the force places one in the Gibbs ensemble, and the average extension is determined by the Gibbs free energy.

Whether the two force-extension relationships are different for a single poly-

mer system has received considerable attention in the literature. Most studies have focused on the freely jointed chain (FJC), or its continuum analogue, the Gaussian chain (GC) [73, 91–93]. A majority have found agreement between the ensembles in the thermodynamic limit as expected from statistical mechanics, although whether the same notion holds in the weakly stretched regime has been debated [94–97].

Experimentally however, the stretching of semiflexible polymers such as double-stranded DNA has been found to be best described by the wormlike-chain model (WLC), which accommodates polymers of varying flexibility [7, 31, 48, 90, 98]. While some theoretical studies have looked at the WLC or generic polymer models, they have focused on the conditions under which a transformation between the partition functions or force-extension relationships provides equivalence. While the ensembles are known to be qualitatively different, a direct comparison has not been made outside of simulations, which have incomplete coverage of the parameter space [44, 73, 99–103].

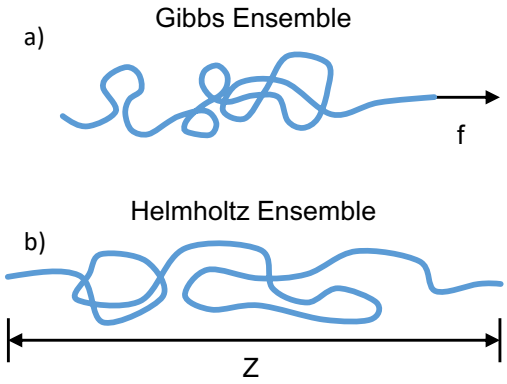


Figure 2.1: Schematic of a stretched WLC under (a): the Gibbs ensemble, and (b) the Helmholtz ensemble. The Gibbs experiment has a constant applied force f, and the average extension $\langle Z \rangle$ can be determined from the Gibbs free energy, yielding an extension-force relationship. The Helmholtz experiments has a fixed extension Z, and the average force $\langle f \rangle$ required to maintain it can be obtained from the Helmholtz free energy, giving a force-extension relationship. The question is when, if at all, the Gibbs force-extension relationship is equivalent to the Helmholtz extension-force version.

Our focus in this chapter is the derivation of the Helmholtz force-extension relationship for a strongly stretched WLC, modelled as a smooth curve with persistence length λ and contour length L. In combination with the force-extension relation in the Gibbs ensemble previously reported [4, 6], this provides us an opportunity to conduct a full analytical assessment of the differences that covers the full range of $L/2\lambda$. These force-extension relationships are valid for

any type of WLC, ranging from rodlike $L/2\lambda \ll 1$ to flexible $L/2\lambda \gg 1$. We showcase the main results here first, while the mathematical derivations are given later in Sections 2.2 and 2.3.

We consider a polymer whose endpoints are left free to rotate, and which is coupled to an external potential that deforms it. The stretched WLC model contains two basic dimensionless parameters, λ/L (from a reduced version of the local bending energy) and $\beta f L$ (from the stretching potential). Hence the dimensionless distance $Z/L = \zeta(L/\lambda, \beta f L)$ is a function of both parameters, as illustrated in Fig. 2.2 (a) where the Kratky-Porod mean square end-to-end distance, $\left\langle R_{\mathrm{KP}}^2 \right\rangle / L^2$, which is a function of L/λ only, is further used for the convenience of accommodating all plots in the figure. When the polymer is strongly stretched, large deviations from the stretching direction are suppressed, and the stretching potential is well approximated as quadratic. Under these conditions, based on the Gibbs ensemble, the mean extension $\langle Z \rangle$ can be expressed as

$$\frac{\langle Z \rangle}{L} = 1 - \frac{D(x)}{\beta f L} \tag{2.1}$$

with

$$D(x) = [1 + x \coth(x)]/2 \tag{2.2}$$

Here, f is the stretching force (Fig. 2.1) and $\beta = 1/k_B T$, where k_B is the Boltzmann constant and T the temperature. This is a known result which has been derived in the flexible limit ($L/2\lambda \gg 1$) by Marko and Siggia [7], and in the full $L/2\lambda$ regime by Kessler and Rabin [6] and by us [4] recently. For completeness, Appendix A.1 contains a summary of the derivation. A scaled parameter $x = L(\beta f/\lambda)^{1/2}$ is used above. This prompts the plotting of

$$\alpha(x) \equiv \left[1 - \frac{\langle Z \rangle}{L}\right] \frac{\lambda}{L} = \frac{D(x)}{x^2} \quad \text{(Gibbs)} \tag{2.3}$$

as a single solid curve in Fig. 2.2 (b).

In the Helmholtz ensemble, we show in Section 2.3 that the mean force $\langle f \rangle$ is expressed in series as,

$$\beta \frac{L^2}{\lambda} \langle f \rangle = \pi^2 \frac{\sum_{n=1}^{\infty} (-1)^{(n+1)} n^2 e^{-\alpha \pi^2 n^2}}{\sum_{n=1}^{\infty} (-1)^n e^{-\alpha \pi^2 n^2} + 1/2} \tag{2.4}$$

where $\alpha = (1 - Z/L)\lambda/L$ follows the same definition as before, but with a fixed Z. Likewise, if we take

$$x = L(\beta \langle f \rangle / \lambda)^{1/2} \quad \text{(Helmholtz)} \tag{2.5}$$

now defined in terms of the mean force, then the relation in (2.4) can also be plotted alongside Eq. (2.3), given as the dashed line in Fig. 2.2 (b). The comparison between the two curves reveals that the equivalence between the stretching experiments in the two ensembles is valid only in the $x \gg 1$ limit, or conversely, the $\alpha \ll 1$ limit. That both curves converge to the same slope is shown analytically in Section 2.3.

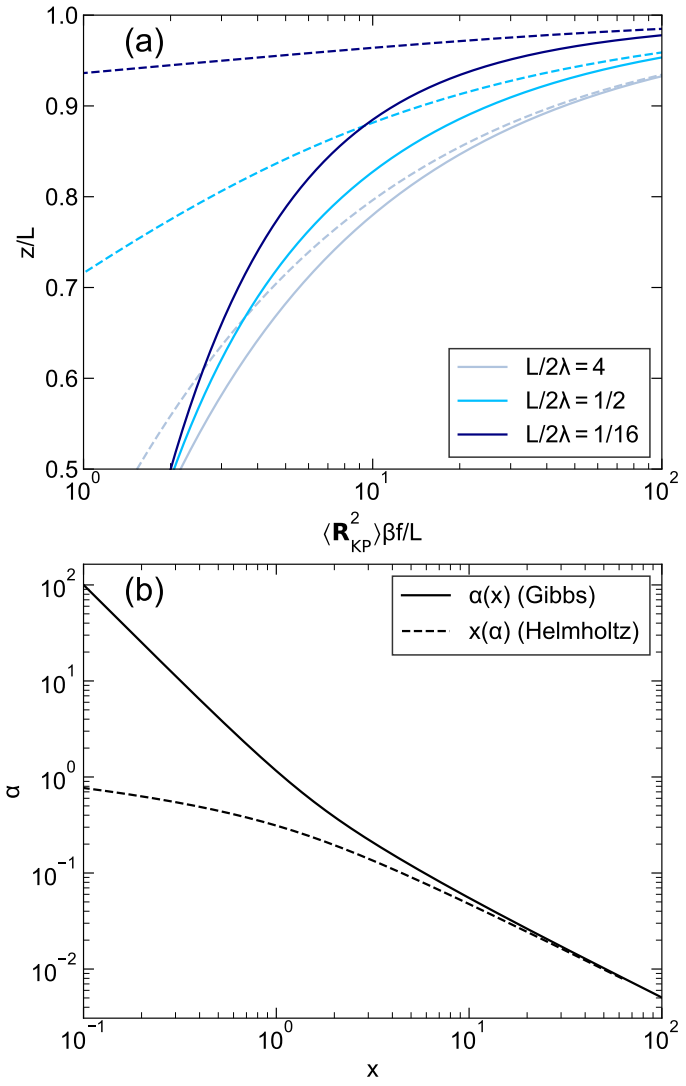


Figure 2.2: Exact solutions of the force-extension relationships for a strongly stretched WLC under the Gibbs and Helmholtz ensembles Eqs. (2.3) and (2.4) (solid and dashed lines, respectively). Plot (a) shows extension-force relationships for $L/2\lambda = 4, 1/2, 1/16$ (flexible, semiflexible, and rodlike), corresponding to the bottom (grey), middle (light blue), and top (dark blue) curves. A reduced force is used to allow plotting of the curves on the same plot [4]. Curves for different $L/2\lambda$ collapse into a single universal scaling curve in (b) with use of the scaling variables, α and x. The Gibbs (solid) and Helmholtz (dashed) curves approach each other only when x is asymptotically large, in the thermodynamic limit.

For each ensemble, the curves $Z/L = \zeta(L/\lambda, \beta f L)$ for different values of L/λ in Fig. 2.2 (a) collapse into a single scaling curve in Fig. 2.2 (b) with the use of α and x. This behaviour reflects the underlying physics of the WLC, for reasons that are explained in Appendix A.2.

Section 2.2 provides the theoretical background needed, and the details of our approach. The results are presented in Section 2.3, with mathematical details placed in Appendices A.3, A.4, and A.5, to avoid overwhelming the unfamiliar reader. Section 2.4 contains a summary of the results, as well as a brief discussion on equivalence for weakly stretched and rodlike WLCs.

2.2 Stretched Wormlike Chain

2.2.1 The Model

The continuum version of the WLC model is known to accurately capture the statistics of stretched semiflexible polymers [6, 7, 46, 50, 104–107]. The model describes a polymer as a smooth space curve of length L, with a persistence length λ corresponding to the tangent vector correlation length along the backbone of the polymer [87]. The ratio $L/2\lambda$ determines the relative stiffness of the chain. A WLC with $L/2\lambda \gg 1$ is flexible, while one with $L/2\lambda \ll 1$ is stiff and behaves as a rodlike molecule. Although we treat the chain as a continuous curve, the number of degrees of freedom is limited by the correlations between separate points along the polymer backbone. The WLC has a number of effective degrees of freedom proportional to the ratio of the length to the Kuhn length b, the distance over which two segments can be considered uncorrelated. For the WLC we have $b = 2\lambda$ [108], and so $L/2\lambda$ is also a measure of the number of thermodynamic degrees of freedom of the system. The $L/2\lambda \gg 1$ flexible limit is therefore also the thermodynamic limit. The chain backbone is parametrized by the variable t, ranging from $t = 0$ at one end, to $t = 1$ at the other. The polymer configuration is given by the position vector $\mathbf{r}(t)$ and tangent unit vector along the backbone $\mathbf{u}(t) = L^{-1}\mathrm{d}\mathbf{r}(t)/\mathrm{d}t$. For an unstretched polymer, the WLC has the Hamiltonian

$$\beta H_0 = \int_0^1 \mathrm{d}t \, \frac{\lambda}{2L} \left| \frac{\mathrm{d}\mathbf{u}(t)}{\mathrm{d}t} \right|^2 \tag{2.6}$$

describing the energy cost of bending the polymer [87].

Figure 2.1 shows a schematic of a WLC being stretched in the constant force Gibbs ensemble, compared to one being stretched in the constant extension Helmholtz ensemble. Describing the WLC in each ensemble requires a different approach, but as will be shown, their partition functions are related through a Fourier transform.

2.2.2 Gibbs Ensemble

In the Gibbs ensemble, the polymer configuration is specified by the temperature T and generalized force $\mathbf{f}$. We consider here the polymer to be coupled to an

external force-field along the z direction $\mathbf{f} = f\hat{z}$. The Gibbs Hamiltonian is then given by [7, 30]

$$\beta H_G = \int_0^1 \mathrm{d}t \left[\frac{\lambda}{2L} \left| \frac{\mathrm{d}\mathbf{u}(t)}{\mathrm{d}t} \right|^2 - \beta L \, \mathbf{f} \cdot \mathbf{u}(\mathbf{t}) \right] \tag{2.7}$$

$$= \beta H_0 - \beta f L \int_0^1 \mathrm{d}t \, u_z(t) \tag{2.8}$$

For an unconfined WLC, translational symmetry means only the orientation dependence needs to be considered. One can then calculate the partition function in the Gibbs ensemble by integrating over the statistical weight $\exp(-\beta H_G)$, yielding

$$Q(f) = \int \mathrm{d}\mathbf{u}(t) \, \exp\left(-\beta H_0[\mathbf{u}(t)] + \beta f L \int_0^1 \mathrm{d}t \, u_z(t) \right) \tag{2.9}$$

where the partition function $Q(f)$ is implicitly reduced by the volume of the system $Q(f) \equiv Q(f)/V$. The average extension $\langle Z \rangle$ is then obtained through the Gibbs free energy $\beta G = -\ln Q(f)$, by the standard thermodynamic relation

$$\langle Z \rangle = -\frac{\partial G(f)}{\partial f} \tag{2.10}$$

This procedure produces a force-extension curve giving the average extension as a function of the applied force $\langle Z \rangle(f)$.

2.2.3 Helmholtz Ensemble

A stretching experiment in the Helmholtz ensemble is instead specified by a given Z. Our central goal is to compute the complementary extension-force relation, giving the average force as a function of the applied extension $\langle f \rangle(Z)$. To obtain the partition function in this ensemble, we modify the free space probability distribution by only allowing configurations whose endpoints have a separation Z. The Helmholtz partition function becomes

$$Q(Z) = \int_0^1 \mathrm{d}\mathbf{u}(t) \, e^{-\beta H_0} \delta\left(Z - L \int_0^1 \mathrm{d}t u_z(t) \right) \tag{2.11}$$

where $\delta(x)$ is the Dirac delta function,

$$\delta(x) = \frac{1}{2\pi} \int_{-\infty}^{\infty} \mathrm{d}p \, e^{ipx} \tag{2.12}$$

Use of this in the above gives the Helmholtz partition function $Q(Z)$ as an inverse Fourier transform

$$Q(Z) = \frac{1}{2\pi} \int_{-\infty}^{\infty} \mathrm{d}p \, e^{ipZ} Q(p) \tag{2.13}$$

where

$$Q(p) = \int \mathrm{d}\mathbf{u}(t) \exp\left[-\beta H_0[\mathbf{u}(t)] - ipL \int_0^1 \mathrm{d}t\, u_z(t)\right] \tag{2.14}$$

is the Fourier transform of $Q(Z)$.

Structurally, Eq. (2.13) has the same form as Eq. (2.9), and they become identical under the mapping $\beta f \to -ip$. If the Gibbs partition function is known, the Helmholtz partition function can then be obtained from the inverse Fourier transform of the Gibbs results evaluated at the imaginary force $f = -ip/\beta$. In other words, $Q(Z)$ can be obtained through Eq. (2.13) using

$$Q(p) = Q(f)\Big|_{f=-ip/\beta} \tag{2.15}$$

assuming the inverse Fourier transform can be found. If found, the Helmholtz free energy $\beta F = -\ln Q(Z)$ can be used to calculate the average force

$$\langle f \rangle = \frac{\partial F(Z)}{\partial Z} \tag{2.16}$$

where we have used the standard thermodynamic relation for the Helmholtz free energy.

This mapping has previously been discussed in the context of FJCs, as well as for the discrete and continuous versions of the WLC [44, 109–112]. In the following sections, we directly compute force-extension relations based on Eqs. (2.10) and (2.16), and compare the results.

2.3 Strongly Stretched WLC in Different Ensembles

The stretching behaviour of a continuous WLC in the Gibbs ensemble is dependent on the relative flexibility $L/2\lambda$ of the polymer, and the relative force $\tilde{f} = \langle \mathbf{R}^2_{\mathrm{KP}} \rangle \beta f / L$ applied to its ends [4]. Here, $\langle \mathbf{R}^2_{\mathrm{KP}} \rangle$ is the Kratky-Porod mean square end-to-end distance for the WLC:

$$\langle \mathbf{R}^2_{\mathrm{KP}} \rangle = 2\lambda^2 \left(L/\lambda + e^{-L/\lambda} - 1 \right) \tag{2.17}$$

There is no closed-form solution of the partition that covers the full range of $L/2\lambda$ and $\tilde{f}$, in either ensemble. However, when the WLC is strongly stretched ($\tilde{f} \gg 1$), the stretching potential is well approximated as quadratic. Under this approximation, a closed form solution for the partition function in the Gibbs ensemble for any $L/2\lambda$ can be derived based on Feynman's formulation for the path integral of a simple harmonic potential in quantum mechanics [4, 73, 113]:

$$Q(f) = \frac{2\pi}{\sqrt{\lambda \beta f}} \frac{e^{\beta f L}}{\sinh(L\sqrt{\beta f/\lambda})} \tag{2.18}$$

valid for $f > 0$. This leads to the Gibbs ensemble extension-force relation

$$\frac{\langle Z \rangle}{L} = 1 - D(x)/\beta f L \tag{2.19}$$

with

$$D(x) = [1 + x \coth(x)]/2 \tag{2.20}$$

and where $x = L\sqrt{\beta f/\lambda}$ acts as the central scaling parameter for the Gibbs ensemble in the strongly stretched region.

To compute the corresponding relationship in the Helmholtz ensemble, we apply the mapping Eq. (2.15), which gives the Fourier transform of the Helmholtz partition function

$$Q(Z) = -\int_{-\infty+i\tau}^{\infty+i\tau} \mathrm{d}p \frac{e^{-ip(L-Z)}}{\sqrt{ip\lambda}\sin(L\sqrt{ip/\lambda})} \tag{2.21}$$

where a small real parameter τ has been introduced, in order to ensure we remain in the $f > 0$ region of validity for the partition function. The central task is then the solving of the above integral, after which the limit of τ going to zero from the right can be taken to recover the exact Helmholtz partition function.

Equation (2.21) is evaluated by means of a contour integral from the real line $+i\tau$, along a semicircle in the bottom half complex plane. Similar contour integrals have been used in evaluating the mapping in the context of discrete chains before [110, 111]. Extending p to be complex, the integrand has poles at $p = -i\lambda\pi^2 n^2/L^2$, for integer n. Appendix A.3 discusses the evaluation of the integral by means of the residue theorem, which leads to

$$Q(Z) = \frac{4\pi}{L}\left[\sum_{n=1}^{\infty}(-1)^n e^{-\alpha\pi^2 n^2} + \frac{1}{2}\right] \tag{2.22}$$

which is the exact form of the Helmholtz partition function for $\tilde{f} \gg 1$. We have introduced

$$\alpha = (1 - Z/L)\,\lambda/L \tag{2.23}$$

which functions as the central scaling parameter characterizing the WLC in the strongly stretched region under the Helmholtz ensemble. The partition function formally takes the form of the partial theta function $\theta(x;q)_p = \sum_{n=0}^{\infty} x^n q^{n^2}$ [114, 115]. In the current chapter the summation form is directly used because of its simplicity for practical use.

Using the free energy obtained from the partition function, through Eq. (2.16) we have the force-extension relationship:

$$\beta\langle f \rangle = \frac{\lambda\pi^2}{L^2}\frac{\sum_{n=1}^{\infty}(-1)^{(n+1)} n^2 e^{-\alpha\pi^2 n^2}}{\sum_{n=1}^{\infty}(-1)^n e^{-\alpha\pi^2 n^2} + 1/2} \tag{2.24}$$

The curves described by Eqs. (2.19) and (2.24) are generally different. Through rearrangement of Eq. (2.19), α is expressed in the Gibbs ensemble in terms of x as

$$\alpha(x) = D(x)/x^2 \tag{2.25}$$

Similarly, re-arrangement of Eq. (2.24) gives x expressed in terms of α in the Helmholtz ensemble:

$$x(\alpha) = \pi \left[\frac{\sum_{n=1}^{\infty} (-1)^{(n+1)} n^2 e^{-\alpha \pi^2 n^2}}{\sum_{n=1}^{\infty} (-1)^n e^{-\alpha \pi^2 n^2} + 1/2} \right]^{1/2} \tag{2.26}$$

Equation (2.25) is the Gibbs ensemble theory, while Eq. (2.26) is the Helmholtz ensemble theory. The results are shown in Figure 2.2, where we see the curves asymptote to each other in the thermodynamic limit but diverge elsewhere, in agreement with expectations from statistical mechanics.

The agreement in the thermodynamic limit can also be seen through direct comparison of Eqs. (2.19) and (2.24). For $\alpha \ll 1$, the series in Eq. (2.24) can be re-summed using the Euler-Maclaurin formula. Keeping leading order terms in Z/L one arrives at

$$\beta\langle f \rangle = \frac{1}{4\lambda(1 - Z/L)^2} \tag{2.27}$$

Similarly in the Gibbs ensemble, for $x \gg 1$, taking the leading order terms in an expansion of Eq. (2.19), one obtains the well-known Marko-Siggia result for a strongly stretched WLC [4, 6, 7]:

$$\frac{\langle Z \rangle}{L} = 1 - \frac{1}{(4\beta f \lambda)^{1/2}} \tag{2.28}$$

A small manipulation of the Helmholtz result gives

$$\frac{Z}{L} = 1 - \frac{1}{(4\beta \langle f \rangle \lambda)^{1/2}} \qquad \text{(Helmholtz)} \tag{2.29}$$

$$\frac{\langle Z \rangle}{L} = 1 - \frac{1}{(4\beta f \lambda)^{1/2}} \qquad \text{(Gibbs)} \tag{2.30}$$

where we see the two curves are identical under the exchanges $\langle f \rangle \to f$ and $Z \to \langle Z \rangle$. In summary: for the case of a strongly stretched WLC, it does not make a difference whether one chooses to perform the stretching experiment in the Gibbs or Helmholtz ensembles if the polymer is long relative to its persistence length, such that it resides in the thermodynamic limit. If the polymer length is on the order of the persistence length or smaller however, results of a stretching experiment will differ between the two ensembles. The definition of x and α, in lieu of the original f and Z, can place experimental data in a unified scaling plot, for any flexibility $L/2\lambda$.

2.4 Other Regions of the Parameter Space

Section 2.2 focused on a strongly stretched WLC in both the Gibbs and Helmholtz ensembles. This is shown in the parameter region on the right-hand side of Fig. 2.4. In this section we briefly discuss two other regions: rodlike polymers, and weakly stretched polymers. Both have been discussed previously in the literature, but are discussed here for completeness.

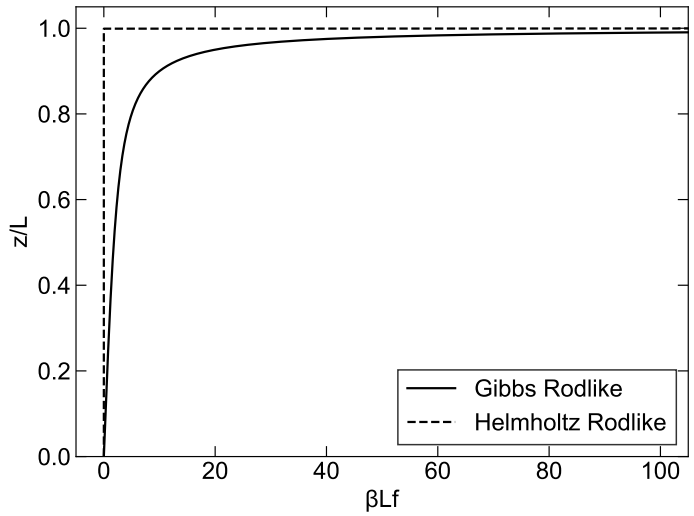


Figure 2.3: Force-extension behaviour for a rodlike polymer in the Gibbs (solid line) and the Helmholtz (dashed line) ensembles. The average force required to maintain a given extension in the Helmholtz ensemble is zero as the thermodynamic fluctuations needing to be suppressed are isotropic. This holds until the rod is fully stretched, at which an infinitely large force is required in the stretching direction in order to completely suppress any deviations.

We first consider rodlike molecules for any magnitude of stretching (the bottom region of Fig. 2.4) where analytic expressions can be obtained. When $L/2\lambda \ll 1$, the persistence length is much larger than the contour length of the polymer, and the WLC behaves as a rigid rod of length L. In this region, the tangent vector no longer varies with t, and instead points in a constant direction. This reduces the integral Eq. (2.9) to

$$Q(f) = \int \mathrm{d}\mathbf{u} \exp(\beta f L u_z) \tag{2.31}$$

The integral is readily evaluated and yields the partition function for a rodlike molecule in the Gibbs ensemble

$$Q(f) = \frac{4\pi}{\beta L f} \sinh(\beta L f) \tag{2.32}$$

which is used to obtain the known result for a stretched rodlike molecule

$$\langle Z\rangle/L = \coth(\beta f L) - 1/\beta f L \tag{2.33}$$

The procedure from Section 2.2 is then followed. Applying the mapping (2.15) to the partition function along with Eq. (2.13) gives

$$Q(Z) = 2\int_{-\infty}^{\infty} \mathrm{d}p\, e^{ipZ}\left(\frac{\sin(Lp)}{Lp}\right) \tag{2.34}$$

The inverse Fourier transform of the sinc function is the rectangular function, leading to the Helmholtz partition function,

$$Q(Z) = \frac{2\pi}{L}\Pi\left(\frac{Z}{2L}\right) = \begin{cases} 0, & \text{if } |Z/L| > 1 \\ 1/2, & \text{if } |Z/L| = 1 \\ 2\pi/L, & \text{if } |Z/L| < 1 \end{cases} \tag{2.35}$$

which matches with the rodlike $\alpha \gg 1$ limit of the strongly stretched Helmholtz partition function Eq. (2.24) that was determined earlier. Using Eq. (2.16) we have the extension-force relationship for the Helmholtz ensemble in the rodlike limit:

$$\beta\langle f\rangle = \frac{1}{\Pi(Z/2L)}\delta(|Z/L| - 1) \tag{2.36}$$

markedly different from the Gibbs result. The result of the derivation here agrees with a previous statement from Ref. [100]. The average force is zero in the partially extended regime, as fluctuations in the extension are uniform in all directions. On the other hand, the average force diverges at full extension, when an infinitely large applied force is needed to completely suppress any deviation from the stretching direction.

We also briefly examine the weakly stretched limit. Disagreement between the Gibbs and Helmholtz ensembles in the rodlike limit for any force or extension excludes the possibility that they might yield equivalent results over the full weakly stretched regime. Therefore, we then focus on the thermodynamic limit: the weakly stretched ($\tilde{f} \ll 1$), long-chain ($L/2\lambda \gg 1$) region of the parameter space (the upper-left region of Fig. 2.4).

A WLC under an external potential becomes indistinguishable from a continuous Gaussian chain when three conditions are satisfied: the WLC is flexible, $L/2\lambda \gg 1$, the system has weak variation, on a length scale of order $\sqrt{L\lambda}$ or larger, and the external potential is weak, on the order of $(\lambda/L)^0 = 1$ or smaller [32, 116]. For the weakly stretched WLC in free space in the thermodynamic limit, all three are satisfied. The problem is then simplified to that of a weakly stretched Gaussian chain, and we refer to this region as the Gaussian limit. This holds even for semiflexible-chain models of other types. It is now indisputable that in the weakly stretched limit, the Gaussian chain model in the two ensembles gives rise to the same force-extension relationship; a detailed discussion is carefully laid out in Ref. [93].

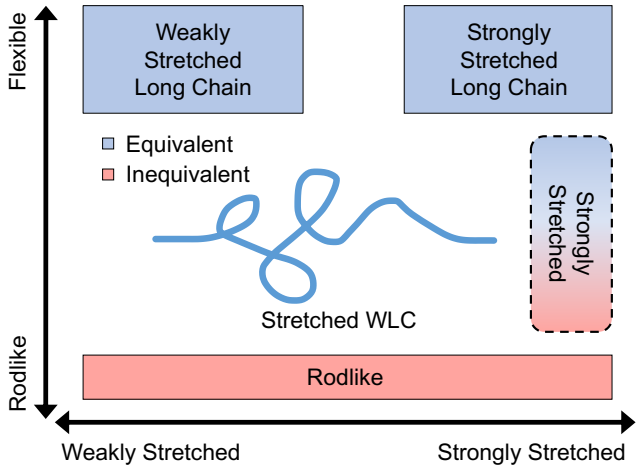


Figure 2.4: Regions of the stretched WLC parameter space. Blue indicates equivalence of the force-extension relations based on the Gibbs and Helmholtz ensembles, while red indicates no such equivalence. The behaviour in the strongly stretched (dashed box) region is the main contribution of this chapter. There, the force-extension relationships converge as the flexible (thermodynamic) limit is approached.

In the Gaussian limit, for the Helmholtz ensemble, it is well known that the average force is that of an entropic spring: $\beta\langle f\rangle = 3Z/R^2$, where $R^2 = 2L\lambda$ is the unperturbed mean square end-to-end distance. The Gibbs version is known to be $\langle Z\rangle = R^2\beta f/3$, readily obtained through the use of the fluctuation theorem in statistical mechanics [4]. The two are same under the exchange of averaged quantities, and so a WLC in the Gaussian limit displays equivalence between Eqs. (2.16) and (2.10). This can also be shown through use of Eq. (2.13), as outlined in Appendix A.5.

The combination of these results with the strongly stretched findings in Section 2.3, are illustrated in Fig. 2.4. Regardless of the applied force or separation, it is found that the force-extension curves are inequivalent for a rodlike $L/2\lambda \ll 1$ WLC, while the differences vanish as the thermodynamic $L/2\lambda \gg 1$ limit is approached. This is consistent with expectations from statistical mechanics, findings for the flexible FJC and GC models, as well as for other semi-flexible chain models similar to the WLC [93, 99, 117].

As a final remark, we note that while Z fixed under the Helmholtz ensemble is equivalent to $\langle Z\rangle$ determined from the fixed force Gibbs ensemble, this is not true for the absolute value of the extension $\langle|Z|\rangle$. For a random coil at zero force in the Gibbs ensemble $\langle Z\rangle = 0$, as the chain is isotropic. The average $\langle|Z|\rangle$, however, maintains a finite value. The ensembles are defined in terms of their generalized coordinates or forces: equivalence, as defined here, is the

agreement of these variables under one ensemble with their averages under the other. The inequivalence of other variables does not invalidate this, but is rather something that must be kept in mind when discussing derived quantities in either ensemble. This is a subtle point, but it has raised much discussion in the literature [44, 93–97, 118–121].

2.5 Conclusion

The WLC is a common model in polymer physics, known to accurately capture the physics of a stretched semiflexible polymer [7]. It describes polymer stiffness through the ratio of its length L to twice of its persistence length λ. We considered the stretching of a WLC with free ends in the Gibbs and Helmholtz ensembles. Using this model, here we provided an exact expression of the force-extension curve under the Helmholtz ensemble in the strongly stretched regime, for the first time. Together with the already known closed-form expression under the Gibbs ensemble, they form a complementary pair providing the basis for interpreting experimental data. The exact results here are in support of existing literature examining the wormlike-chain behaviour through simulation and other means [44, 73, 99–103, 122]. It also complements existing work for the WLC under different boundary conditions [73, 123].

Experimental verification of the results presented here could be done within the existing framework of single molecule manipulation. One common approach is to attach a bead to the polymer terminal end, and manipulate the entire chain with either magnetic or optical tweezers. Classic experiments have been performed on long semiflexible double-stranded DNA molecules (in the thermodynamic limit) under both the Gibbs and Helmholtz ensembles [31, 48]. These methods have also been applied to shorter DNA segments (outside the thermodynamic limit), as well as other short molecules [37, 40, 42, 50, 58, 124]. This suggests an experimental study of single molecule stretching outside the thermodynamic limit, in both ensembles, is feasible with current techniques.

Finally, what is the meaning of the "thermodynamic limit"? One limit that can be taken is to increase the number of chemical units used to link the polymer chain and decrease the energy penalty associated with the bond angles. A finite limit can be achieved to arrive at the concept of the persistence length (a finite quantity), as stated in the classic books [30, 125]. While the density of segments becomes infinite in this continuum limit, it is not a thermodynamic limit, as the range of correlations relative to the length remains constant. The thermodynamic limit for a polymer system is achieved when the number of uncorrelated segments is taken to infinity. For the WLC this is given by the ratio $L/2\lambda$, and therefore conceptually there is no surprise that equivalence only arises for $L/2\lambda \gg 1$. The merger of the dashed and solid curves in Fig. 2.2 (b) is a demonstration of that limit. Conversely, there is no surprise that the statement of ensemble equivalence fails for $L/2\lambda \lesssim 1$.

Chapter 3

Stretching Semiflexible Polymers: Gibbs Versus Helmholtz Ensembles

The previous chapter introduced the idea that the behaviour of a stretched semiflexible polymer depends on how it was stretched. More specifically, it was shown that the choice of statistical ensemble for the experiment will change the results in all cases except for the thermodynamic limit of an infinitely long polymer, where the behaviour under both ensembles converges. This chapter asks of how this prediction compares to the existing literature and results reported therein. Here, over 20 years worth of experiments from both ensembles, covering a range of polymer lengths, is compared with classical predictions and the ensemble dependent finite length wormlike chain. It is found that the new statistical mechanical analysis captures previously unexplained behaviour remarkably well. Potential regions of the parameter space that could benefit from further experimental investigation are also suggested. The contents of this chapter was published in Ref. [2] in 2025.

3.1 Introduction

The physical properties of single polymers and biopolymers are often probed using a stretching experiment, where the polymer's response to the forced separation of its ends is measured. The resulting behaviour follows from fundamental statistical physics [1, 73, 91, 99–101, 103, 126]. In the case where a force f is applied to the terminal ends, and the average extension is measured, the system corresponds to the Gibbs statistical ensemble. If instead the ends are held at a fixed separation Z, and the average restoring force measured, then the system corresponds to the Helmholtz ensemble. Active research in stretching polymers and biopolymers has resulted in the accumulation of more than thirty years

of experimental/computer simulation data [31, 33–68] , yet despite this, these data remain uninterpreted by such concepts. In light of recent analytical developments, we reveal here that for semiflexible polymers, an important class including polymers such as DNA, all data falls into two characteristic scaling curves.

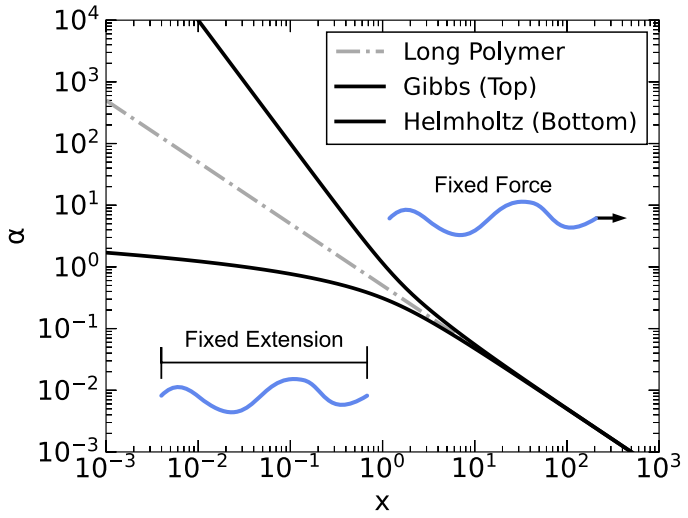


Figure 3.1: Theoretical behaviour for the two different types of polymer stretching experiment. The upper curve is the expected behaviour when the force is fixed and the fluctuating extension is measured by averaging [4–6]. The lower curve is when the extension is fixed and the fluctuating force is measured by averaging [1]. When the polymer is strongly stretched, only two scaled variables are relevant, regardless of polymer stiffness: the extension variation α defined in (3.1), and the reduced force x in (3.2). As the polymer length increases, they merge to the same asymptotic power law represented by the grey dash-dot line for a strongly stretched, infinitely long WLC [7].

An elementary statistical-physics model in polymer physics is the wormlike chain (WLC), which is particularly useful in studies of the conformational properties of biopolymers (see Appendix B.1). Two essential length scales appear, the total polymer contour length L and the persistence length λ, the orientation-orientation correlation length along the chain. The early experimental data for stretched semiflexible polymers focused on long DNA segments ($L/\lambda \gg 1$), which follow the asymptotic approximation of the WLC very well [7, 31, 33]. However, modern techniques enable the stretching of polymers short enough, where a large body of literature exists covering the small-L/λ region from the perspective of both experiments and computer simulations and shows that the $L/\lambda \gg 1$ approximation is no longer valid [31, 33–47] .

When the force f is fixed, the general problem of finding a solution of the strongly stretched WLC can be tackled by mapping the Green's function of a

quantum particle in a simple harmonic field (the Feynman integral [113]) to the WLC system, allowing the calculation of the partition function for finite $L/2\lambda$. This was first carried out by Odijk in Ref. [127], and stated more directly later in Ref. [5], which provided exact coefficients to the general form in Ref. [128]. The exact form has been verified in Ref. [6], and by us in Ref. [4] recently. When the extension Z is fixed, to obtain an analytical expression, a Fourier transform of the Gibbs ensemble theory evaluated at an imaginary force must be performed. For the current problem, this was derived for the first time in Ref. [1].

Two scaled variables emerge from the theoretical development, as explained in Appendix B.2. One measures the deviation of the extension Z from the total length L in a reduced form,

$$\alpha = (1 - Z/L)\lambda/L \tag{3.1}$$

and the other is the reduced external force

$$x = L(\beta f/\lambda)^{1/2}. \tag{3.2}$$

They are rooted in the quadratic form between the neighbouring bending angles used in the WLC model and the quadratic dependence of the polymer orientational angle from the preferred stretching direction [7, 127]. Both Refs. [104] and [1] explain the origin of the scaling and the two scaled variables are used here. Strictly speaking, for the fixed-f curve, $\langle Z \rangle$ should be used in (3.1), and for the fixed-Z curves, $\langle f \rangle$ in (3.2). In the first case, the analytic expression for

$$\alpha = G(x) = \frac{1}{2x^2}\left[1 + x\coth(x)\right] \tag{3.3}$$

which is plotted as the upper solid black curve in Fig. 3.1, and in the second case,

$$x = H(\alpha) = \pi\left[\frac{\sum_{n=1}^{\infty}(-1)^{(n+1)}n^2 e^{-\alpha\pi^2 n^2}}{\sum_{n=1}^{\infty}(-1)^n e^{-\alpha\pi^2 n^2} + 1/2}\right]^{1/2} \tag{3.4}$$

which is plotted as the lower solid black curve. They both approach the Marko-Siggia asymptote

$$\alpha = (2x)^{-1} \tag{3.5}$$

in a power-law form, plotted as the dashed line [129].

3.2 Results

3.2.1 Review of Experimental Results and Computer Simulations

The first studies on the deformation of semiflexible polymers were done firmly within this limit. Smith et al. used a combination of magnetic tweezers and

constant fluid flow to provide low noise data for the force-extension of 32.7 μm dsDNA (dsDNA has a persistence length of around 50 nm), which was analyzed by Marko and Siggia and used to demonstrate the validity of the WLC model [7, 31]. In a similar vein, Perkins et al. used flow to study the deformation and hydrodynamics of single dsDNA molecules, with contour lengths also on the order of 10s of μm [33]. Around the same time, Baumann et al. were investigating similar length dsDNA segments under different ionic strengths (its charged backbone means the salt concentration will affect the apparent persistence length) [34]. Ortiz and Hadziioannou investigated single molecule stretching of Poly(methacrylic acid) (PMAA) in 1999 using atomic force microscopy (AFM). They measured the force as a function of the polymer end-to-end separation, instead of using a constant force as was done in the flow experiments. This is an important distinction. However, although the PMAA used was short compared to dsDNA (120nm for PMAA), it is so flexible that the behaviour was sufficiently captured by both the WLC and freely-jointed chain models [35]. More modern microfluidics has been used to good effect by Ref. [41] in the stretching of long dsDNA [41]. Li et al. used MC to simulate long polymers, with a focus on excluded volume effects [46].

As techniques improved, shorter semiflexible segments were measured. Baumann et al. again investigated dsDNA but with shorter segments on the nanometre scale, measuring a 1324 nm molecule. F-actin (a biopolymer found in muscles) was measured by Liu and Pollack using microfabricated cantilevers (MFC) in a process similar to an AFM measurement [37]. Although the filaments were long, from several micrometers to 10s of micrometers, its persistence length also being on the order of μm means the relative length $L/2\lambda$ of the polymers used in the measurements was shorter than the dsDNA experiments done previously. Rosa et al. as well as Cifra and Bleha both used Monte Carlo (MC) simulations to model very short WLCs. Cifra and Bleha used MC to simulate the extension of a WLC by fixing its length, placing their simulations in the Helmholtz ensemble [39]. The relative length of the simulated polymers ranged from 10 to 0.7, leading to noticeable finite length effects. Rosa et al. was motivated by the work of [36], and performed MC simulations with a fixed force [38]. With relative lengths from 0.625 to 1.25 the polymers were also quite short, and being conducted in the Gibbs ensemble, provide a direct contrast of behaviour with the results in Ref. [39]. Similarly, Manca et al. used MC to investigate both fixed extension and fixed force WLC behaviour, with $L/2\lambda$ ranging from 2.5 to 0.2, showing strong finite length and ensemble dependent effects [44]. Optical trapping was employed by Seol et al. with the specific goal of investigating moderate lengths of dsDNA where finite length effects could be observed, and where traditional analysis with the long chain WLC broke down. They explain the behaviour by using the WLC model with an effective persistence length calibrated to the polymer contour length [40]. Chen et al. used a method with optical tweezers that enabled stretching of short polymers segments with a constant force without electronic feedback, which they used to probe dsDNA segments ranging from 84 to 441 nm, quite short relative to its persistence length of 50 nm [42, 43]. Molecular dynamics has been employed by

Cortini et al. mainly to model dsDNA condensation, but with force-extension simulated as well [45]. Kurzthaler used pseudo-Brownian dynamics to back up analytic theory on compression of short molecules. The free end and constant force compression is equivalent to stretching, and provides good insight to the Gibbs ensemble behaviour [47].

3.2.2 Ensemble Dependent Analysis

In our analysis of these works, each parameter (L, f, λ, Z) was taken directly from the studies themselves. For the data from Refs. [40, 42, 43] which fitted an effective persistence length to capture finite length effects, the long chain (regular) persistence length of $\lambda = 51.51$ determined in Ref. [40] was used for plotting the data instead. A universal temperature of 298K was assumed unless otherwise stated in the original work, giving a value of $k_bT = 4.114$ pN $\cdot$ nm. The data in Ref. [33] is plotted against flow velocity. To compare against the WLC model, we apply their empirical constant shift of 122, as was done in the original work. In the MC simulations performed by Rosa et al., a shift in behaviour can occur for strongly stretched chains, especially at higher temperature [38]. The reasons are explained in detail in their publication, and arise from the finite nature of the chain segments in their model, contrasted against the continuum version of the WLC employed here. As a result we only used $k_bT = 1$ data from their study.

Data was taken at the earliest point at which it became distinguishable from noise or other data. In all cases, data was included up to the longest extension measured, which often displayed extension of the polymer backbone in an overstretching regime. Although overstretching beyond the contour length is not considered here, we kept this data displayed regardless. While Fig. 3.2 contains the full set of extracted data, the scaled variables x and α only apply to strongly-stretched polymers, so only data where $Z/L \geq 0.5$ is shown in Fig. 3.3.

Table 3.1 gives a summary of each study. The authors, experimental system, single molecule studied, and representative symbol in the figures are listed. Figure 3.2 displays the data from these references according to their ensemble, and whether or not they display finite length behaviour. Short semifleixlble polymers are shown in for fixed-f in (a) and for fixed-Z in (c). To better distinguish the short polymer data, long polymer data is universally given a circular marker, and plotted separately in (b). There they are plotted in unscaled Z/L -vs-f style plot, commonly used. The data are coloured by their relative length $L/2\lambda$, from high ratio (red) to low ratio (yellow). Together in the background, two curves are presented: the dashed black curve representing the Marko-Siggia power law, (3.5), and the grey curve the Marko-Siggia interpolation formula that takes low-f behaviour into consideration: $\beta f\lambda = Z/L + 4(1 - Z/L)^{2^{-1}} - 1/4$. Most red data points [Fig. 3.2 (b)] fall into the Marko-Siggia power law, as expected for long polymers. Noticeably, the yellow data points, representing the shorter polymers [Fig 3.2 (a) and (c)], show significant deviations from the dashed curves. Most data in Fig. 3.2(a) lies below the dashed line, and most data in Fig. 3.2(c) above. In terms of force, they could be a few orders of magnitude

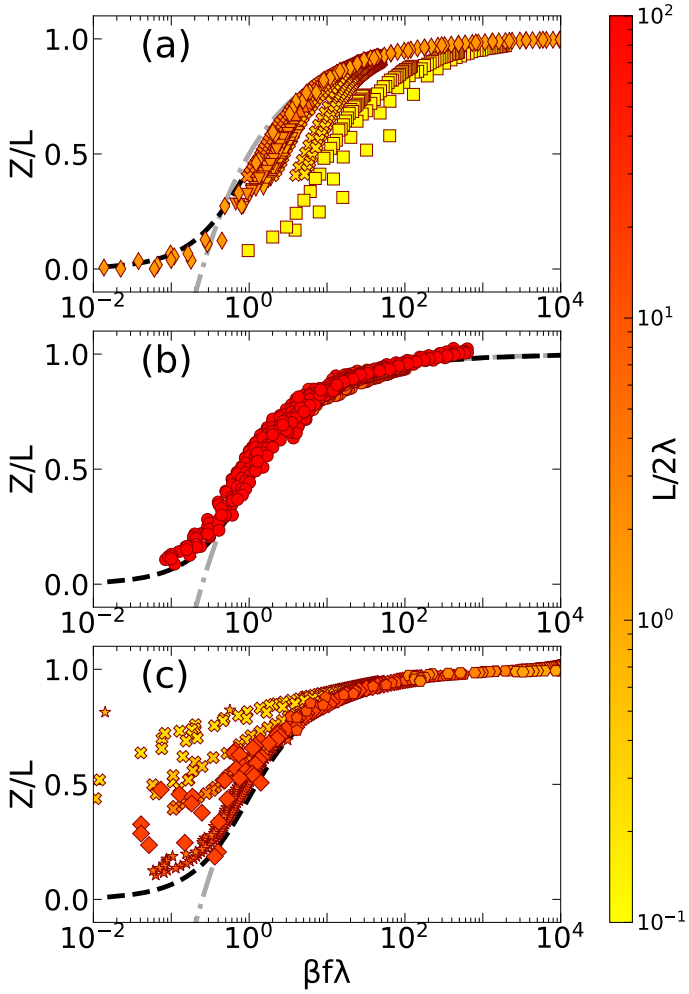


Figure 3.2: Collection of force-extension data from different experiments and computer simulations of semiflexible polymers in the literature. Table 3.1 lists the details for each study, including the molecule used, experimental setup, and corresponding symbols in the plots. Each data point is coloured based on its relative length, given by the ratio $L/2\lambda$, as indicated by the sidebar. (a) contains data for lower $L/2\lambda$, where the force was fixed, and the average extension measured. This is common in simulations, and some special experimental setups. (b) contains data for high $L/2\lambda$, such as the long dsDNA data used to validate the WLC model in Ref. [7]. A wide mix of techniques is employed with this data. (c) contains data for lower $L/2\lambda$ as well, but for cases where the extension was fixed, and the force was measured. This is typical for optical tweezers and AFM, or special simulations. In the background of each is the power law in (3.5) (grey dash-dot line), and the Marko-Siggia interpolation formula commonly used to fit experimental data (black dashed line) [7].

Table 3.1: Summary of the data used from experiments and computer simulations. The first column lists the first authors only. The method of study is labelled as Flow (applied fluid flow), OT (optical tweezers), MT (magnetic tweezers), AFM (atomic force microscopy), MFC (microfabricated cantilevers), MC (Monte Carlo simulation), PBD (pseudo-Brownian dynamics), or MD (molecular dynamics). The data has been categorized by fixed-f or fixed-Z and by symbols used for plotting in Figs. 3.2 and 3.3. Data with circles indicate high-$L/2\lambda$ data, plotted as one set in Fig. 3.2 (b) and Fig. 3.3 (b).

Study	Method	Molecule	Fixed	Symbol
Smith [31]	Flow + MT	dsDNA	f	$\circ$
Perkins [33]	Flow	dsDNA	f	$\circ$
Baumann [34]	OT	dsDNA	Z	$\circ$
Ortiz [35]	AFM	PMAA	Z	$\circ$
Baumann [36]	OT	dsDNA	Z	$\diamond$
Liu [37]	MFC	F-Actin	Z	$\hexagon$
Rosa [38]	MC	Generic	f	$\lozenge$
Cifra [39]	MC	Generic	Z	$\star$
Seol [40]	OT	dsDNA	Z	$\circ$
Wang [41]	Flow	dsDNA	f	$\circ$
Chen [42]	OT	dsDNA	f	$\triangle$
Chen [43]	OT	dsDNA	f	$\triangledown$
Manca [44]	MC	Generic	f or Z	$\times$
Cortini [45]	MD	Generic	Z	$\pentagon$
Li [46]	MC	Generic	f	$\circ$
Kurzthaler [47]	PBD	Generic	f	$\square$

different. It is clear that the deviations are due to finite length effects.

These deviations are accounted for by considering the full scaling functions, G and H, in (3.3) and (3.4). Using the scaled parameters, x and α, reduces the collection of length-dependent curves down to two universal curves. The result of this exercise is shown in Fig. 3.3. The scaled fixed-f data is plotted in the top graph (a), along with the scaled Gibbs ensemble curve, $G(x)$. Bottom (c) contains the fixed-Z data, along with the Helmholtz curve $G(\alpha)$. For both cases, we find the curves do an excellent job of capturing the data presented in Fig. 3.2. Here, the bottom right of each (large x small α) is the long-chain region, where both curves become identical and follow a simple power law. The long polymer data, given by the red circular markers in (b), is exclusively situated here, indicating it is well captured by the Marko-Siggia asymptote. The shorter yellow data occupies the finite length region in the top left (large α small x), and follows no such simple power law. There are a few exceptions in the behaviour, notably the diamonds deviating from the asymptote in (a), the hexagons curving down in (c), and the stars, curving to the left below the curve in (c). The diamonds' shift is due to discrete chain segments in Ref. [38], while the bending of the hexagon data from Ref. [37] is due to overstretching.

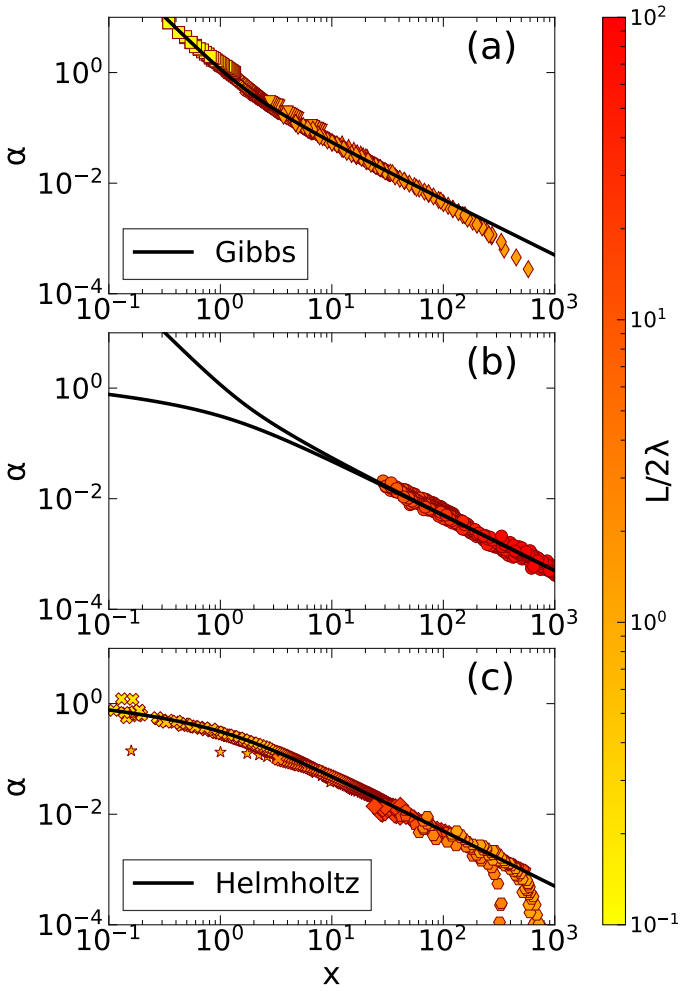


Figure 3.3: The same data as Fig. 3.2 (a)-(c), re-plotted using the reduced variables α and x. The same colour scheme is employed. The solid lines are from the theoretical predictions, (3.3) and (3.4). Low- to mid-$L/2\lambda$ polymers follow different scaling behaviour, depending on how the experiment was conducted. This ensemble dependence is displayed in (a) and (c). High-$L/2\lambda$ experiments in (b) reside only along the asymptotic limit described by (3.5).

The curving of the stars from Ref. [39] could be due to residual low force data or numerical effects from the MC simulations. The broad agreement of the data shows that the ensemble dependent effects explain the behaviour that was previously taken into account using empirical, size dependent persistence lengths [40, 43].

3.3 Summary

In summary, we showed through analysis of a range of experiments and computer simulations, that previously unexplained deviations from WLC behaviour arise from standard statistical mechanics. By using two scaling parameters, x and α, two universal curves emerge for the force-extension behaviour under the Gibbs and Helmholtz ensembles. When polymer stretching data is presented in this way, a universal collapse onto one of the two curves is seen, depending on if the experiment was conducted with fixed force f, or fixed extension Z. An aspect to highlight is the differences between the red data, having a large relative length $L/2\lambda$ and residing on the well-known WLC asymptote, and the yellow data, which lies in the short polymer, small $L/2\lambda$ region.

While the computer-simulation works probe deep into the short chain region, further investigation with real polymers systems to the same degree would be interesting. Already, Refs. [42, 43] probe within this region for the constant force Gibbs ensemble with a dsDNA segment around 80 nm in length. The persistent nature and low extensibility of dsDNA make it an obvious candidate for further investigations on even shorter segments. Such additional experimental work on near rodlike polymer systems would further validate the physical picture presented here.

The concerns regarding different ensemble effects for Gaussian chains in the weakly stretched regime have been discussed previously [96, 97, 121]. The study presented here focuses on the strongly stretched regime of a wormlike chain, which differs from that problem.

Chapter 4

Helical Wrapping of Cylindrical Tubes by Wormlike-Chain Polymers

When a semiflexible polymer wraps around a solid cylinder with a radius comparable to the persistence length, it displays a helical conformation. What is the confinement free energy of this particular conformation and what is the pitch, the basic geometric measure of the helix, as a function of the persistence length to cylinder radius ratio? Here this is explored on the basis of a standard wormlike-chain model, by using the Green's function approach in statistical physics and numerical computation of the resulting differential equation. In the asymptotic limits of small and large cylinder radius, a power-law scaling relationship is also established from a scaling argument and from the exact solution to the theoretical model. The results from the calculation agree well with experimental data, computer-simulation data, and a previous theoretical estimate. This chapter sheds light on recent developments in the area of single-walled carbon nanotubes wrapped by various types of long polymers. An initial formulation of this problem was presented in Ref. [130]. The problem was then re-analyzed completely, with the resulting work published in Ref. [3] in 2023. It is this published work that forms the basis of this chapter.

4.1 Introduction

The helical wrapping of polymers on nanotubes has been recognized as an important problem in nanotechnology. In particular, the wrapping of single-walled carbon nanotubes (SWNTs) has received much experimental and theoretical attention, owing to physicochemical properties that can be exploited for nanotube solvation and separation, with minimal modification to the underlying electronic properties [76, 78–82]. For example, polymer wrapping has proved particularly

useful for the purification of SWNTs from commercial samples, as it allows the separation of semiconducting nanotubes with specific diameters [74, 131]. Polymer wrapping has also shown potential to improve certain practical applications of SWNTs, for example, developing sensitive CO_2 detectors [132], as well as serving as a useful material for solar cells [133].

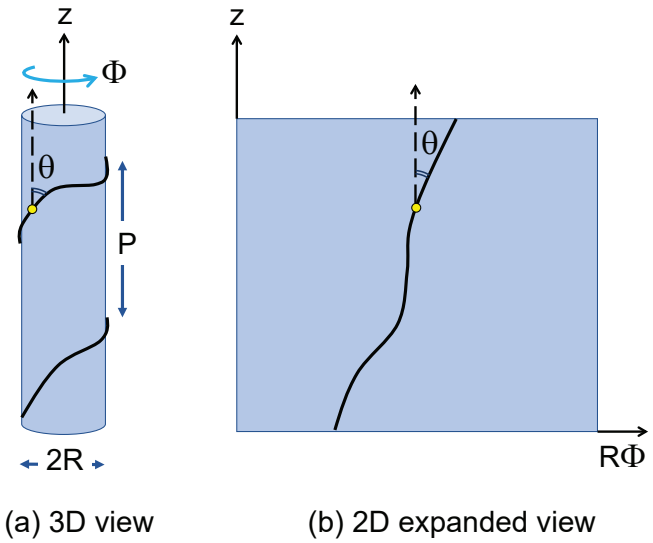


Figure 4.1: Schematic of a WLC wrapped on the surface of a nanotube in (a) 3D view, and (b) 2D expanded view. A nanotube having a smaller radius in comparison with the persistence length has a higher degree of confinement, yielding in a larger pitch P. The general behaviour of P depends on the polymer length, stiffness, and the nanotube radius. In the expanded view, the WLC can be thought of moving on a flat surface spanned by the spatial variables $[R, \Phi, z]$, subject to an effective potential $U_{\text{eff}}(\theta)$, as a function of the bond direction θ. The effective orientational ordering potential $U_{\text{eff}}(\theta)$ is caused by the cylinder's curvature.

To form a complete understanding of a polymer wrapped SWNT, two related but separable problems need to be examined. The first is the adsorption process, describing the physics between a free, unconfined state, and an adsorbed state where the polymer partially wraps around the nanotube. Especially for single-stranded DNA (ssDNA), this has been studied extensively both experimentally and theoretically [15, 83, 84, 134–136]. Here we focus on the second problem: what conformation does the polymer spontaneously adopt after it has been adsorbed onto the nanotube surface? Although the adsorbed polymer can form a hairpin-like structure, the lowest-free-energy conformation is known to be a helix [83, 84]. Helically wrapped SWNTs have been observed experimentally,

as well as by molecular dynamics (MD) and Monte Carlo (MC) simulations for several polymers, with ssDNA being a prominent choice [8–17].

In this chapter, we theoretically study the conformational properties of a long semi-flexible polymer of persistence length λ confined on the surface of an infinitely long cylinder of radius R, over a large range of the ratio λ/R, representing the relative size of the cylinder. Both the scaling analysis commonly used in polymer physics, and the more rigorous Green's function approach are employed, with numerical computation as an additional aid. The chapter is organized in such a way that the main results from our calculation are summarized in Fig. 4.2 first, before the presentation of the theoretical details. Experimental and molecular dynamics data for ssDNA, Chitosan, Alginic Acid, PNES, and PPES [8–17] is overlaid on the figure, and compares to our theoretical curve favourably.

As described in Section 4.2, the essential relations between the helix pitch P (see Fig. 4.1) (as well as the confinement free energy ΔG) and λ/R can be established in a power law. This can already be used to capture some large-λ/R data in the literature. A more careful study is presented in Section 4.3 for other parameter regions of λ/R, on the basis of solving a standard wormlike-chain (WLC) model by accounting for the cylinder's curvature through an effective potential (see Section 4.3.2). The theoretical approach of solving for the Green's function is used, which enables the construction of the distribution function of the on-surface angle θ (see Fig. 4.1) that a polymer segment makes from the tube axis direction. Numerical solutions of the Green's function are obtained. In particular, the density distribution function of P is obtained, which allows us to calculate the most probable value of P.

4.2 Scaling and Comparison with Experiment

Before indulging in the mathematical details, we first present a simplified physical picture where the WLC is confined in a tube having a small-R/λ ratio. The scaling analysis gives rise to power-law relations, which can be verified through a more rigorous treatment in Sections 4.3.3 and 4.3.7.

The conformational properties of a WLC are dominated by the bending energy of the chain, measured by the quadratic change of the tangential unit vector along the chain with the energy penalty proportional to the persistence length λ. For the monomer coloured yellow in Fig. 4.1, the tangential vector change contains two contributions: a rotational change of θ about the monomer, and the bending of the curve along the chain path due to the cylindrical confinement. These are two orthogonal variations and hence can be decoupled. The latter amounts to an energy penalty [137],

$$U_{\text{eff}} = \lambda L \kappa^2/2 \tag{4.1}$$

where $\kappa^2 = R^{-2}\sin^4\theta$ is the square curvature of the cylinder surface along the direction specified by θ. A polymer having a long contour length L is assumed, hence on average a factor L is included in the above. This three-dimensional

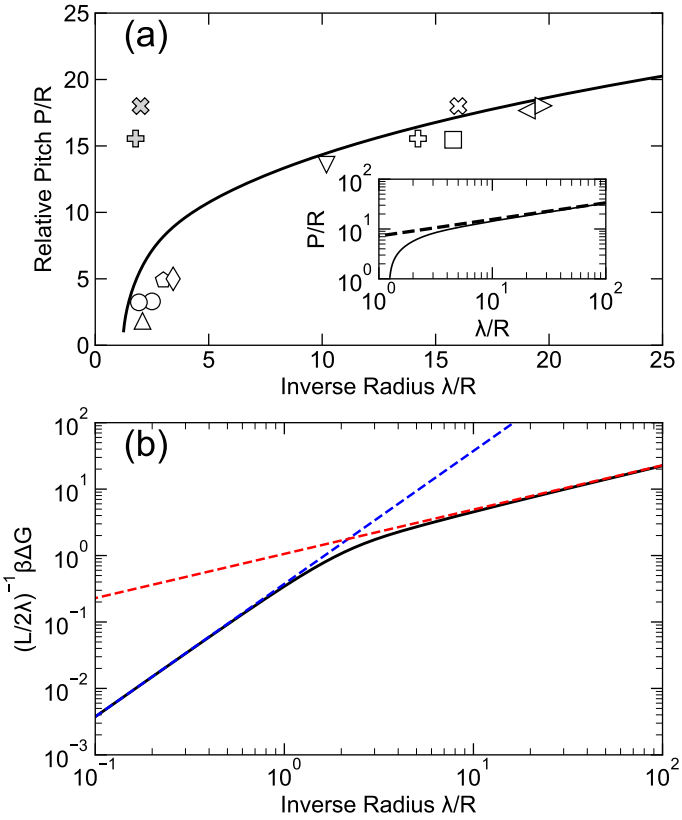


Figure 4.2: (a) Helix pitch ratio P/R, and (b) reduced change in Gibbs free energy, for a polymer wrapped as a helix on a cylindrical surface. The numerical solution to the full WLC model is given by the solid black line in both figures. Data adopted from 10 different experimental and computer simulation studies in the literature is displayed by symbols. The data points are sourced as follows: The upwards pointing triangle marker is from [8], the downwards pointing triangle is from [9], the circles are from [10], the left pointing triangle is from [11], the right pointing triangle is from [12], the square is from [13], the pentagon is from [14], and the diamond is from [15]. The grey cross and plus in the top left, are data from Zheng et al. [16] and Campbell et al. [17] respectively, while the white plus and cross to the right are the same data points, shifted to approximate the persistence length of the "charge strip" 2x ssDNA structure suggested by Zheng et al. [16, 17]. Details are discussed in the text. The persistence lengths for each of the polymers were estimated based on the experimental conditions and existing literature [18–25]. The inset shows the power-law behaviour (dashed line) of the solution (solid line) for large λ/R as presented in Section 4.3.7. (b) is the difference between the reduced Gibbs free energy of the cylinder surface-confined WLC, and a 2D free-space WLC. The blue and red dashed lines are the respective small λ/R and large λ/R scaling laws, as presented in Sections 4.3.3 and 4.3.5.

(3D) view can be mapped into a two-dimensional (2D) view of a WLC on a flat surface (see Fig. 4.1(b)), where the bending energy is solely described by the change of θ and the curvature effects are captured by an effective potential energy given above. Then the problem becomes a 2D WLC in an orientationally ordered field $U_{\text{eff}}(\theta)$.

Taking this mapping, a number of scaling laws can then be immediately drawn for the case of strong confinement (large λ/R) of a long WLC (large L/λ). In a seminal work, Odijk deduced the relations between the mean magnitude of the angle $\langle|\theta|\rangle$ as well as the confinement free energy per segment and the field strength [127, 138]. In our language, for $\lambda \gg R$, they can be expressed by

$$\langle|\theta|\rangle \sim (\lambda/R)^{-1/3} \quad (\text{when } |\theta| \ll 1) \tag{4.2}$$

$$(L/2\lambda)^{-1}\beta\Delta G \sim (\lambda/R)^{2/3} \tag{4.3}$$

where the characteristic exponents 1/3 and 2/3 are due to a clever scaling argument [127, 138]. One then has an estimate

$$\frac{P}{R} = \frac{2\pi}{\tan(|\theta|)} \approx \frac{2\pi}{|\theta|} \sim \left(\frac{\lambda}{R}\right)^{1/3} \quad (\text{for } \lambda \gg R), \tag{4.4}$$

for the reduced pitch.

These power laws are justified below in a full Green's-function treatment based on the standard WLC model. Taking the ground-state-dominance (GSD) approach (valid for large L/λ and a small-θ asymptote, we show

$$(L/2\lambda)^{-1}\,\beta\Delta G = a\,(\lambda/R)^{2/3} \quad (\text{for } \lambda \gg R) \tag{4.5}$$

$$P/R = 2\pi b\,(\lambda/R)^{1/3} \quad (\text{for } \lambda \gg R) \tag{4.6}$$

where

$$a = 1.060 \pm 0.001 \tag{4.7}$$

$$b = 1.150 \pm 0.001. \tag{4.8}$$

The reduced pitch in (4.6) is the most probable value, after the entire distribution density function of P is obtained, in closer match to experimental procedures. The dashed lines in the double-logarithmic plots in Fig. 4.2 represent this asymptotic behaviour.

The opposite to the strong-confinement limit is the small λ/R, weak-confinement limit. Here the free energy is expected to follow the usual scaling $\beta\Delta G \sim 2L\lambda/R^2$ where $2L\lambda$ is the mean square end-to-end distance. More precisely,

$$(L/2\lambda)^{-1}\,\beta\Delta G = c\,(\lambda/R)^2 \quad (\text{for } \lambda \ll R) \tag{4.9}$$

A perturbation theory presented in Section 4.3.5 gives the exact value for the coefficient

$$c = 3/8 \tag{4.10}$$

analytically. This is presented in Fig. 4.2(b) by the dashed line with slope 2.

Overall, one then expects a crossover from the weak to strong behaviour of these physical quantities, in terms of changing the ratio λ/R. Staying within the GSD approach, we have numerically solved the resulting differential equations to obtain the theoretical results, presented as the solid curves in Fig. 4.2.

A direct comparison can be made between the theoretical results obtained in this chapter and other observations in the literature. The most probable helix pitch as a function of λ/R is plotted in Fig. 4.2(a), alongside experimental and computer simulation data for ssDNA, Chitosan, Alginic Acid, PNES, and PPES, taken from 10 different studies [8–17]. The data are presented and discussed in detail in Appendix C. Good agreement is seen with the data over the full range, save for two exceptions in the top left (grey cross and plus). These points correspond to atomic force microscopy (AFM) measurements by Zheng et al., and Campbell et al. [16, 17]. Both use the same ssDNA sequence, $(GT)_{30}$, and use SWNTs of similar radii. Zheng et al. posited that the repeating structure allowed two ssDNA segments to interact and form a "charge strip"; a single long polymer with both segments linked through hydrogen bonding [16]. The WLC theory predicts for this ratio of P/R, a persistence length $\approx 8\times$ that of the separated ssDNA molecules used in the experiments, which is plotted as the white cross and plus in Fig. 4.2. This 8-fold increase is consistent with the formation of an ssDNA dimer on the surface of the SWNT, which should exhibit a much higher persistence length than individual ssDNA molecules. Hence, our theory qualitatively supports the existence of such a structure, although the existence of this "charge strip" has been disputed by other studies [135].

4.3 Theory

4.3.1 WLC Model

The continuum version of the wormlike-chain (WLC) model describes the statistics of a semiflexible polymer chain of length L. The chain is represented by a continuous space curve, labelled by a path parameter t, which has a value $t = 0$ at one end and $t = 1$ at another. The polymer configuration is specified by the coordinates of the monomer located at t, through the vector $\mathbf{r}(t)$. The unit tangent vector of the space curve at t is then $\mathbf{u}(t) = L^{-1}\mathrm{d}\mathbf{r}(t)/\mathrm{d}t$.

The statistical probability of observing the configuration specified by $\mathbf{r}(t)$ is given by

$$P \propto \exp\left(-\beta H\right), \tag{4.11}$$

where the reduced Hamiltonian is [87, 139]

$$\beta H = \int_0^1 \mathrm{d}t \left[\frac{\lambda}{2L}\left|\frac{\mathrm{d}\mathbf{u}(t)}{\mathrm{d}t}\right|^2 + U[\mathbf{r}(t), \mathbf{u}(t)]\right]. \tag{4.12}$$

The first term in the integrand describes the energy cost for bending the polymer, while the second is the contribution from a generic external potential field.

The persistence length λ is the tangent vector correlation length along the backbone of the polymer, a measure of its stiffness, for a WLC in a 3D free-space [87].

In a WLC problem, the probability density function $\rho(\mathbf{r}, \mathbf{u})$, is a key physical quantity that can be used to understand the spatial and orientational ordering of the polymer, for spatial location $\mathbf{r}$ and the polymer's orientational direction $\mathbf{u}$. The calculation of the free energy G and $\rho(\mathbf{r}, \mathbf{u})$ can be performed through use of the reduced Green's function (the propagator) $q(\mathbf{r}, \mathbf{u}; t)$, which describes the statistical probability of finding a polymer of segment length t, with its t terminal located at $\mathbf{r}$ and pointing at $\mathbf{u}$. Within such a formalism [32],

$$\beta G = -\ln Q \tag{4.13}$$

and

$$\rho = Q^{-1} \int_0^1 \mathrm{d}t \, q(\mathbf{r}, \mathbf{u}; t) q(\mathbf{r}, -\mathbf{u}; 1-t) \tag{4.14}$$

where

$$Q = \int \mathrm{d}\mathbf{r}\mathrm{d}\mathbf{u} q(\mathbf{r}, \mathbf{u}; t = 1) \tag{4.15}$$

is the partition function. When the WLC is embedded on a curved surface, $q(\mathbf{r}, \mathbf{u}; t)$ satisfies [137]

$$\frac{\partial}{\partial t} q(\mathbf{r}, \mathbf{u}, t) = \Big\{ -U(\mathbf{r}, \mathbf{u}) - \frac{L\lambda}{2} \kappa^2(\mathbf{r}, \mathbf{u}) - L\mathbf{u} \cdot \nabla_{\mathbf{r}} + \frac{L}{2\lambda} \nabla_{\mathbf{u}}^2 + L\big[(\mathbf{u} \cdot \nabla_{\mathbf{r}})\mathbf{u}\big] \cdot \nabla_{\mathbf{u}} \Big\} q(\mathbf{r}, \mathbf{u}, t) \tag{4.16}$$

with an initial condition $q(\mathbf{r}, \mathbf{u}, t = 0) = 1$. In comparison with the same equation for a flat-space polymer, the additional κ^2 curvature term plays the role of a bending energy penalty, pushing the polymer to follow the curvature κ of the surface [137]. Such a term has no effects on a spherical surface where the curvature is constant, and drives the WLC to form a specific orientational order when it is forced onto a toroidal surface [140], or cylindrical surface (as described here).

4.3.2 Cylindrical Surface

On a cylinder of radius R, the vector $\mathbf{r}$ for a spatial point on the surface is specified by variables $[z, \Phi]$, in terms of cylindrical coordinates (see Fig. 4.1(a)). At a given $\mathbf{r}$, the polymer's orientation, $\mathbf{u}$, can be specified by the polar angle θ, measured from the vertical direction along the cylinder's axis. Using this parameterization, one can show

$$\kappa = R^{-1} \sin^2 \theta \tag{4.17}$$

which is independent of $\mathbf{r}$. The range of θ is $[0, 2\pi]$.

Here, for a problem where there is no external field, $U(\mathbf{r}, \mathbf{u}) = 0$, and we are not concerned about the positional dependence of the probability distribution. The dependence on $(\mathbf{r}, \mathbf{u})$ is simplified to a dependence on θ only. The differential equation (4.16) can then be rewritten as

$$\frac{\partial}{\partial t} q(\theta, t) = \left[\frac{L}{2\lambda} \frac{\partial^2}{\partial \theta^2} - \frac{L}{2\lambda} \left(\frac{\lambda}{R} \right)^2 \sin^4 \theta \right] q(\theta, t). \tag{4.18}$$

In the above, the net effects of the curvature term have been represented by the effective potential energy,

$$U_{\text{eff}}(\theta) = \frac{L\lambda}{2} \kappa^2 = \frac{L}{2\lambda} \left(\frac{\lambda}{R} \right)^2 \sin^4 \theta, \tag{4.19}$$

which plays the role of a directionally ordering field. In a 2D expended view, illustrated in Fig. 4.1(b), the basic structure of the theory is equivalent to a WLC in a flat, 2D space, under an orientational field preferring the z-direction. The properties are similar to some well-established physical pictures known previously [7, 127]. The monomer-averaged, orientational probability distribution density, for example, can be expressed in a simple form,

$$\rho(\theta) = B^{-1} \int_0^1 \mathrm{d}t \, q(\theta, t) q(\theta, 1 - t) \tag{4.20}$$

where B is a normalization constant. The free energy of confinement is obtained from,

$$\beta \Delta G = -\ln Q - \beta G_0 \tag{4.21}$$

with

$$Q = \int_0^{2\pi} \mathrm{d}\theta \, q(\theta, t = 1), \tag{4.22}$$

where the free energy G_0 of a unconfined WLC in 2D (ie, that of $U_{\text{eff}} = 0$)) is taken as the reference.

4.3.3 Ground-State-Dominance Solution

In a typical experimental system, the polymer length L is much greater than the persistence length λ. This has prompted us to take the $L/\lambda \gg 1$ limit, known as the ground-state-dominance (GSD) theory. In this asymptotic limit, the propagator takes the form,

$$q(\theta, t) = \exp[-\mu (L/2\lambda) t] \, \psi(\theta). \tag{4.23}$$

The problem of solving the differential equation in (4.18) then becomes a problem of finding the ground-state eigenvalue μ and eigenfunction $\psi(\theta)$ of the equation

$$-\mu \psi(\theta) = \left[\frac{\partial^2}{\partial \theta^2} - \left(\frac{\lambda}{R} \right)^2 \sin^4 \theta \right] \psi(\theta). \tag{4.24}$$

The reduced free energy difference, is then determined from μ only,

$$\beta(L/2\lambda)^{-1}\Delta G = \mu + \mathcal{O}(L/2\lambda)^{-1}, \tag{4.25}$$

which is exact in the $L/2\lambda \gg 1$ limit. The solution presented in this chapter is based on the GSD theory, which contains only one system parameter λ/R, showing up in Eq. (4.24). The eigenfunction $\psi(\theta)$ also gives the (unnormalized) distribution function, $\rho(\theta) \sim [\psi(\theta)]^2$.

4.3.4 Small-R Theory

Before we present the full solution to the one-parameter GSD theory, it is instructive to examine the asymptotic behaviour in the $\lambda/R \gg 1$ limit, when the WLC is strongly confined in a tube with small radius. In such a case, the function $\psi(\theta)$ is strongly peaked near $\theta = 0$, π, and 2π, and a scaling relation can be drawn. Taking the peak at $\theta = 0$ as an example, through the variable-replacement

$$\theta = \zeta\,(\lambda/R)^{-1/3} \tag{4.26}$$

and the approximation $\sin\theta \sim \theta$, the eigenproblem in (4.24) can be further reduced to

$$-\mu\,(\lambda/R)^{-2/3}\,\psi_1(\zeta) = \left[\frac{\partial^2}{\partial\zeta^2} - \zeta^4\right]\psi_1(\zeta) \tag{4.27}$$

where

$$\psi_1(\zeta) \propto \psi[\theta = \zeta\,(\lambda/R)^{-1/3}]. \tag{4.28}$$

Solving this reduced eigenproblem numerically gives $\mu\,(\lambda/R)^{-2/3} = a = 1.060 \pm 0.001$, hence

$$\beta(L/2\lambda)^{-1}\Delta G = (1.060 \pm 0.001)\,(\lambda/R)^{2/3} \tag{4.29}$$

as listed in Eqs. (4.5) and (4.7) in the introduction.

4.3.5 Large-R Theory

When the radius of the cylinder is made large relative to the persistence length of the polymer ($R \gg \lambda$), the WLC feels only a weak perturbation from the cylindrical potential ($U_{\text{eff}} \ll 1$). The overall conformation is then marginally compressed from its 2D free-space form perturbatively. In this limit, the effective potential can be treated as a perturbation to the ground state 2D free-space WLC, and the theory can be solved for exactly up to first order in the perturbing potential.

Starting from the GSD equation, Eq. (4.24), to first order the reduced free energy is

$$\mu = \mu_0 + \epsilon\mu_1. \tag{4.30}$$

Here, μ_0 is the 2D unconfined GSD free energy, and ϵ is the perturbation strength

$$\epsilon = (\lambda/R)^2 \ll 1. \tag{4.31}$$

The perturbation reduced free energy μ_1 is

$$\mu_1 = \langle \sin^4 \theta \rangle, \tag{4.32}$$

where the average is taken over the free space probability distribution. Overall, the confinement free energy in this limit then becomes

$$\beta(L/2\lambda)^{-1}\Delta G = \epsilon\mu_1 + \mathcal{O}((L/2\lambda)^{-1}) + \mathcal{O}(\epsilon^2) \tag{4.33}$$

$$= \langle \sin^4 \theta \rangle (\lambda/R)^2 \tag{4.34}$$

when $L/2\lambda \gg 1$ and $\lambda/R \ll 1$. Or, by evaluating the average,

$$\beta \left(\frac{L}{2\lambda} \right)^{-1} \Delta G = \frac{3}{8} \left(\frac{\lambda}{R} \right)^2 \tag{4.35}$$

one then finds $c = 3/8$, as presented in Eqs. (4.9) and (4.10) in the introduction. This scaling can be seen in Fig. 4.2(b) as the red dashed line.

4.3.6 Numerical Solution

The full numerical solution to (4.24) can also be found by numerically solving for the eigenfunctions of the operator on the right-hand side. This is done numerically by discretizing the right-hand side into 10^5 grid points in θ, and approximating the differential operator as a second order central difference over the grid. The eigenvectors and eigenvalues of the resulting matrix are then solved for using a sparse matrix eigenproblem solver, as implemented by the SciPy Python software library, which internally uses an implicit restarted Arnoldi method [141, 142].

The resulting eigenvalues and eigenvectors are used to construct the full solution to the WLC problem for a range of finite values of λ/R. The eigenvectors are used to determine the helix-pitch distribution functions. From the distributions the observed pitch, taken as the most probable value of the distribution, is computed numerically. The relative pitch P/R is plotted in Fig. 4.2(a) as the solid black line. Convergence to the large-λ/R limit found in Section 4.3.7 is shown in the inset. The smallest eigenvalue $\mu_{\min}$ for a given λ/R ratio gives the corresponding reduced free energy. The resulting free-energy curve as a function of λ/R is presented in Fig. 4.2(b). The free-energy curve approaches both the large- and small-λ/R asymptotic limits determined in Sections 4.3.4 and 4.3.5. For all data the error bars are smaller than the line width of the curves (solid black lines).

4.3.7 Helix Pitch

For the $0 \leq \theta \leq \pi/2$ region, the reduced pitch P/R is related to θ through

$$P = 2\pi R \cot(\theta). \tag{4.36}$$

Based on the distribution function $\rho(\theta) \propto \psi^2(\theta)$, the pitch distribution function can be determined,

$$\rho_P(P) = \rho(\theta) \left| \frac{\mathrm{d}\theta}{\mathrm{d}P} \right| = \frac{C}{2\pi R} [\psi(\theta)]^2 \sin^2 \theta \tag{4.37}$$

where θ on the right-hand side needs to be substituted by inverting (4.36) to yield P, and where

$$C^{-1} = \int_0^{\pi/2} [\psi(\theta)]^2 d\theta \tag{4.38}$$

is a normalization constant.

Figure 4.3(a) is a plot of the pitch distribution based on the eigenfunction $\psi(\theta)$, found through the GSD theory presented in Section 4.3.3. The distribution functions are plotted for three representative values of the relative cylindrical confinement $\lambda/R = 1, 5, 25$. The observed pitch of the spontaneous helix formed by the WLC on the surface of the cylinder is taken to be the most probable value of the distribution function $\rho_P(P)$. This is numerically computed by finding the maximum of each distribution for an expanded range of λ/R values, and plotted from $\lambda/R \approx 1$ to 25 in Fig. 4.2(a). Below $\lambda/R \approx 1$, the polymer feels weak confinement and starts to approach its free space 2D random coil configuration. Under these conditions, the wrapping of the WLC on the cylinder has no clear indication of a helix. Therefore, the idea of a helix pitch ceases to be well-defined.

Approaching the large-λ/R limit, the pitch distribution functions asymptotically merge into a universal scaling function, $H(x)$, in the form

$$R\rho_P(P) = (\lambda/R)^{-1/3} H[(P/R)(\lambda/R)^{-1/3}]. \tag{4.39}$$

To see this, in Fig. 4.3(b) the reduced $R\rho_P(P)(\lambda/R)^{1/3}$ for various of λ/R are plotted as functions of the reduced parameter

$$x = (P/R)(\lambda/R)^{-1/3}. \tag{4.40}$$

The full solution, represented by the dashed grey lines, converges onto the large-λ/R distribution given by the solid black line, as λ/R is increased. According to Eqs. (4.36) and (4.26), close to the asymptotic limit $x \approx 2\pi/[\theta(\lambda/R)^{1/3}] = 2\pi/\zeta$. Therefore,

$$H(2\pi/\zeta) = \alpha_1 [\psi_1(\zeta)]^2 \zeta^2, \tag{4.41}$$

where $\psi_1(\zeta)$ is the eigenfunction found based on the solution to Eq. (4.27) instead of Eq. (4.24). The solid curve is plotted according to this transformation, within a numerical normalization constant $\alpha_1^{-1} = 2\pi \int_0^{\pi} [\psi_1(\zeta)]^2 d\zeta$. The vertical red dotted line in the plot numerically identifies the location of the most probable value $x_{\mathrm{mpv}} = 7.227...$, which is used to determine the coefficient for the large-λ/R pitch scaling,

$$P/R = x_{\mathrm{mpv}} (\lambda/R)^{1/3}. \tag{4.42}$$

The constant in Eqs. (4.6) and (4.8) is then

$$b = 1.150 \pm 0.001. \tag{4.43}$$

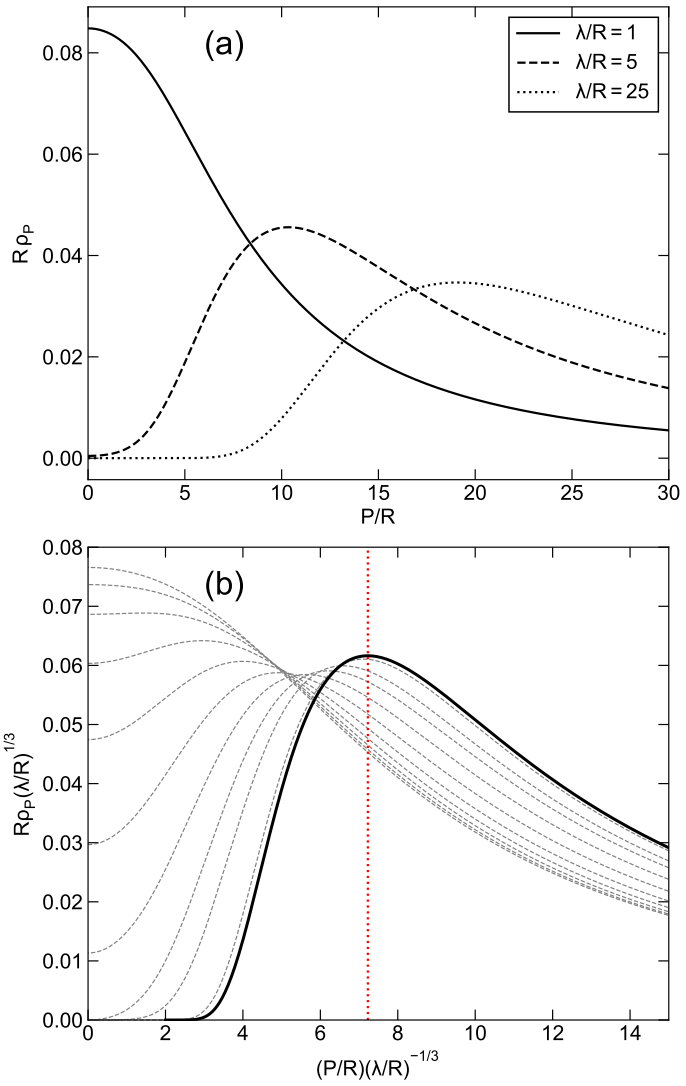


Figure 4.3: (a) Density distribution function for the relative helix pitch as a function of said pitch, $R\,\rho_P(P)$, for three different values of the relative confinement; $\lambda/R = 1, 5, 25$. For $\lambda/R = 1$, the polymer is in a weakly confined, random coil configuration on the surface of the nanotube, and the most probable pitch is $P/R = 0$. As the nanotube radius is decreased relative to the persistence length λ, the most probable value for the pitch increases. (b) Rescaled pitch distributions showing convergence to the large-λ/R result as λ/R is increased. The dashed grey curves are the full solution, corresponding to 10 even spaced curves for λ/R values in the range $[1, 10^2]$. The dashed red line corresponds to the peak of the large-λ/R distribution (solid black line), the location of which determines the coefficient of the large-λ/R scaling law given in Eq. (4.6) and illustrated in Fig. 4.2 (a).

4.4 Comparison to a Previous Theory

In addition to computer simulations for specific systems, there has been another theoretical study that aimed to explain the observed helix pitch over a large range of system parameters. Based on the same WLC model but depending on multiple approximate procedures, Lundberg and Strano constructed an implicit equation for the helix pitch, which was compared to many of the same experimental measurements and simulation studies mentioned here [26]. It is worth noting that there is a discrepancy between our independent interpretation of the literature data and the interpretation presented in their work. To the best of our ability, we have accounted for the change in persistence length of the polymers due to the differing ionic strengths of the experimental solutions, and believe that the data points presented in our Fig. 4.2 are accurate. All data points we used, and their associated references, can be found in the Appendix C.

A comparison between the pitch calculations from both theories over the same domain is presented in Fig. 4.4, where the numerical solution to their implicit Eq. (23) is plotted as the dashed curve. Among other approximations, Lundberg and Strano used two main steps, which could be attributed as the origin of the differences. The first is the use of a modified WLC force-extension interpolation formula, based on the original proposed by Marko-Sigga [7, 143], which is known to contain errors [4]. The second is the restriction of such a virtual force to apply only along the direction of the nanotubes central axis. These approximations become more valid in the strong confinement region, $\lambda/R \gg 1$, which naturally yields the same power law but with a different numerical coefficient. The relative percent difference between their result and our full WLC solution done in this chapter is plotted in red as the dot-dashed curve in Fig. 4.4. The aim of our calculation here is to provide an independent, precise numerical solution to the WLC model, with no approximations introduced. It is not our aim to justify the validity of all steps taken in [26], some of which could be debated. In general, both theories predict similar qualitative trends, as presented in the figure.

4.5 Summary

In this chapter, using the wormlike-chain (WLC) polymer model, we present a scaling argument and numerical solution for a polymer of persistence length λ wrapped around a cylinder of radius R, using the Green's function approach. A wide range of λ/R is examined, including the two extreme cases, $\lambda/R \ll 1$ (weakly confined) and $\lambda/R \gg 1$ (strongly confined), where the scaling relations for the most probable helix pitch and confinement free energy as power laws of λ/R are predicted, along with their numerical prefactors.

The physical picture presented here fits into the general area of theoretical research of the standard WLC model in confinement. Theoretical efforts based on solving the WLC models exactly [138, 144–149], or computing the scaling relations by computer simulations [150–176], have been made to present

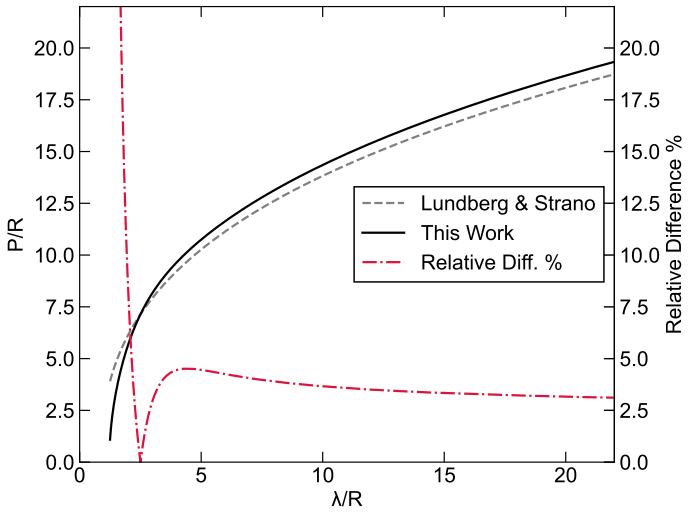


Figure 4.4: Numerical comparison between the helix-pitch predictions from the current chapter (solid curve) and from Ref. [26] (dashed curve). The relative percent difference is plotted as the dot-dashed line.

the scaling properties of a WLC in slit confinement and in tube confinement. Adding to the complexity of the problem is the inclusion of the excluded-volume interaction between polymer segments and the finite polymer-length effects. For the current problem, when the WLC is in a well-organized helix formation, the effects due to excluded-volume interactions are not expected to be significant.

A numerical solution is also obtained in the crossover region between these limits. The helix pitch calculation agrees well with those determined by experiments and molecular-level computer simulations, which mostly concern the wrapping on single-walled carbon nanotubes by a range of polymers types, including ssDNA, Chitosan, Algenic Acid, PNES, and PPES [8–17]. The result is presented in Section 4.3.7, and compared against the 10 different studies considered in Fig. 4.2.

The polymers studied in this chapter were all taken to have a total contour length much greater than their persistence length (i.e. $L \gg \lambda$). Most of the reference data we compared to in Fig. 4.2(a) falls into this regime. The theoretical formalism for a finite L/λ is readily made in Section 4.3.2, which can be used to explain any finite L/λ effects, with a required introduction of L/λ as an additional parameter in the theory.

Chapter 5

Conclusion

5.1 Summary

This thesis dealt with the statistical mechanics of the wormlike-chain (WLC) model, and its application to the classic problem of polymer stretching, and on the modern system of polymer-nanotube complexes. The WLC is a fundamental model in the field of polymer physics, itself a broader subset of condensed and soft matter physics. It treats a semiflexible polymer as a smooth curve in space, characterized by its length L, persistence length λ (decay length of tangent vector correlations, describing the stiffness), position at a point Lt along the backbone $\mathbf{r}(t)$, and the tangent vector at the same point $\mathbf{u}(t)$. By incorporating techniques from quantum field theory, the model can be stated in terms of a diffusion equation (Eq. (1.18)) for the Green's function $q(\mathbf{r}(t), \mathbf{u}(t))$, also called the propagator. Solving the diffusion equation under the appropriate external field $U(\mathbf{r}(t), \mathbf{u}(t))$ allows one to obtain the partition function Q for the system of interest, and compute the thermodynamic quantities of interest, such as the free energy.

Chapter 1 broadly introduced polymers, and the basic models, including the WLC. It also outlined the basic structure of the thesis and motivation for the updated treatment of the statistical mechanics of the WLC in the context of polymer stretching.

Chapter 2 investigated the stretching of finite length semiflexible polymers under the Gibbs and Helmholtz (canonical) statistical ensembles. Stretching is one of the key experiments in polymer physics, and involves the deformation of the polymer by either applying a force to its endpoints, or fixing them at a predetermined separation. In the first case, the average extension is measured in response to the applied force, while in the second the average restoring force is measured in response to the fixed extension. This corresponds to a measurement being performed in the fixed-force Gibbs ensemble, or the fixed extension Helmholtz ensemble. Early studies on dsDNA, a semiflexible polymer, were situated within the thermodynamic limit, where the number of uncorrelated

segments along the chain was large ($L/2\lambda \gg 1$). This suppressed any ensemble dependent behaviour. The early work on explaining these results using the WLC was also done firmly within the thermodynamic limit, and its resulting success at explaining the results meant broadly that these ensemble effects where never directly investigated. This chapter investigated the differences by directly computing the exact force-extension behaviour in the Helmholtz ensemble, which together with the Gibbs ensemble result provides a basis for the analysis of finite length polymer stretching experiments.

Chapter 3 built on the theories proposed in Chapter 2. Using the large body of literature that has been produced on stretched semiflexible polymers, data was compiled from a range of experiments and simulations done in both ensembles, for a range of polymer lengths. This was then compared against the classic predictions for an infinitely long WLC, and the ensemble dependent force-extension curves for finite length polymers. It was found that while the early works were firmly situated in the thermodynamic limit, many studies had since been done on systems outside this limit, and these showed marked deviations from the expected behaviour. By placing the data on a universal plot, the exact scaling behaviours of the observed force-extension relationships could be observed. These showed that the data had a remarkable adherence to the ensemble dependent curves, with clear finite length effects becoming noticeable as shorter, more rodlike polymer segments were stretched.

Chapter 4 investigated the wrapping of cylindrical tubes by WLC polymers. This served as a broad abstraction of DNA wrapped carbon-nanotubes. Wrapping of the nanotubes by DNA can aid in their solvation without largely affecting their properties, as untreated nanotubes form large aggregates in solution and are hard to disperse individually without treatment. When DNA is introduced to the system, it forms a helix around the nanotube, with a regular pitch. The central question was if this pitch could be explained through the WLC model. To this end, several studies measuring the helix pitch of polymer wrapped nanotubes were compared against predictions from the WLC. A numerical solution assuming an infinitely long polymer found good agreement with the experiments. Scaling behaviour under different limits of nanotube size was also determined analytically, with a numerical prefactor determining exact behaviour when required. A comparison was also made with an earlier approximate theory.

5.2 Outlook

The three core chapters of this thesis showed the continued applicability of the WLC model in polymer physics. Advances on the experimental front mean that new systems become available for study, and that a new analysis of the existing models can be required to explain their behaviour. The first two of these chapters focused on behaviour outside of the thermodynamic limit, while the last dealt firmly with polymers within it. It would be interesting to bridge these two systems, and see how the behaviour of confined or otherwise restricted

polymers changes as they become more rodlike. Other long range effects, such as excluded volume, were ignored completely here. While their effects diminish with decreasing polymer size, evaluating and mapping this behaviour and its importance within the context of the statistical mechanics discussed here could be interesting.

Bibliography

[1] Andersen, N. T.; Chen, J. Z. Y. Forced extension of a wormlike chain in the Gibbs and Helmholtz ensembles. *J. Chem. Phys.* **2024**, *160*, 084903.

[2] Andersen, N. T.; Chen, J. Z. Y. Stretching semiflexible polymers: Gibbs versus Helmholtz ensembles. *Phys. Rev. E* **2025**, *111*, 045402.

[3] Andersen, N. T.; Chen, J. Z. Y. Helical Wrapping of Cylindrical Tubes by Wormlike-Chain Polymers. *Macromolecules* **2023**, *56*, 3246–3254.

[4] Andersen, N. T.; Teng, Y.; Chen, J. Z. Y. Stretching a semiflexible polymer of finite length. *Macromolecules* **2021**, *55*, 210–216.

[5] Odijk, T. Stiff chains and filaments under tension. *Macromolecules* **1995**, *28*, 7016–7018.

[6] Kessler, D. A.; Rabin, Y. Distribution functions for filaments under tension. *J. Chem. Phys.* **2004**, *121*, 1155–1164.

[7] Marko, J. F.; Siggia, E. D. Stretching DNA. *Macromolecules* **1995**, *28*, 8759–8770.

[8] Cathcart, H.; Nicolosi, V.; Hughes, J. M.; Blau, W. J.; Kelly, J. M.; Quinn, S. J.; Coleman, J. N. Ordered DNA wrapping switches on luminescence in single-walled nanotube dispersions. *J. Am. Chem. Soc.* **2008**, *130*, 12734–12744.

[9] Deria, P.; Sinks, L. E.; Park, T.-H.; Tomezsko, D. M.; Brukman, M. J.; Bonnell, D. A.; Therien, M. J. Phase transfer catalysts drive diverse organic solvent solubility of single-walled carbon nanotubes helically wrapped by ionic, semiconducting polymers. *Nano Lett.* **2010**, *10*, 4192–4199.

[10] Yarotski, D. A.; Kilina, S. V.; Talin, A. A.; Tretiak, S.; Prezhdo, O. V.; Balatsky, A. V.; Taylor, A. J. Scanning tunneling microscopy of DNA-wrapped carbon nanotubes. *Nano Lett.* **2009**, *9*, 12–17.

[11] Kang, Y. K.; Lee, O.-S.; Deria, P.; Kim, S. H.; Park, T.-H.; Bonnell, D. A.; Saven, J. G.; Therien, M. J. Helical wrapping of single-walled carbon nanotubes by water soluble poly (p-phenyleneethynylene). *Nano Lett.* **2009**, *9*, 1414–1418.

[12] Liu, Y.; Chipot, C.; Shao, X.; Cai, W. Free-energy landscape of the helical wrapping of a carbon nanotube by a polysaccharide. *J. Phys. Chem. C* **2011**, *115*, 1851–1856.

[13] Liu, Y.; Chipot, C.; Shao, X.; Cai, W. Solubilizing carbon nanotubes through noncovalent functionalization. Insight from the reversible wrapping of alginic acid around a single-walled carbon nanotube. *J. Phys. Chem. B* **2010**, *114*, 5783–5789.

[14] Zerze, G. H.; Stillinger, F. H.; Debenedetti, P. G. The Handedness of DNA Assembly around Carbon Nanotubes Is Determined by the Chirality of DNA. *J. Phys. Chem. B* **2020**, *124*, 5362–5369.

[15] Gurevitch, I.; Srebnik, S. Conformational behavior of polymers adsorbed on nanotubes. *J. Chem. Phys.* **2008**, *128*, 144901.

[16] Zheng, M.; Jagota, A.; Strano, M. S.; Santos, A. P.; Barone, P.; Chou, S. G.; Diner, B. A.; Dresselhaus, M. S.; Mclean, R. S.; Onoa, G. B.; others Structure-based carbon nanotube sorting by sequence-dependent DNA assembly. *Science* **2003**, *302*, 1545–1548.

[17] Campbell, J. F.; Tessmer, I.; Thorp, H. H.; Erie, D. A. Atomic force microscopy studies of DNA-wrapped carbon nanotube structure and binding to quantum dots. *J. Am. Chem. Soc.* **2008**, *130*, 10648–10655.

[18] Chen, H.; Meisburger, S. P.; Pabit, S. A.; Sutton, J. L.; Webb, W. W.; Pollack, L. Ionic strength-dependent persistence lengths of single-stranded RNA and DNA. *Proc. Natl. Acad. Sci. U.S.A.* **2012**, *109*, 799–804.

[19] Murphy, M.; Rasnik, I.; Cheng, W.; Lohman, T. M.; Ha, T. Probing single-stranded DNA conformational flexibility using fluorescence spectroscopy. *Biophys. J.* **2004**, *86*, 2530–2537.

[20] Morris, G. A.; Castile, J.; Smith, A.; Adams, G. G.; Harding, S. E. Macromolecular conformation of chitosan in dilute solution: A new global hydrodynamic approach. *Carbohydr. Polym.* **2009**, *76*, 616–621.

[21] Vold, I. M. N.; Kristiansen, K. A.; Christensen, B. E. A study of the chain stiffness and extension of alginates, in vitro epimerized alginates, and periodate-oxidized alginates using size-exclusion chromatography combined with light scattering and viscosity detectors. *Biomacromolecules* **2006**, *7*, 2136–2146.

[22] Grell, M.; Bradley, D.; Long, X.; Chamberlain, T.; Inbasekaran, M.; Woo, E.; Soliman, M. Chain geometry, solution aggregation and enhanced dichroism in the liquidcrystalline conjugated polymer poly (9, 9-dioctylfluorene). *Acta Polym.* **1998**, *49*, 439–444.

[23] Fytas, G.; Nothofer, H.; Scherf, U.; Vlassopoulos, D.; Meier, G. Structure and dynamics of nondilute polyfluorene solutions. *Macromolecules* **2002**, *35*, 481–488.

[24] Jeschke, G.; Sajid, M.; Schulte, M.; Ramezanian, N.; Volkov, A.; Zimmermann, H.; Godt, A. Flexibility of shape-persistent molecular building blocks composed of p-phenylene and ethynylene units. *J. Am. Chem. Soc.* **2010**, *132*, 10107–10117.

[25] Cotts, P. M.; Swager, T. M.; Zhou, Q. Equilibrium flexibility of a rigid linear conjugated polymer. *Macromolecules* **1996**, *29*, 7323–7328.

[26] Lundberg, D. J.; Strano, M. S. Approximate Corona Phase Hamiltonian for Individual Cylindrical Nanoparticle–Polymer Interactions. *J. Phys. Chem. B* **2021**, *126*, 347–354.

[27] Rubinstein, M.; Colby, R. H. *Polymer Physics*; Oxford University Press, 2003.

[28] Brydson, J. A. *Plastics materials*; Elsevier, 1999.

[29] Neidle, S.; Sanderson, M. *Principles of nucleic acid structure*; Academic Press, 2021.

[30] Doi, M.; Edwards, S. F. *The Theory of Polymer Dynamics*; Oxford University Press, 1988.

[31] Smith, S. B.; Finzi, L.; Bustamante, C. Direct mechanical measurements of the elasticity of single DNA molecules by using magnetic beads. *Science* **1992**, *258*, 1122–1126.

[32] Chen, J. Z. Y. Theory of wormlike polymer chains in confinement. *Prog. Polym. Sci.* **2016**, *54*, 3–46.

[33] Perkins, T. T.; Smith, D. E.; Larson, R. G.; Chu, S. Stretching of a single tethered polymer in a uniform flow. *Science* **1995**, *268*, 83–87.

[34] Baumann, C. G.; Smith, S. B.; Bloomfield, V. A.; Bustamante, C. Ionic effects on the elasticity of single DNA molecules. *Proc. Natl. Acad. Sci. U.S.A.* **1997**, *94*, 6185–6190.

[35] Ortiz, C.; Hadziioannou, G. Entropic elasticity of single polymer chains of poly (methacrylic acid) measured by atomic force microscopy. *Macromolecules* **1999**, *32*, 780–787.

[36] Baumann, C. G.; Bloomfield, V. A.; Smith, S. B.; Bustamante, C.; Wang, M. D.; Block, S. M. Stretching of single collapsed DNA molecules. *Biophys. J.* **2000**, *78*, 1965–1978.

[37] Liu, X.; Pollack, G. H. Mechanics of F-actin characterized with microfabricated cantilevers. *Biophys. J.* **2002**, *83*, 2705–2715.

[38] Rosa, A.; Hoang, T. X.; Marenduzzo, D.; Maritan, A. Elasticity of semiflexible polymers with and without self-interactions. *Macromolecules* **2003**, *36*, 10095–10102.

[39] Cifra, P.; Bleha, T. Stretching of self-interacting wormlike macromolecules. *Polymer* **2007**, *48*, 2444–2452.

[40] Seol, Y.; Li, J.; Nelson, P. C.; Perkins, T. T.; Betterton, M. D. Elasticity of short DNA molecules: theory and experiment for contour lengths of 0.6–7 μm. *Biophys. J.* **2007**, *93*, 4360–4373.

[41] Wang, J.; Lu, C. Single molecule λ-DNA stretching studied by microfluidics and single particle tracking. *J. Appl. Phys.* **2007**, *102*.

[42] Chen, Y.-F.; Blab, G. A.; Meiners, J.-C. Stretching submicron biomolecules with constant-force axial optical tweezers. *Biophys. J.* **2009**, *96*, 4701–4708.

[43] Chen, Y.-F.; Wilson, D. P.; Raghunathan, K.; Meiners, J.-C. Entropic boundary effects on the elasticity of short DNA molecules. *Phys. Rev. E* **2009**, *80*, 020903.

[44] Manca, F.; Giordano, S.; Palla, P. L.; Zucca, R.; Cleri, F.; Colombo, L. Elasticity of flexible and semiflexible polymers with extensible bonds in the Gibbs and Helmholtz ensembles. *J. Chem. Phys.* **2012**, *136*, 154906.

[45] Cortini, R.; Caré, B. R.; Victor, J.-M.; Barbi, M. Theory and simulations of toroidal and rod-like structures in single-molecule DNA condensation. *J. Chem. Phys.* **2015**, *142*.

[46] Li, X.; Schroeder, C. M.; Dorfman, K. D. Modeling the stretching of wormlike chains in the presence of excluded volume. *Soft Matter* **2015**, *11*, 5947–5954.

[47] Kurzthaler, C. Elastic behavior of a semiflexible polymer in 3D subject to compression and stretching forces. *Soft Matter* **2018**, *14*, 7634–7644.

[48] Wang, M. D.; Yin, H.; Landick, R.; Gelles, J.; Block, S. M. Stretching DNA with optical tweezers. *Biophys. J.* **1997**, *72*, 1335–1346.

[49] Bemis, J. E.; Akhremitchev, B. B.; Walker, G. C. Single polymer chain elongation by atomic force microscopy. *Langmuir* **1999**, *15*, 2799–2805.

[50] Sun, Y.-L.; Luo, Z.-P.; An, K.-N. Stretching short biopolymers using optical tweezers. *Biochem. Biophys. Res. Commun.* **2001**, *286*, 826–830.

[51] Dessinges, M.-N.; Maier, B.; Zhang, Y.; Peliti, M.; Bensimon, D.; Croquette, V. Stretching single stranded DNA, a model polyelectrolyte. *Phys. Rev. Lett.* **2002**, *89*, 248102.

[52] Sun, Y.-L.; Luo, Z.-P.; Fertala, A.; An, K.-N. Direct quantification of the flexibility of type I collagen monomer. *Biochem. Biophys. Res. Commun.* **2002**, *295*, 382–386.

[53] Leake, M. C.; Wilson, D.; Gautel, M.; Simmons, R. M. The elasticity of single titin molecules using a two-bead optical tweezers assay. *Biophys. J.* **2004**, *87*, 1112–1135.

[54] Sun, Y.-L.; Luo, Z.-P.; Fertala, A.; An, K.-N. Stretching type II collagen with optical tweezers. *J. Biomech.* **2004**, *37*, 1665–1669.

[55] Aumann, F.; Lankas, F.; Caudron, M.; Langowski, J. Monte Carlo simulation of chromatin stretching. *Phys. Rev. E* **2006**, *73*, 041927.

[56] Miller, E.; Garcia, T.; Hultgren, S.; Oberhauser, A. F. The mechanical properties of E. coli type 1 pili measured by atomic force microscopy techniques. *Biophys. J.* **2006**, *91*, 3848–3856.

[57] Nakajima, K.; Watabe, H.; Nishi, T. Single polymer chain rubber elasticity investigated by atomic force microscopy. *Polymer* **2006**, *47*, 2505–2510.

[58] Khalil, A. S.; Ferrer, J. M.; Brau, R. R.; Kottmann, S. T.; Noren, C. J.; Lang, M. J.; Belcher, A. M. Single M13 bacteriophage tethering and stretching. *Proc. Natl. Acad. Sci. U.S.A.* **2007**, *104*, 4892–4897.

[59] Buehler, M. J.; Wong, S. Y. Entropic elasticity controls nanomechanics of single tropocollagen molecules. *Biophys. J.* **2007**, *93*, 37–43.

[60] Kauert, D. J.; Kurth, T.; Liedl, T.; Seidel, R. Direct mechanical measurements reveal the material properties of three-dimensional DNA origami. *Nano Lett.* **2011**, *11*, 5558–5563.

[61] Hsu, H.-P.; Binder, K. Stretching semiflexible polymer chains: Evidence for the importance of excluded volume effects from Monte Carlo simulation. *J. Chem. Phys.* **2012**, *136*.

[62] Wieczorek, A.; Rezaei, N.; Chan, C. K.; Xu, C.; Panwar, P.; Brömme, D.; Merschrod S, E. F.; Forde, N. R. Development and characterization of a eukaryotic expression system for human type II procollagen. *BMC Biotechnol.* **2015**, *15*, 112.

[63] Liese, S.; Gensler, M.; Krysiak, S.; Schwarzl, R.; Achazi, A.; Paulus, B.; Hugel, T.; Rabe, J. P.; Netz, R. R. Hydration effects turn a highly stretched polymer from an entropic into an energetic spring. *ACS Nano* **2017**, *11*, 702–712.

[64] Kolberg, A.; Wenzel, C.; Hackenstrass, K.; Schwarzl, R.; Ruittiger, C.; Hugel, T.; Gallei, M.; Netz, R. R.; Balzer, B. N. Opposing temperature dependence of the stretching response of single PEG and PNiPAM polymers. *J. Am. Chem. Soc.* **2019**, *141*, 11603–11613.

[65] Shon, M. J.; Rah, S.-H.; Yoon, T.-Y. Submicrometer elasticity of double-stranded DNA revealed by precision force-extension measurements with magnetic tweezers. *Sci. Adv.* **2019**, *5*, eaav1697.

[66] Dutta, S.; Sing, C. E. Two stretching regimes in the elasticity of bottle-brush polymers. *Macromolecules* **2020**, *53*, 6946–6955.

[67] Gutiérrez-Medina, B.; Maldonado, A. I. P.; García-Meza, J. V. Mechanical testing of particle streaming and intact extracellular mucilage nanofibers reveal a role of elastic force in diatom motility. *Phys. Biol.* **2022**, *19*, 056002.

[68] Bibeau, J. P.; Pandit, N. G.; Gray, S.; Shatery Nejad, N.; Sindelar, C. V.; Cao, W.; De La Cruz, E. M. Twist response of actin filaments. *Proc. Natl. Acad. Sci. U.S.A.* **2023**, *120*, e2208536120.

[69] Kardar, M. *Statistical physics of particles*; Cambridge University Press, 2007.

[70] Strick, T. R.; Allemand, J.-F.; Bensimon, D.; Bensimon, A.; Croquette, V. The elasticity of a single supercoiled DNA molecule. *Science* **1996**, *271*, 1835–1837.

[71] Rief, M.; Oesterhelt, F.; Heymann, B.; Gaub, H. E. Single molecule force spectroscopy on polysaccharides by atomic force microscopy. *Science* **1997**, *275*, 1295–1297.

[72] Strunz, T.; Oroszlan, K.; Schäfer, R.; Güntherodt, H.-J. Dynamic force spectroscopy of single DNA molecules. *Proc. Natl. Acad. Sci. U.S.A.* **1999**, *96*, 11277–11282.

[73] Keller, D.; Swigon, D.; Bustamante, C. Relating single-molecule measurements to thermodynamics. *Biophys. J.* **2003**, *84*, 733–738.

[74] Samanta, S. K.; Fritsch, M.; Scherf, U.; Gomulya, W.; Bisri, S. Z.; Loi, M. A. Conjugated polymer-assisted dispersion of single-wall carbon nanotubes: the power of polymer wrapping. *Acc. Chem. Res.* **2014**, *47*, 2446–2456.

[75] Chen, J.; Hamon, M. A.; Hu, H.; Chen, Y.; Rao, A. M.; Eklund, P. C.; Haddon, R. C. Solution properties of single-walled carbon nanotubes. *Science* **1998**, *282*, 95–98.

[76] O'Connell, M. J.; Boul, P.; Ericson, L. M.; Huffman, C.; Wang, Y.; Haroz, E.; Kuper, C.; Tour, J.; Ausman, K. D.; Smalley, R. E. Reversible water-solubilization of single-walled carbon nanotubes by polymer wrapping. *Chem. Phys. Lett.* **2001**, *342*, 265–271.

[77] Vigolo, B.; Penicaud, A.; Coulon, C.; Sauder, C.; Pailler, R.; Journet, C.; Bernier, P.; Poulin, P. Macroscopic fibers and ribbons of oriented carbon nanotubes. *Science* **2000**, *290*, 1331–1334.

[78] Zheng, M.; Jagota, A.; Semke, E. D.; Diner, B. A.; McLean, R. S.; Lustig, S. R.; Richardson, R. E.; Tassi, N. G. DNA-assisted dispersion and separation of carbon nanotubes. *Nat. Mater.* **2003**, *2*, 338–342.

[79] Liu, P. Modifications of carbon nanotubes with polymers. *Eur. Polym. J.* **2005**, *41*, 2693–2703.

[80] Gomulya, W.; Costanzo, G. D.; De Carvalho, E. J. F.; Bisri, S. Z.; Derenskyi, V.; Fritsch, M.; Fröhlich, N.; Allard, S.; Gordiichuk, P.; Herrmann, A.; others Semiconducting single-walled carbon nanotubes on demand by polymer wrapping. *Adv. Mater.* **2013**, *25*, 2948–2956.

[81] Star, A.; Stoddart, J. F.; Steuerman, D.; Diehl, M.; Boukai, A.; Wong, E. W.; Yang, X.; Chung, S.-W.; Choi, H.; Heath, J. R. Preparation and properties of polymer-wrapped single-walled carbon nanotubes. *Angew. Chem.* **2001**, *113*, 1771–1775.

[82] Enyashin, A.; Gemming, S.; Seifert, G. DNA-wrapped carbon nanotubes. *Nanotechnology* **2007**, *18*, 245702.

[83] Tallury, S. S.; Pasquinelli, M. A. Molecular dynamics simulations of flexible polymer chains wrapping single-walled carbon nanotubes. *J. Phys. Chem. B* **2010**, *114*, 4122–4129.

[84] Kumar, S.; Pattanayek, S. K.; Pereira, G. G. Organization of polymer chains onto long, single-wall carbon nano-tubes: Effect of tube diameter and cooling method. *J. Chem. Phys.* **2014**, *140*, 024904.

[85] Sakurai, J. J.; Napolitano, J. *Modern quantum mechanics*; Cambridge University Press, 2020.

[86] Kratky, O.; Porod, G. Röntgenuntersuchung gelöster Fadenmoleküle. *Recueil des Travaux Chimiques des Pays-Bas* **1949**, *68*, 1106–1122.

[87] Saitô, N.; Takahashi, K.; Yunoki, Y. The statistical mechanical theory of stiff chains. *J. Phys. Soc. Jpn.* **1967**, *22*, 219–226.

[88] Odijk, T. Polyelectrolytes near the rod limit. *J. Polym. Sci., Polym. Phys. Ed.* **1977**, *15*, 477–483.

[89] Skolnick, J.; Fixman, M. Electrostatic persistence length of a wormlike polyelectrolyte. *Macromolecules* **1977**, *10*, 944–948.

[90] Perkins, T. T.; Smith, D. E.; Larson, R. G.; Chu, S. Stretching of a single tethered polymer in a uniform flow. *Science* **1995**, *268*, 83–87.

[91] Titantah, J.; Pierleoni, C.; Ryckaert, J.-P. Different statistical mechanical ensembles for a stretched polymer. *Phys. Rev. E* **1999**, *60*, 7010.

[92] Van der Straeten, E.; Naudts, J. A one-dimensional model for theoretical analysis of single molecule experiments. *J. Phys. A* **2006**, *39*, 5715.

[93] Winkler, R. G. Equivalence of statistical ensembles in stretching single flexible polymers. *Soft Matter* **2010**, *6*, 6183–6191.

[94] Neumann, R. M. Nonequivalence of the stress and strain ensembles in describing polymer-chain elasticity. *Phys. Rev. A* **1985**, *31*, 3516.

[95] Neumann, R. M. Implications of using the entropy spring model for an ideal polymer chain. *Phys. Rev. A* **1986**, *34*, 3486.

[96] Neumann, R. M. On the precise meaning of extension in the interpretation of polymer-chain stretching experiments. *Biophys. J.* **2003**, *85*, 3418–3420.

[97] Süzen, M.; Sega, M.; Holm, C. Ensemble inequivalence in single-molecule experiments. *Phys. Rev. E* **2009**, *79*, 051118.

[98] Schurr, J. M.; Smith, S. B. Theory for the extension of a linear polyelectrolyte attached at one end in an electric field. *Biopolymers* **1990**, *29*, 1161–1165.

[99] Winkler, R. G. Deformation of semiflexible chains. *J. Chem. Phys.* **2003**, *118*, 2919–2928.

[100] Sinha, S.; Samuel, J. Inequivalence of statistical ensembles in single molecule measurements. *Phys. Rev. E* **2005**, *71*, 021104.

[101] Manca, F.; Giordano, S.; Palla, P. L.; Cleri, F.; Colombo, L. Two-state theory of single-molecule stretching experiments. *Phys. Rev. E* **2013**, *87*, 032705.

[102] Manca, F.; Giordano, S.; Palla, P. L.; Cleri, F.; Colombo, L. Theory and Monte Carlo simulations for the stretching of flexible and semiflexible single polymer chains under external fields. *J. Chem. Phys.* **2012**, *137*.

[103] Dhar, A.; Chaudhuri, D. Triple minima in the free energy of semiflexible polymers. *Phys. Rev. Lett.* **2002**, *89*, 065502.

[104] Kierfeld, J.; Niamploy, O.; Sa-Yakanit, V.; Lipowsky, R. Stretching of semiflexible polymers with elastic bonds. *Eur. Phys. J. E* **2004**, *14*, 17–34.

[105] Hori, Y.; Prasad, A.; Kondev, J. Stretching short biopolymers by fields and forces. *Phys. Rev. E* **2007**, *75*, 041904.

[106] Li, X.; Dorfman, K. D. Effect of excluded volume on the force-extension of wormlike chains in slit confinement. *J. Chem. Phys.* **2016**, *144*.

[107] Vologodskii, A. DNA extension under the action of an external force. *Macromolecules* **1994**, *27*, 5623–5625.

[108] Kratky, O.; Porod, G. Röntgenuntersuchung gelöster Fadenmoleküle. *Rec. Trav. Chim.* **1949**, *68*, 1106–1122.

[109] Flory, P. J. *Statistical Mechanics of Chain Molecules*, reprinted ed.; Hanser Publishers, 1989.

[110] Giordano, S. Spin variable approach for the statistical mechanics of folding and unfolding chains. *Soft Matter* **2017**, *13*, 6877–6893.

[111] Benedito, M.; Giordano, S. Thermodynamics of small systems with conformational transitions: The case of two-state freely jointed chains with extensible units. *J. Chem. Phys.* **2018**, *149*.

[112] Chaudhuri, D. Semiflexible polymers: Dependence on ensemble and boundary orientations. *Phys. Rev. E* **2007**, *75*, 021803.

[113] Feynman, R. P. *Statistical Mechanics: A Set Of Lectures*; Westview Press, 1998.

[114] Andrews, G. E. Ramanujan's "lost" notebook. I. Partial θ-functions. *Adv. Math.* **1981**, *41*, 137–172.

[115] Warnaar, S. O. Partial theta functions. I. Beyond the lost notebook. *Proc. London Math. Soc.* **2003**, *87*, 363–395.

[116] Jiang, Y.; Chen, J. Z. Y. Self-consistent field theory and numerical scheme for calculating the phase diagram of wormlike diblock copolymers. *Phys. Rev. E* **2013**, *88*, 042603.

[117] Benetatos, P. Ensemble inequivalence and negative extensibility in a strongly stretched wormlike chain with fluctuating bending stiffness. *J. Chem. Phys.* **2022**, *157*.

[118] Manca, F.; Giordano, S.; Palla, P. L.; Cleri, F. On the equivalence of thermodynamics ensembles for flexible polymer chains. *Physica A* **2014**, *395*, 154–170.

[119] Neumann, R. M. Comment on "Elasticity of flexible and semiflexible polymers with extensible bonds in the Gibbs and Helmholtz ensembles"[J. Chem. Phys. 136, 154906 (2012)]. *J. Chem. Phys.* **2013**, *138*.

[120] Manca, F.; Giordano, S.; Palla, P. L.; Cleri, F.; Colombo, L. Response to "Comment on 'Elasticity of flexible and semiflexible polymers with extensible bonds in the Gibbs and Helmholtz ensembles"'[J. Chem. Phys. 138, 157101 (2013)]. *J. Chem. Phys.* **2013**, *138*.

[121] Ivanov, V. A.; Klushin, L. I.; Skvortsov, A. M. How to understand the ensemble equivalence during stretching of a single macromolecule. *Polym. Sci. Ser. A* **2012**, *54*, 602–613.

[122] Spakowitz, A. J.; Wang, Z.-G. Exact results for a semiflexible polymer chain in an aligning field. *Macromolecules* **2004**, *37*, 5814–5823.

[123] Dutta, S.; Benetatos, P. Inequivalence of fixed-force and fixed-extension statistical ensembles for a flexible polymer tethered to a planar substrate. *Soft Matter* **2018**, *14*, 6857–6866.

[124] Chen, H.; Fu, H.; Zhu, X.; Cong, P.; Nakamura, F.; Yan, J. Improved high-force magnetic tweezers for stretching and refolding of proteins and short DNA. *Biophys. J.* **2011**, *100*, 517–523.

[125] De Gennes, P.-G. *Scaling concepts in polymer physics*; Cornell University Press, 1979.

[126] Everaers, R.; Becker, N. B.; Rosa, A. Single-molecule stretching experiments of flexible (wormlike) chain molecules in different ensembles: Theory and a potential application of finite chain length effects to nick-counting in DNA. *J. Chem. Phys.* **2021**, *154*.

[127] Odijk, T. Theory of lyotropic polymer liquid crystals. *Macromolecules* **1986**, *19*, 2313–2329.

[128] Fixman, M.; Kovac, J. Polymer conformational statistics. III. Modified Gaussian models of stiff chains. *J. Chem. Phys.* **1973**, *58*, 1564–1568.

[129] Note The coeffient of 1/2 in (3.5) in the small-α limit of (3.4) is not obvious. To leading order, the quantity in the square brackets of (3.4) reduces to $(1/\pi^2)(L/\lambda)[1/(4\lambda(1-Z/L)^2)]$ after re-summation for small α [1].

[130] Andersen, N. Wormlike Chain Polymers Under External Fields with Applications to Nanotechnology. M.Sc. thesis, University of Waterloo, 2022.

[131] Chik, M. W.; Hussain, Z.; Zulkefeli, M.; Tripathy, M.; Kumar, S.; Majeed, A. B. A.; Byrappa, K. Polymer-wrapped single-walled carbon nanotubes: A transformation toward better applications in healthcare. *Drug Deliv. Transl. Res.* **2019**, *9*, 578–594.

[132] Li, Y.; Li, G.; Wang, X.; Zhu, Z.; Ma, H.; Zhang, T.; Jin, J. Poly (ionic liquid)-wrapped single-walled carbon nanotubes for sub-ppb detection of CO2. *Chem. Commun.* **2012**, *48*, 8222–8224.

[133] Gomulya, W.; Gao, J.; Loi, M. A. Conjugated polymer-wrapped carbon nanotubes: physical properties and device applications. *Eur. Phys. J. B* **2013**, *86*, 1–13.

[134] Li, Z.; Song, Y.; Li, A.; Xu, W.; Zhang, W. Direct observation of the wrapping/unwrapping of ssDNA around/from a SWCNT at the single-molecule level: towards tuning the binding mode and strength. *Nanoscale* **2018**, *10*, 18586–18596.

[135] Johnson, R. R.; Johnson, A. C.; Klein, M. L. Probing the structure of DNA- carbon nanotube hybrids with molecular dynamics. *Nano Lett.* **2008**, *8*, 69–75.

[136] Arkin, H.; Janke, W. Polymer adsorption on curved surfaces. *Phys. Rev. E* **2017**, *96*, 062504.

[137] Liang, Q.; Li, J.; Zhang, P.; Chen, J. Z. Y. Modified diffusion equation for the wormlike-chain statistics in curvilinear coordinates. *J. Chem. Phys.* **2013**, *138*, 244910.

[138] Odijk, T. The statistics and dynamics of confined or entangled stiff polymers. *Macromolecules* **1983**, *16*, 1340–1344.

[139] Freed, K. F. *Advances in Chemical Physics*; John Wiley & Sons, Ltd, 1972; pp 1–128.

[140] Ye, S.; Zhang, P.; Chen, J. Z. Y. Nematic ordering of semiflexible polymers confined on a toroidal surface. *Soft Matter* **2016**, *12*, 5438–5449.

[141] Virtanen, P. et al. SciPy 1.0: Fundamental Algorithms for Scientific Computing in Python. *Nat. Methods* **2020**, *17*, 261–272.

[142] Lehoucq, R. B.; Sorensen, D. C.; Yang, C. *ARPACK users' guide: solution of large-scale eigenvalue problems with implicitly restarted Arnoldi methods*; SIAM, 1998.

[143] Ogden, R. W.; Saccomandi, G.; Sgura, I. Computational aspects of Worm-Like-Chain interpolation formulas. *Comput. Math. with Appl.* **2007**, *53*, 276–286.

[144] Burkhardt, T. W. Free energy of a semiflexible polymer confined along an axis. *J. Phys. A: Math. Gen.* **1995**, *28*, L629–L635.

[145] Chen, J. Z. Y.; Sullivan, D. E. Free energy of a wormlike polymer chain confined in a slit: crossover between two scaling regimes. *Macromolecules* **2006**, *39*, 7769–7773.

[146] Odijk, T. DNA confined in nanochannels: Hairpin tightening by entropic depletion. *J. Chem. Phys.* **2006**, *125*, 204904.

[147] Odijk, T. Scaling theory of DNA confined in nanochannels and nanoslits. *Phys. Rev. E* **2008**, *77*, 060901.

[148] Chen, J. Z. Y. Conformational properties of a back-folding wormlike chain confined in a cylindrical tube. *Phys. Rev. Lett.* **2017**, *118*, 247802.

[149] Teng, Y.; Andersen, N. T.; Chen, J. Z. Y. Statistical properties of a slit-confined wormlike chain of finite length. *Macromolecules* **2021**, *54*, 8008–8023.

[150] Dijkstra, M.; Frenkel, D.; Lekkerkerker, H. N. Confinement free energy of semiflexible polymers. *Physica A* **1993**, *193*, 374 – 393.

[151] Bicout, D. J.; Burkhardt, T. W. Simulation of a semiflexible polymer in a narrow cylindrical pore. *J. Phys. A Math. Gen.* **2001**, *34*, 5745–5750.

[152] Chen, Y.-L.; Graham, M. D.; de Pablo, J. J.; Randall, G. C.; Gupta, M.; Doyle, P. S. Conformation and dynamics of single DNA molecules in parallel-plate slit microchannels. *Phys. Rev. E* **2004**, *70*, 060901.

[153] Yang, Y.; Burkhardt, T. W.; Gompper, G. Free energy and extension of a semiflexible polymer in cylindrical confining geometries. *Phys. Rev. E* **2007**, *76*, 011804.

[154] Cui, T.; Ding, J.; Chen, J. Z. Y. Dynamics of a self-avoiding polymer chain in slit, tube, and cube confinements. *Phys. Rev. E* **2008**, *78*, 061802.

[155] Burkhardt, T. W.; Yang, Y.; Gompper, G. Fluctuations of a long, semiflexible polymer in a narrow channel. *Phys. Rev. E* **2010**, *82*, 041801.

[156] Wang, Y.; Tree, D. R.; Dorfman, K. D. Simulation of DNA Extension in Nanochannels. *Macromolecules* **2011**, *44*, 6594–6604.

[157] Dai, L.; Jones, J. J.; van der Maarel, J. R. C.; Doyle, P. S. A systematic study of DNA conformation in slitlike confinement. *Soft Matter* **2012**, *8*, 2972–2982.

[158] Dai, L.; Tree, D. R.; van der Maarel, J. R. C.; Dorfman, K. D.; Doyle, P. S. Revisiting blob theory for DNA diffusivity in slitlike confinement. *Phys. Rev. Lett.* **2013**, *110*, 168105.

[159] Benkova, Z.; Cifra, P. Simulation of semiflexible cyclic and linear chains moderately and strongly confined in nanochannels. *Macromolecules* **2012**, *45*, 2597–2608.

[160] Cifra, P.; Bleha, T. Free energy of polymers confined in open and closed cavities. *Macromol. Theory Simul.* **2012**, *21*, 15–23.

[161] Smyda, M. R.; Harvey, S. C. The entropic cost of polymer confinement. *J. Phys. Chem. B* **2012**, *116*, 10928–10934.

[162] Chen, Y.-L.; Lin, Y.-H.; Chang, J.-F.; Lin, P.-k. Dynamics and conformation of semiflexible polymers in strong quasi-1D and -2D confinement. *Macromolecules* **2014**, *47*, 1199–1205.

[163] Muralidhar, A.; Tree, D. R.; Dorfman, K. D. Backfolding of wormlike chains confined in nanochannels. *Macromolecules* **2014**, *47*, 8446–8458.

[164] Dai, L.; van der Maarel, J.; Doyle, P. S. Extended de Gennes Regime of DNA Confined in a Nanochannel. *Macromolecules* **2014**, *47*, 2445–2450.

[165] Tree, D. R.; Reinhart, W. F.; Dorfman, K. D. The Odijk regime in slits. *Macromolecules* **2014**, *47*, 3672–3684.

[166] Vargas-Lara, F.; Stavis, S. M.; Strychalski, E. A.; Nablo, B. J.; Geist, J.; Starr, F. W.; Douglas, J. F. Dimensional reduction of duplex DNA under confinement to nanofluidic slits. *Soft Matter* **2015**, *11*, 8273–8284.

[167] Mansfield, M. L.; Tsortos, A.; Douglas, J. F. Persistent draining crossover in DNA and other semi-flexible polymers: Evidence from hydrodynamic models and extensive measurements on DNA solutions. *J. Chem. Phys.* **2015**, *143*, 124903.

[168] Dai, L.; Renner, C. B.; Doyle, P. S. The polymer physics of single DNA confined in nanochannels. *Adv. Colloid Interface Sci.* **2016**, *232*, 80–100, Proceedings from the International Workshop on Polyelectrolytes in Chemistry, Biology and Technology.

[169] Muralidhar, A.; Dorfman, K. D. Backfolding of DNA confined in nanotubes: Flory theory versus the two-state cooperativity model. *Macromolecules* **2016**, *49*, 1120–1126.

[170] Muralidhar, A.; Quevillon, M. J.; Dorfman, K. D. The backfolded Odijk regime for wormlike chains confined in rectangular nanochannels. *Polymers* **2016**, *8*, 79.

[171] Leith, J. S.; Kamanzi, A.; Sean, D.; Berard, D.; Guthrie, A. C.; McFaul, C. M. J.; Slater, G. W.; de Haan, H. W.; Leslie, S. R. Free energy of a polymer in slit-like confinement from the Odijk regime to the bulk. *Macromolecules* **2016**, *49*, 9266–9271.

[172] Polson, J. M.; Tremblett, A. F.; McLure, Z. R. N. Free energy of a folded polymer under cylindrical confinement. *Macromolecules* **2017**, *50*, 9515–9524.

[173] Hayase, Y.; Sakaue, T.; Nakanishi, H. Compressive response and helix formation of a semiflexible polymer confined in a nanochannel. *Phys. Rev. E* **2017**, *95*, 052502.

[174] Bleha, T.; Cifra, P. Stretching and compression of DNA by external forces under nanochannel confinement. *Soft Matter* **2018**, *14*, 1247–1259.

[175] Cheong, G. K.; Li, X.; Dorfman, K. D. Evidence for the extended de Gennes regime of a semiflexible polymer in slit confinement. *Phys. Rev. E* **2018**, *97*, 022502.

[176] Wang, J.; Li, K. Statistical behaviors of semiflexible polymer chains stretched in rectangular tubes. *Polymers* **2019**, *11*, 260.

[177] Moffitt, J. R.; Chemla, Y. R.; Smith, S. B.; Bustamante, C. Recent advances in optical tweezers. *Annu. Rev. Biochem.* **2008**, *77*, 205–228.

[178] Bustamante, C. J.; Chemla, Y. R.; Liu, S.; Wang, M. D. Optical tweezers in single-molecule biophysics. *Nat. Rev. Methods Primers* **2021**, *1*, 25.

[179] Heller, I.; Hoekstra, T. P.; King, G. A.; Peterman, E. J. G.; Wuite, G. J. L. Optical tweezers analysis of DNA–protein complexes. *Chem. Rev.* **2014**, *114*, 3087–3119.

[180] Hugel, T.; Seitz, M. The study of molecular interactions by AFM force spectroscopy. *Macromol. Rapid Commun.* **2001**, *22*, 989–1016.

[181] Gurevitch, I.; Srebnik, S. Monte Carlo simulation of polymer wrapping of nanotubes. *Chemical Physics Letters* **2007**, *444*, 96–100.

Appendices

Appendix A

Forced Extension of a Wormlike Chain in the Gibbs and Helmholtz Ensembles Appendix

This appendix contains the mathematical details of derivations and results mentioned in Chapter 2.

A.1 Derivation of the Strongly Stretched Gibbs Result

When the WLC is strongly stretched, tangent vector deviations from the stretching direction become small, and the Hamiltonian in (2.7) can be expanded to have the quadratic form

$$\beta H = \int_0^1 \mathrm{d}t \left[\frac{\lambda}{2L} \left| \frac{\mathrm{d}\mathbf{u}_{xy}(t)}{\mathrm{d}t} \right|^2 + \frac{1}{2} \beta L f \mathbf{u}_{xy}^2(t) \right] - \beta f L \tag{A.1}$$

Here, $\mathbf{u}_{xy}$ is the projection of the tangent vector $\mathbf{u}$ into the xy plane. The calculation of the partition function can then be mapped to the quantum problem of carrying out the Feynman path integral of the Green's function for a particle in a 2D harmonic potential [113]. From this procedure, the known two-point Green's function is

$$G(\mathbf{u}_{xy}, \mathbf{u}'_{xy}; \tau) = A e^{-B(\mathbf{u}_{xy}^2 + \mathbf{u}_{xy}'^2) - 2C \mathbf{u}_{xy} \cdot \mathbf{u}'_{xy}} \tag{A.2}$$

with

$$A = \frac{\alpha}{2\pi} \frac{1}{\sinh(\gamma\tau)} \tag{A.3}$$

$$B = \pi A \cosh(\gamma\tau) \tag{A.4}$$

$$C = -\pi A \tag{A.5}$$

and

$$\alpha = (\lambda\beta f)^{1/2} \tag{A.6}$$

$$\gamma = L(\beta f/\lambda)^{1/2} \tag{A.7}$$

The parameter $\tau = t - t'$ is the segment length between the two endpoints, where t and t' refer to the terminal ends with $\mathbf{u}_{xy}$ and $\mathbf{u}'_{xy}$ respectively.

The full partition function is obtained by integrating the full chain ($\tau = 1$) over all possible coordinates

$$\frac{Q}{V} = \int \mathrm{d}\mathbf{u}_{xy}\mathrm{d}\mathbf{u}'_{xy}\, G(\mathbf{u}_{xy}, \mathbf{u}'_{xy}; 1) = \frac{2\pi}{\alpha \sinh(\gamma)} \tag{A.8}$$

where V is the volume of the system. The free energy of the system is then

$$\beta G = -\ln Q - \beta f L \tag{A.9}$$

which is then used to obtain the extension

$$\langle z \rangle / L = 1 - D(L\sqrt{\beta f/\lambda})/\beta f L \tag{A.10}$$

where

$$D(x) = (1 + \coth(x))/2 \tag{A.11}$$

as presented in Eqs. (2.1) and (2.2).

A.2 Scaling Argument

In the text, especially Fig. 2.2, force-extension curves for different flexibility L/λ are represented by a universal relation, after the use of the scaling variables α and x. Here, a simple argument that requires no path integrals, etc., is given for the scaling relation.

When strongly stretched, the WLC makes small deviations from the main stretching direction, where the angle θ from the direction is small. Both the bending energy $(\lambda/2)[(\Delta\theta)^2/(\Delta s)^2]\Delta s$ and stretching potential $\beta f \Delta s(\cos\theta - 1) \sim -\beta f \Delta s\, \theta^2/2$ on a length element Δs are quadratic in θ, for any L/λ. Using the dimensionless element $\Delta t = \Delta s/L$ and fluctuation $v = (\lambda/2L)^{1/2}\theta$, the two energies can be cleanly written as $[(\Delta v)^2/(\Delta t)^2]\Delta t$ and $x^2 v^2 \Delta t$. Hence, we see the first scaling parameter x.

The extension comes from $Z/L \sim 1 - \langle\theta^2\rangle/2$. This gives $1 - Z/L \sim \langle\theta^2\rangle/2 = (L/\lambda)\langle v^2\rangle$. Therefore, the entire $\alpha = (1 - Z/L)\lambda/L \sim \langle v^2\rangle$ is a function of x only, in the statistical physics of variable v. The second scaling parameter, α, emerges on the left-hand side.

A.3 Contour Integral

The Helmholtz ensemble partition function is obtained first by starting with the known result for the partition function of a strongly stretched ($\tilde{f} = \langle \mathbf{R}^2_{\mathrm{KP}} \rangle \beta f / L \gg 1$) WLC, given in Eq. (2.18) in the main text,

$$Q(f) = \frac{2\pi}{\sqrt{\lambda \beta f}} \frac{e^{\beta f L}}{\sinh(L\sqrt{\beta f/\lambda})}$$

This is valid for any $L/2\lambda$, covering rodlike through to flexible WLCs. However, the partition function is only valid for $f > 0$, and so a direct application of the mapping, Eq. (2.15), is not possible. Instead, we make the mapping $\beta f \to -ip + \tau$, where τ is a small, real parameter, to ensure we remain on the $f > 0$ branch. We denote functions under this modified mapping with a prime. The modified Helmholtz partition function $Q'(Z)$ is then obtained through Eq. (2.13). By taking the limit of $Q'(Z)$ as τ goes to zero from the right after the transformation has been performed, the exact Helmholtz partition function $Q(Z)$ is obtained.

Applying this modified mapping along with Eq. (2.13) gives

$$Q'(Z) = \int_{-\infty}^{\infty} \mathrm{d}p \frac{e^{ipZ} e^{(-ip+\tau)L}}{\sqrt{\lambda(-ip+\tau)} \sinh(L\sqrt{(-ip+\tau)/\lambda})} \tag{A.12}$$

Making the change of variable $p' = p + i\tau$ changes it into the convenient form

$$Q'(Z) = (-1)e^{\tau Z} \int_{-\infty+i\tau}^{\infty+i\tau} \mathrm{d}p' \frac{e^{-ip'(L-Z)}}{\sqrt{ip'\lambda} \sin(L\sqrt{ip'/\lambda})} \tag{A.13}$$

The above integral can be evaluated by means of a contour integral in the complex plane. We define the contour C to be the curve that follows the real line $+i\tau$, and makes a semicircle in the bottom half plane, going counter-clockwise (see Fig. A.1). We take the integrand to be that of Eq. (A.13), with p' replaced by the complex variable z. It is straightforward to show that when C is made infinitely large so as a cover the entire real line, the contribution from the semicircular portion in the bottom half plane vanishes, and we have the resulting equation

$$\oint_C \mathrm{d}z \frac{e^{-iz(L-Z)}}{\sqrt{iz\lambda} \sin(L\sqrt{iz/\lambda})} = \int_{\infty+i\tau}^{-\infty+i\tau} \mathrm{d}p \frac{e^{-ip'(L-Z)}}{\sqrt{ip'\lambda} \sin(L\sqrt{ip'/\lambda})} \tag{A.14}$$

Evaluation of the left-hand side is done by means of the residue theorem

$$\oint_C f(z)\mathrm{d}z = 2\pi i \sum_n \mathrm{Re}_n \tag{A.15}$$

where Re_n denotes the nth residue. In this case, the poles are at $z = 0$, and $z = -in^2\pi^2\lambda/L$, where n is an integer. The resulting residue at $z = 0$ is

$$\mathrm{Re}_0 = (1/iL) \tag{A.16}$$

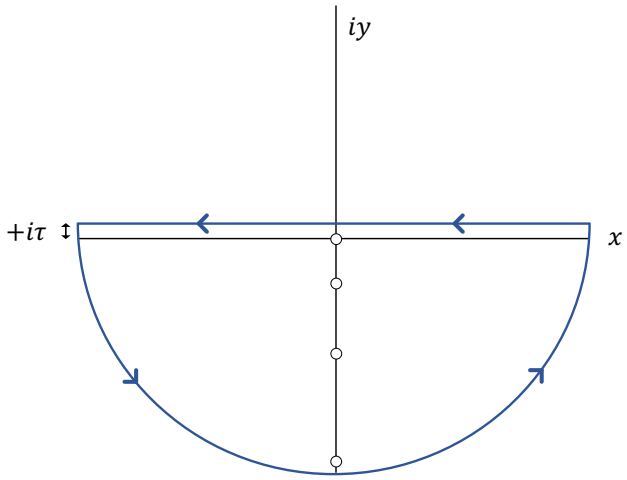


Figure A.1: Diagram of the contour C running counter-clockwise over the complex plane $z = x + iy$, used to evaluate the Fourier transform integral. First-order poles are at $z = 0$, and at $z = -in^2\pi^2\lambda/L$, represented by circles. The contributions from the semicircle in the bottom half plane vanish as the radius of C is increased to infinity. The component along the real line is offset by $i\tau$, where τ is a small real parameter used to ensure we remain within the region of validity of the partition function.

while the remaining residues are

$$\mathrm{Re}_n = (2i/L)(-1)^{n+1} e^{-\alpha\pi^2 n^2} \tag{A.17}$$

where $\alpha = (L - Z)\,\lambda/L^2$ as defined in Eq. (2.23). Summing over the residues gives

$$\oint_C \mathrm{d}z \frac{e^{-iz(L-Z)}}{\sqrt{iz\lambda}\sin(L\sqrt{iz/\lambda})} = \frac{4\pi}{L}\left[\sum_{n=1}^{\infty}(-1)^n e^{-\alpha\pi^2 n^2} + \frac{1}{2}\right] \tag{A.18}$$

and so the partition function is then

$$Q'(Z) = e^{\tau Z}\frac{4\pi}{L}\left[\sum_{n=1}^{\infty}(-1)^n e^{-\alpha\pi^2 n^2} + \frac{1}{2}\right] \tag{A.19}$$

Taking the limit $\tau \to 0^+$ turns the above into the exact results for the Helmholtz partition function of a strongly stretched WLC:

$$Q(Z) = \frac{4\pi}{L}\left[\sum_{n=1}^{\infty}(-1)^n e^{-\alpha\pi^2 n^2} + \frac{1}{2}\right] \tag{A.20}$$

This readily reduces to the Helmholtz partition function for a rodlike ($\alpha \gg 1$):

$$Q(Z)_{\text{rod}} = \frac{2\pi}{L} \tag{A.21}$$

which agrees with the independently calculated Eq. (2.35).

A.4 Re-summation

The partition function can also be re-summed, to directly show the ensemble equivalence in the thermodynamic limit, in the strongly stretched region. Through some small manipulation one obtains

$$Q(Z) = \frac{4\pi}{L}\left[\frac{1}{2}\sum_{n=-\infty}^{\infty}(-1)^n e^{-\alpha\pi^2 n^2}\right] \tag{A.22}$$

which puts the sum in a form readily approximated by the Euler-Maclaurin formula:

$$\sum_{i=m}^{n} f(i) \approx \int_m^n f(x)\mathrm{d}x \tag{A.23}$$

Any error in the above vanishes as $\alpha \to 0$. This gives

$$Q(Z) = \frac{2\pi}{L}\int_{-\infty}^{\infty}\mathrm{d}n\,(-1)^n e^{-\alpha\pi^2 n^2} \tag{A.24}$$

We then note that $(-1)^n = e^{n\ln(-1)}$, and so $\ln(-1) = \ln(e^{i\pi}) = i\pi$, giving

$$Q(Z) = \frac{2\pi}{L}\int_{-\infty}^{\infty} e^{-\alpha\pi^2 n^2 + i\pi n}\mathrm{d}n \tag{A.25}$$

The above evaluates to

$$Q(Z) = \frac{2}{L}\sqrt{\frac{\pi}{\alpha}}e^{-1/4\alpha} \tag{A.26}$$

which is the Helmholtz partition function in the thermodynamic limit. The force-extension relationship can then be calculated using Eq. (2.16). The Helmholtz free energy F is

$$\beta F = \frac{L}{4\lambda(1-Z/L)} + \ln\left[(1-Z/L)(\lambda/2\pi)\right] \tag{A.27}$$

and so the mean force is

$$\beta\langle f\rangle = \frac{1}{4\lambda(1-Z/L)^2} - \frac{1}{L(1-Z/L)} \tag{A.28}$$

Keeping only the leading order term, we arrive at the force-extension equation presented in the main text

$$\beta\langle f\rangle = \frac{1}{4\lambda(1-Z/L)^2} \tag{A.29}$$

equivalent to the Marko-Siggia result [7].

A.5 Gaussian Limit

As the free space stretched WLC reduces to the continuous Gaussian chain if $L/2\lambda \gg 1$ and $\tilde{f} \ll 1$, here we review the known fact that the force-extension curves are identical based on the Gaussian formalism. We start from the Helmholtz partition function for the Gaussian chain, obtained from the well-known Green's function by fixing the end points [30]

$$Q(Z) = \left(\frac{3}{2\pi R}\right)^{3/2} e^{-(3Z^2)/(2R^2)} \tag{A.30}$$

where $R^2 = 2L\lambda$ is the unperturbed mean square end-to-end distance. Use of Eq. (2.16) then gives

$$\beta\langle f\rangle = \frac{3Z}{R^2} \tag{A.31}$$

which is the well-known result for an entropic spring in the Helmholtz ensemble [27]. Rearranging gives rise to

$$\frac{Z}{L} = \frac{R^2\beta\langle f\rangle}{3L}. \tag{A.32}$$

Examining Eq. (2.13), the Gibbs partition function can be obtained from the Fourier transform of $Q(Z)$, followed by a mapping from p to f. Performing this transform, we obtain

$$Q(p) = \int_{-\infty}^{\infty} \left(\frac{3}{2\pi R^2}\right)^{3/2} e^{-3x^2/2R^2} e^{-ipZ}\,\mathrm{d}Z \tag{A.33}$$

$$= e^{-p^2R^2/6} \tag{A.34}$$

Then as $\beta f = -ip$, $\beta^2 f^2 = -p^2$,

$$Q(f) = e^{\beta^2 f^2 R^2/6}. \tag{A.35}$$

Through Eq. (2.10) the average extension is

$$\frac{\langle Z\rangle}{L} = \frac{R^2\beta f}{3L} \tag{A.36}$$

which is the identical to Eq. (A.32) under the transformations $\langle Z\rangle \to Z$, $f \to \langle f\rangle$.

Appendix B

Stretching Semiflexible Polymers: Gibbs Versus Helmholtz Ensembles Appendix

This appendix contains the mathematical details of derivations and results mentioned in Chapter 3. In addition, Section B.4 contains a derivation of results for different boundary conditions at the polymer endpoints, to facilitate a comparison against the free-end case discussed in the main text of the chapter.

B.1 Wormlike-chain Theory

Here, a brief outline of the wormlike-chain (WLC) theory, high force scaling, and the relationship between the two ensembles for a strongly stretched polymer, is given.

The WLC polymer is described as a smooth curve in space, parameterized by a variable t, which ranges from 0 at one end, to $t = 1$ at the other. The polymer has a contour length L, and a persistence length λ, equal to twice its Kuhn length b, which characterizes its stiffness. The position of any point along the curve is given by $\mathbf{r}(t)$, and the tangent vector to that point described by $\mathbf{u}(t) = \mathrm{d}\mathbf{r}(t)/\mathrm{d}t$. An unstretched, ideal WLC, is then described by the Hamiltonian:

$$\beta H_0 = \int_0^1 \mathrm{d}t \frac{\lambda}{2L} \left| \frac{\mathrm{d}\mathbf{u}(t)}{\mathrm{d}t} \right|^2 \tag{B.1}$$

where $\beta = 1/k_b T$, with k_b is the Boltzmann constant and T the temperature.

The conformational statistics of the WLC can be obtained from its partition function. If a WLC is stretched with a fixed applied force f along a direction

$\hat{z}$, where the desired quantity is the average extension along this direction $\langle Z \rangle$, then the correct choice is the Gibbs ensemble partition function

$$Q(f) = \int \mathrm{d}\mathbf{u}(t) \, \exp\left(-\beta H_0[\mathbf{u}(t)] + \beta f L \int_0^1 \mathrm{d}t \, u_z(t) \right) \tag{B.2}$$

where the applied force term has been introduced as the integral over the tangent vector component along the $\hat{z}$ direction, $u_z(t)$, at a point t. Here, we have implicitly reduced the partition function by the volume of phase space V.

If instead, the average force $\langle f \rangle$ is desired from a WLC system with a fixed extension Z, then the Helmholtz ensemble is employed, with partition function

$$Q(Z) = \int_0^1 \mathrm{d}\mathbf{u}(t) \, e^{-\beta H_0} \delta\left(Z - L \int_0^1 \mathrm{d}t u_z(t) \right) \tag{B.3}$$

where again the partition function has been implicitly reduced. The average force and average extension are then derived from the Gibbs free energy $\beta G = -\ln G(f)$ and the Helmholtz free energy $\beta F = -\ln F(Z)$ respectively, using the standard thermodynamic relationships

$$\langle Z \rangle = -\frac{\partial G(f)}{\partial f} \tag{B.4}$$

$$\langle f \rangle = -\frac{\partial F(Z)}{\partial Z} \tag{B.5}$$

It is not possible to find general closed form formulas for WLC force-extension relationships over the entire range of Z or f. However, it is possible for a subset of the parameter space. Here, we consider strongly stretched polymers, defined as when deviations of the WLC tangent vector from the stretching direction are well approximated as quadratic. When both polymer ends are unconstrained, the force-extension relationships for a strongly stretched WLC in both ensembles are known [1, 4–6]. For the Gibbs ensemble, we have

$$\begin{aligned} \frac{\langle Z \rangle}{L} &= 1 - D(x)/\beta f L \\ D(x) &= [1 + x \coth(x)]/2 \\ x &= L(\beta f/\lambda)^{1/2} \end{aligned} \tag{B.6}$$

While for the Helmholtz ensemble we get

$$\begin{aligned} \beta \langle f \rangle &= \frac{\lambda \pi^2}{L^2} \frac{\sum_{n=1}^{\infty} (-1)^{(n+1)} n^2 e^{-\alpha \pi^2 n^2}}{\sum_{n=1}^{\infty} (-1)^n e^{-\alpha \pi^2 n^2} + 1/2} \\ \alpha &= (1 - Z/L) \, \lambda / L \end{aligned} \tag{B.7}$$

Under the thermodynamic limit $L/2\lambda \gg 1$, both of the above equations ap-

proach the same result:

$$\frac{Z}{L} = 1 - \frac{1}{(4\beta\langle f\rangle\lambda)^{1/2}} \quad \text{(Helmholtz)} \tag{B.8}$$

$$\frac{\langle Z\rangle}{L} = 1 - \frac{1}{(4\beta f\lambda)^{1/2}} \quad \text{(Gibbs)} \tag{B.9}$$

which can be expressed concisely as

$$\alpha = \frac{1}{2x} \tag{B.10}$$

where there is no longer any distinction between the thermodynamic variables f, Z and their averages $\langle f\rangle$, $\langle Z\rangle$.

B.2 Scaling Argument

The two scaled variables x and α used throughout the text emerge during the discussion in Appendix B.1. However, they can also be derived with a short scaling argument, which perhaps provides more insight. Under the strongly stretching limit considered here, deviations of the WLC are small and quadratic in nature. The bending energy, in terms of the bending angle θ, for a small segment Δs, is $(\lambda/2)[(\Delta\theta)^2/(\Delta s)^2]\Delta s$. The stretching potential under quadratic deviations is $\beta f\Delta s(\cos\theta - 1) \sim -\beta f\Delta s\theta^2/2$. Considering a dimensionless length element $\Delta t = \Delta s/L$ and dimensionless fluctuation $v = (\lambda/2L)^{1/2}\theta$, the bending energies and stretching potential take on the simplified forms $[(\Delta v)^2/(\Delta t)^2]\Delta t$ and $x^2v^2\Delta t$, and x has naturally emerged from the stretching potential.

The second scaling parameter can be seen be considering the extension under the strongly stretched regime $Z/L\ 1 - \langle\theta^2\rangle/2$. This gives $1 - Z/L \sim \langle\theta^2\rangle/2 = (L/\lambda)\langle v^2\rangle/2$, or more concisely, $\alpha \sim \langle v^2\rangle$ where the second scaling variable α appears.

B.3 Helmholtz Interpolation Formula

The function $H(\alpha)$ used here is expressed in Eq. (3.4) in the main text by series summation. It can also be identically expressed by the partial theta functions $\theta(x;q)_p = \sum_{n=0}^{\infty} x^n q^{n^2}$ [114, 115]. Both are not the most convenient form. A simple replacement can be the interpolation formula,

$$H(\alpha) = \frac{e^{-\alpha\pi^2/2}}{2\alpha}\left(1 + 8\pi^2\alpha^2\right)^{1/2} \tag{B.11}$$

For $\alpha \approx 10^{-1}$, the above exhibits its worst error at around 10%. It should be accurate enough for practical use, and a comparison is presented in Fig. B.1.

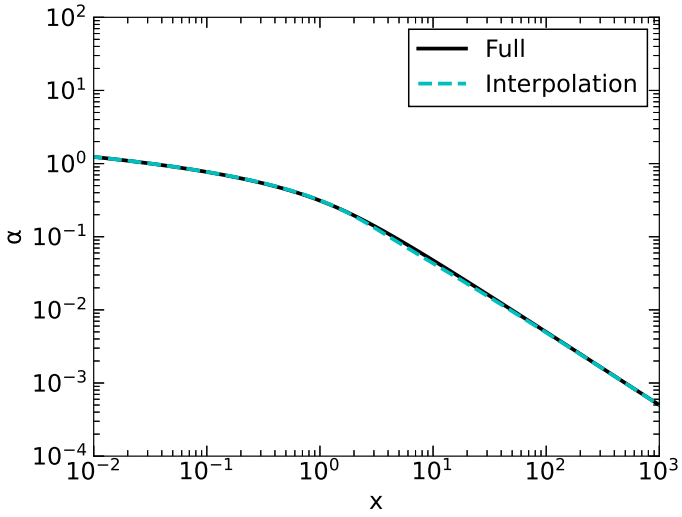


Figure B.1: Comparison of the exact Helmholtz result Eq. (3.4) in the main text, and the interpolation formula Eq. (B.11), which limits to the exact behaviour for both small and large α, and provides a reasonably accurate result in the intermediate regime, in a simple formula.

B.4 Derivation of Solutions for Different Boundary Conditions

B.4.1 General Theory and Mapping

The exact solutions for the Gibbs ensemble partition functions under the strongly stretched regime can be found by directly carrying out a path integral. By reducing the propagator by a factor of $\exp(\beta f L)$ equation under the strongly stretched harmonic approximation is identical to the 2D quantum harmonic oscillator. Evaluation of the path integral can be following a similar approach as done for the quantum harmonic oscillator as formulated by Feynman [113]. This gives the 1D propagator for the strongly stretched polymer in the Gibbs ensemble

$$K(x_i, x_f; L) = A \exp[B(x_i^2 + x_f^2) - 2C x_i x_f] \tag{B.12}$$

where

$$A = \left(\frac{1}{2\pi} \frac{\sqrt{\beta\lambda f}}{\sinh(L\sqrt{\beta f/\lambda})} \right)^{1/2} \tag{B.13}$$

$$B = -\frac{1}{2} \frac{\sqrt{\beta\lambda f}\cosh(L\sqrt{\beta f/\lambda})}{\sinh(L\sqrt{\beta f/\lambda})} \tag{B.14}$$

$$C = -\frac{1}{2} \frac{\sqrt{\beta\lambda f}}{\sinh(L\sqrt{\beta f/\lambda})} \tag{B.15}$$

The propagator end points correspond to the angles in the polymer system through

$$\theta_i = \sqrt{x_i^{(x)} + x_i^{(y)}} \tag{B.16}$$

$$\theta_f = \sqrt{x_f^{(x)} + x_f^{(y)}} \tag{B.17}$$

where θ_i and θ_f represent the angles of the tangent vector $\mathbf{u}$ for the initial and final points relative to the stretching direction, respectively. This analysis was previously carried out in Ref. [4] following this approach, and in an appendix of Ref. [6] through different means. The 1D partition function is obtained by integrating the propagator

$$Q_{1D} = \int \mathrm{d}x_i \mathrm{d}x_f K(x_i, x_f, L) \tag{B.18}$$

through the symmetry of the system, the desired 2D partition function is $Q_{2D} = Q_{1D}^2 \exp \beta f L$. In all cases, the partition functions have been reduced by the volume of phase space. Translational invariance of the system means 2D function captures the full behaviour of the polymer system, and the force-extension relationship is found through standard thermodynamics. The result is Eq. (2.19) in the main text:

$$\frac{\langle Z \rangle}{L} = 1 - D(x)/\beta f L \tag{B.19}$$

$$D(x) = [1 + x\coth(x)]/2 \tag{B.20}$$

The Helmholtz result was determined in Ref. [1], by evaluating the Gibbs result at the imaginary force $f = -ip/\beta$ and taking the inverse Fourier transform of the result with respect to p. The result corresponds to Eq. (2.24) in the main text

$$\beta\langle f \rangle = \frac{\lambda\pi^2}{L^2} \frac{\sum_{n=1}^{\infty}(-1)^{(n+1)} n^2 e^{-\alpha\pi^2 n^2}}{\sum_{n=1}^{\infty}(-1)^n e^{-\alpha\pi^2 n^2} + 1/2} \tag{B.21}$$

$$\tag{B.22}$$

Both of the above results represent a polymer system where the terminal ends are free to rotate. This is the case focused on in the main text, and the results of which provide good agreement with experimental measurements, regardless of the boundary conditions employed in these experiments. However, it is useful nonetheless to have a grasp of the behaviour under different boundary conditions. This is treated in the following two sections.

B.4.2 Two Fixed Ends

The polymer ends can be alternatively forced to align along the stretching direction. The tangent vector of the initial point and end point both point along the stretching direction, giving $\theta_i = 0$ and $\theta_f = 0$. Both ends are forced to be co-axial. This implies $x_i = 0$ and $x_f = 0$.

The propagator in this case is

$$K(0,0;L) = A \tag{B.23}$$

and integrating gives the Gibbs ensemble result

$$Q_{1D} = \left[\frac{1}{2\pi}\frac{\sqrt{\beta\lambda f}}{\sinh(L\sqrt{\beta f/\lambda})}\right]^{1/2} \tag{B.24}$$

therefore,

$$Q_{2D} = \frac{1}{2\pi}\frac{\sqrt{\beta\lambda f}}{\sinh(L\sqrt{\beta f/\lambda})}e^{\beta f L} \tag{B.25}$$

Which is used to determine the force-extension relationship in the Gibbs ensemble for the two fixed ends case

$$\frac{\langle Z\rangle}{L} = 1 - \frac{1}{2}\frac{1}{\sqrt{\beta f\lambda}}\coth(L\sqrt{\beta f/\lambda}) + \frac{1}{2}\frac{1}{\beta f L} \tag{B.26}$$

The above derivation agrees with the results found in Ref. [105].

Starting from the partition function Eq. (B.25) and obtaining the Helmholtz partition function through the mapping $\beta f = -i$ followed by the contour integral. This gives

$$Q(Z) = \frac{1}{2\pi}\int_{-\infty}^{\infty}\mathrm{d}p\frac{1}{2\pi}\frac{\sqrt{ip\lambda}}{\sin(L\sqrt{ip/\lambda})}e^{-ip(L-Z)} \tag{B.27}$$

$$= \frac{1}{4\pi^2}\oint\mathrm{d}z\frac{\sqrt{iz\lambda}}{\sin(L\sqrt{iz/\lambda})}e^{-iz(L-Z)} \tag{B.28}$$

$$= \frac{1}{4\pi^2}2\pi i\sum_n R_n \tag{B.29}$$

where R_n is the residue of the nth pole. The poles of the integrand occur for

$$z_0 = -\frac{in^2\pi^2\lambda}{L^2} \quad n = 1,2,3... \tag{B.30}$$

and have the values

$$R(z_0) = 2i\left(\frac{n^2\pi^2\lambda^2}{L^3}\right)(-1)^{n+1}e^{-n^2\pi^2\alpha} \tag{B.31}$$

Summing over the residues and simplifying gives the partition function for the two coaxially fixed ends case:

$$Q(Z) = \pi\frac{\lambda^2}{L^3}\sum_{n=1}(-1)^{n+1}n^2e^{-n^2\pi^2\alpha} \tag{B.32}$$

$$\tag{B.33}$$

The force-extension relationship derived from the above partition function is

$$\beta\langle f\rangle = \frac{\lambda\pi^2}{L^2}\left[\frac{\sum_{n=1}(-1)^n n^4 e^{-n^2\pi^2\alpha}}{\sum_{n=1}(-1)^{n+1}n^2e^{-n^2\pi^2\alpha}}\right] \tag{B.34}$$

Using the two parameters α and x, both equations can be reformatted to show their scaling behaviour

$$\alpha(x) = \frac{1}{2x^2}\left[x\coth(x) - 1\right] \qquad \text{(Gibbs)} \tag{B.35}$$

$$x(\alpha) = \pi\left[\frac{\sum_{n=1}(-1)^n n^4 e^{-n^2\pi^2\alpha}}{\sum_{n=1}(-1)^{n+1}n^2e^{-n^2\pi^2\alpha}}\right]^{1/2} \qquad \text{(Helmholtz)} \tag{B.36}$$

B.4.3 One Fixed End

One polymer end can be fixed to point along the stretching direction, while the other is left free to rotate. We call this the one fixed end case, and it can be treated analogously to the other two. Here, the first end is taken to be fixed ($x_i = 0$) while the other end is left free.

The propagator then becomes

$$K(0, x_f; L) = A\exp Bx_f^2 \tag{B.37}$$

which leads to the partition function

$$Q_{2D} = \frac{1}{4\pi}\frac{(\beta\lambda f)\cosh(L\sqrt{\beta f/\lambda})}{\sinh^2(L\sqrt{\beta f/\lambda})}e^{\beta fL} \tag{B.38}$$

From the above, the force-extension relationship in the Gibbs ensemble is found to be

$$\frac{\langle z\rangle}{L} = 1 - \frac{1}{\sqrt{\beta fL}}\left[\coth(L\sqrt{\beta f/\lambda}) - \frac{1}{1}\tanh(L\sqrt{\beta f/\lambda})\right] + \frac{1}{2}\frac{1}{\beta fL} \tag{B.39}$$

Performing the mapping $\beta f = -ip$ and writing the Helmholtz partition function in terms of the inverse Fourier transform gives

$$Q(Z) = \frac{1}{2\pi}\frac{1}{4\pi}\int_{\infty}^{\infty} \mathrm{d}p \frac{1}{4\pi}\frac{(ip\lambda)\cos(L\sqrt{ip/\lambda})}{\sin^2(L\sqrt{ip/\lambda})} e^{-ip(L-Z)} \tag{B.40}$$

Evaluating the integrand by means of the contour integral

$$\oint \mathrm{d}z \frac{1}{4\pi}\frac{(iz\lambda)\cos(L\sqrt{iz/\lambda})}{\sin^2(L\sqrt{iz/\lambda})} e^{-iz(L-Z)} \tag{B.41}$$

where the poles are located at

$$z_0 = -\frac{in^2\pi^2\lambda}{L^2} \tag{B.42}$$

with corresponding residues

$$R(z_0) = i\frac{n^4\pi^4\lambda^3}{L^4}(-1)^{n+1}e^{-n^2\pi^2\alpha} \tag{B.43}$$

The Helmholtz partition function is given then by the sum over the residues

$$Q(Z) = \frac{\pi^3}{4}\frac{\lambda^3}{L^4}\sum_n (-1)^n n^4 e^{-n^2\pi^2\alpha} \tag{B.44}$$

which leads to the force-extension relationship for the one fixed end case in the Helmholtz ensemble

$$\beta\langle f\rangle = \frac{\lambda\pi^2}{L^2}\left[\frac{\sum_{n=1}(-1)^{n+1}n^6 e^{-n^2\pi^2\alpha}}{\sum_{n=1}(-1)^n n^4 e^{-n^2\pi^2\alpha}}\right] \tag{B.45}$$

The relationships for both ensembles can be recast in terms of α and x

$$\alpha(x) = \frac{1}{x}\left[\coth(x) - \frac{1}{2}\tanh(x)\right] - \frac{1}{2x^2} \quad \text{(Gibbs)} \tag{B.46}$$

$$x(\alpha) = \pi\left[\frac{\sum_{n=1}(-1)^{n+1}n^6 e^{-n^2\pi^2\alpha}}{\sum_{n=1}(-1)^n n^4 e^{-n^2\pi^2\alpha}}\right] \quad \text{(Helmholtz)} \tag{B.47}$$

Differences between the free end, two fixed ends, and one fixed end cases are discussed in the main text.

B.4.4 Scaling behaviour for 1 and 2 fixed ends

The curves in Fig. 2.2 corresponding to Eqs. (2.19) and (2.24) are for a WLC with two unconstrained ends, meaning that each end point is free to rotate. This is not a fundamental constraint, and either one or both of the ends can be made fixed instead. The choice of boundary conditions for the WLC will then

affect the observed scaling behaviour. Although we found the free-end curves best explained the data, we present alternative boundary conditions here, where we hope that further experimental investigations might be able to probe this aspect of the theory.

The possible configurations are unconstrained (free) ends, one fixed end, and two fixed ends. All three can be accessed experimentally, for example, using optical tweezers, unconstrained ends can be achieved using two tweezers in tandem, and one fixed end by using a single tweezer and grafting the other end to a coverslip [177–179]. Two fixed ends can be achieved using atomic force microscopy [180].

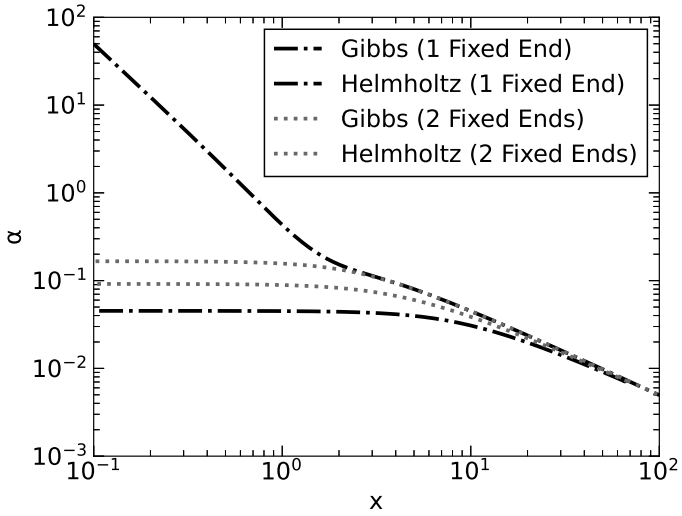


Figure B.2: Finite length scaling behaviour for a strongly stretched WLC under different boundary conditions. The outer dot-dashed curves are with one end fixed, and one end free to rotate, as is the common setup in optical tweezer experiments. The inner dotted curves are for both ends fixed, as might be achieved in AFM experiments. In both cases, the Gibbs result is the upper curve, while the Helmholtz result is the lower curve.

The derivation follows similarly from the free end case (details can be found in Appendix B.4 and Ref. [1]). By changing the boundary conditions from two free ends, to one free end and one fixed end, the following force-extension relationships are obtained:

$$\alpha(x) = \frac{1}{x}[\coth(x) - \frac{1}{2}\tanh(x)] \qquad \text{(Gibbs)} \qquad \text{(B.48)}$$

$$x(\alpha) = \pi \left[\frac{\sum_{n=1}^{\infty}(-1)^{n+1} n^6 e^{-n^2\pi^2\alpha}}{\sum_{n=1}^{\infty}(-1)^{n} n^4 e^{-n^2\pi^2\alpha}} \right]^{1/2} \qquad \text{(Helmholtz)} \qquad \text{(B.49)}$$

while fixing both of the ends gives:

$$\alpha(x) = \frac{1}{2x^2}[x\coth(x) - 1] \qquad \text{(Gibbs)} \tag{B.50}$$

$$x(\alpha) = \pi \left[\frac{\sum_{n=1}^{\infty}(-1)^n n^4 e^{-n^2\pi^2\alpha}}{\sum_{n=1}^{\infty}(-1)^{n+1} n^2 e^{-n^2\pi^2\alpha}} \right]^{1/2} \qquad \text{(Helmholtz)} \tag{B.51}$$

These two sets of curves are plotted in Fig. B.2. The inner dotted curves are for two fixed ends, while the outer curves are dashed curves are for one fixed end. In both cases the upper curves correspond to the Gibbs ensemble, while the lower curves are for the Helmholtz ensemble. Several of the experiments have one end fixed to a coverslip during the force-extension measurements. However, we find the compiled data best agrees with the two free end results, regardless of which boundary conditions were employed in practice.

B.5 Other Studies

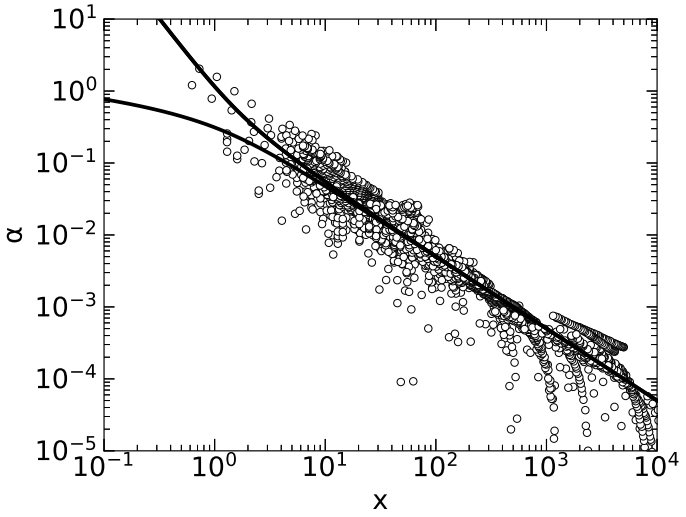


Figure B.3: Set of extra data not presented in the main text, see Table B.1 for the full list and corresponding systems. The studies are of high quality, but the force-extension data within does not have the resolution necessary to resolve the fine theoretical difference presented here.

The literature covered in the main text focused on studies that examined the strongly stretched limit for both short and long polymers. In general, we used studies that contained the lowest amount of noise, as these were able to clearly resolve details in the critical region of interest. There is, however, a body of literature without sufficient resolution to probe the finite length effects. These

Table B.1: Collection of force-extension data not presented in the main text. The method of study is labelled by Flow (applied fluid flow), OT (optical tweezer), MT (magnetic tweezer), AFM (atomic force microscopy), MC (Monte Carlo simulation), PBD (pseudo-Brownian dynamics), or MD (molecular dynamics). All data points are represented by unfilled circles in Fig. B.3

Study	Method	Molecule	Fixed
Wang [48]	OT	dsDNA	f[1]
Bemis [49]	AFM	PbP2V[2]	Z
Sun [50]	OT	Procollagen I	Z
Dessinges [51]	MT	ssDNA[3]	Z
Sun [52]	OT	Procollagen II	Z
Leake [53]	OT	Titin	Z
Sun [54]	OT	Procollagen II	Z
Aumann [55]	MC	Chromatin	f
Miller [56]	AFM	E. Coli Type 1 Pili	Z
Nakajima [57]	AFM	Polystyrene	Z
Khalil [58]	OT	m13 + dsDNA	f[4]
Buehler [59]	MD	Tropocollagen	f
Kauert [60]	MT	DNA Bundle	f
Hsu [61]	MC	Generic	f
Wieczorek [62]	OT	Procollagen II	Z
Liese [63]	AFM + MD	PEG	f or Z
Kolberg [64]	AFM	PEG + PNiPAM	Z
Shon [65]	MT	dsDNA	f
Dutta [66]	MC	Branched Polymer	f
Gutiérrez-Medina [67]	OT	Diatom EPS Fiber[5]	Z
Bibeau [68]	Flow	Actin	f

1 Switches to fixed f partway through measurement, only this data included
2 Polystyrene-b-poly-2-vinylpyridine
3 0.5 mM Mg^{++} data only, see Ref. [51] for effects of high ionic conditions.
4 Stated in the original work, but unconfirmed by us
5 Extracellular polymeric substances

are still high quality studies on their respective topics, and we include them here for completeness. Figure B.3 contains this set of extra data, plotted in the same style as Fig. 3.3 in the main text. The two solid lines are the fixed-f (top) and fixed-Z (bottom). The data is given in Table B.1.

Appendix C

Helical Wrapping of Cylindrical Tubes by Wormlike-Chain Polymers Appendix

This appendix contains a discussion and explanation of the experimental data from Chapter 4. It also contains a discussion on the theory by Lundberg and Strano [26], which was compared against the WLC solution presented in the main text of the chapter.

C.1 Experimental Data

The experimental data values for the helix pitch of single-walled carbon nanotubes (SWNTs) wrapped by various polymers, as presented in Figure 2 in the main text, are given here. Values for the helix pitch were taken directly from the studies of interest. If the paper gave a value for the persistence length λ of the system, it was used. If no value for λ was given, it was estimated using separate experimental studies, with the specific value selected to properly account for the ionic strength of the experimental or theoretical system. See the table C.1 below for details. The radius of the nanotube was taken as the radius of the SWNT, plus the distance from the surface of the nanotube to the polymer backbone; we refer to this as the hybrid radius. All values for the hybrid radius were taken from their respective papers, save for one exception noted in the table.

C.2 Comparison Against Lundberg and Strano

For the comparison against the theory by Lundberg and Strano [26], we solved their theory over the same data range, and using the same number of points in λ/R, as was used for our solution to the wormlike-chain (WLC) model. Their theory, given as the dashed grey curve in Figure 4 in the main text, was obtained by solving their Eq. (23). Using our notation, this equation is

$$-2\lambda\frac{R^2P/2\pi}{(R^2+(P/2\pi)^2)^{3/2}}+F(\alpha)\left[\frac{1}{\sqrt{R^2+(P/2\pi)^2}}-\left(\frac{(P/2\pi)^2}{(R^2+(P/2\pi)^2)^{3/2}}\right)\right]=0 \tag{C.1}$$

Where $F(\alpha)$ is

$$F(\alpha)=\frac{k_BT}{l_p}\left(\alpha-\frac{1}{4}+\frac{1}{4(1-\alpha)^2}-\frac{3}{4}\alpha^2\right) \tag{C.2}$$

and $\alpha=(P/2\pi)/\sqrt{R^2+(P/2\pi)^2}$.

For each data point, the ratio λ/R was fixed, and the value of $P/2\pi$ that satisfies the equation was numerically solved for.

Table C.1: Experimental data points, estimated persistence length, and nanotube radii

Authors	Exp / Sim	System	l_p (nm)	P (nm)	R [Hybrid Radius] (nm)
Cathcart 2008 [8]	Exp	2x ssDNA	2.5 [18, 19]	2.2	1.2
Liu 2011 [12]	Sim (MD)	Chitosan	16 ± 2 [20]	14.6 ± 1.7	0.81
Liu 2010 [13]	Sim(MD)	Alginic Acid	15.3 ± 0.5 [21]	15*	0.97
Deria 2010 [9]	Exp	PNES	7.5 [22, 23]	10 ± 2	0.736[a]
Yarotski 2009 [10]	Exp + Sim (MD)	ssDNA	2.5 [18, 19]	3.3 ± 0.2 ; 4.2**	1 ; 1.3[b]
Kang 2009 [11]	Exp + Sim (MD)	PPES	14 [24, 25]	13 ± 2	0.736
Zheng 2003 [16]	Exp	ssDNA	2 [18, 19]	18	1
Campbell 2008 [17]	Exp	ssDNA	1.6 [18, 19]	14 ± 5	0.9
Zerze 2020 [14]	Sim (MD)	ssDNA	3 [18, 19]	4.9 ± 0.7	1
Gurevitch 2008 [15]	Sim (MC)	Generic[c]	10.3σ [181]	15σ	3σ

* Estimated based off Figure 1.

** Semicolon separates experimental data from simulation data (Experimental ; Theory)

a Assumed same as Kang et al., similar polymer, same nanotube batch [9, 11]

b Taken from Figure 4 [10]

c A general parameter σ was used in the work instead of specific values